UNIVERSITY
OF TRENTO - Italy

Doctoral School in
Engineering of Civil and Mechanical
Structural Systems
XXVIII Cycle

Francesco Longo

NUMERICAL MODELLING OF UNREINFORCED MASONRY INFILL WALLS UNDER SEISMIC LOAD CONSIDERING IN-PLANE / OUT-OF-PLANE INTERACTION

April, 2016

University of Trento
University of Brescia
University of Bergamo
University of Padova
University of Trieste
University of Udine
University IUAV of Venezia

Francesco Longo (Ph.D. Student)

Numerical Modelling of Unreinforced Masonry Infill Walls under Seismic Load Considering In-Plane - Out-Of-Plane Interaction

Prof. Claudio Modena (Supervisor)
Dr. Lydell A. Wiebe (Co-supervisor)

2016

UNIVERSITY OF TRENTO
Engineering of Civil and Mechanical Structural Systems - XXVIII Cycle

Prof. Paolo Scardi (PhD. Head's)

Final Examination 04/04/2016

Board of Examiners:

Prof. Claudia Battaino	(University of Trento, Italy)
Prof. Elisabeth Vintzileou	(National Technical University of Athens, Greece)
Prof. Andrea Vignoli	(University of Firenze, Italy)
Prof. Hervé Degée	(Hasselt University, Belgium)

ABSTRACT

Numerical Modelling of
Unreinforced Masonry Infill Walls under Seismic Load
Considering In-Plane - Out-Of-Plane Interaction

Francesco Longo, Ph.D. Candidate
Prof. Claudio Modena, University of Padova, Italy (Supervisor)
Dr. Lydell A. Wiebe, McMaster University, Hamilton; Canada (Co-supervisor)
Prof. Paolo Scardi, University of Trento, Italy (Ph. D. Head's)

Many studies and post-earthquake investigations have recognized that masonry infill walls play a major role in the seismic response of structures. Although their effect may be beneficial in some situations, the walls are also susceptible to high levels of damage, including collapse that can be life-threatening because of the heavy debris. Despite the critical importance of infill walls for life safety, infill walls are often neglected in numerical models and analyses implemented by designers because they are traditionally considered to be non-structural elements. Moreover, the majority of experimental studies and numerical models include only the in-plane behaviour of the panels: indeed, until recently, only sophisticated micro-models incorporated the out-of-plane response of unreinforced masonry infill walls. Recently, however, researchers have started to advance proposals for simplified macro-models that are capable of modelling in-plane/out-of-plane interaction, paving the way for the consideration of the associated issues in design practice. However, very few studies have applied these models to the dynamic seismic response history analysis of realistic structures.
In this context, this thesis focuses on the numerical modelling of unreinforced masonry (URM) infill walls, with particular attention to the combined in-plane/out-of-plane response of panels in reinforced concrete (RC) frame buildings during seismic events.

In the first part of this research, existing studies for URM masonry infill walls are reviewed, with an emphasis on the out-of-plane response of the panels. Significant experimental tests, modeling strategies and post-earthquake surveys are presented, stressing the parameters that influence the behaviour of the infills. An in-depth description is dedicated to the infill wall macro-model that is adopted for the analyses performed in this work, emphasizing its capabilities and limitations. This model consists of a single diagonal formed by two beam elements representing the wall; lumped modal mass is concentrated at the midpoint node of the diagonal. In-plane axial force and out-of-plane bending of the equivalent element interact by means of two fibre sections located adjacent to the central node. User defined domains limit axial/bending strengths and in-plane/out-of-plane ultimate displacements of the wall. When the response of an element exceeds these domains, the model simulates the collapse of this infill wall by removing it from the analysis.

Next, the numerical model is calibrated in the OpenSees software framework by comparing existing experimental results with numerical outputs. The laboratory tests comprise in-plane cyclic and out-of-plane quasi-static results on 1-bay and 1-storey frame specimens with two different types of clay URM infill walls that are frequently found in Italian and other Mediterranean countries. The calibrated model is then applied to the static pushover analysis of a set of planar frames, while the wall elements are simultaneously loaded in both orthogonal directions.

The nucleus of present study is the application of the calibrated model to the dynamic response history analysis of planar RC frames. Frame dimensions, number of stories, design and infill configurations are selected to be representative of the Italian building stock. Acceleration time histories consist of a suite of a bidirectional ground motions that are scaled to be compatible with Eurocode 8 elastic spectra. Cracking and collapse of the infill walls are monitored during the analysis. The infill walls reach their ultimate displacement capacity by a combination of in-plane and out-of-plane displacements, with the out-of-plane component usually playing the dominant role. The intensity of seismic load that is required to fail the infill walls, as well as the patterns of failure, are shown to be consistent with observed damage to URM infill walls in similar buildings during recent earthquakes.

This research suggests that simplified macro-elements are suitable for design-oriented models of URM infill walls in RC framed structures, capturing the critical interaction between in-plane and out-of-plane response of the infill walls but without making the models excessively complex.

SOMMARIO

Il comportamento sismico degli edifici è influenzato in modo determinante dalla presenza di pannelli di tamponamento in muratura, come è ormai riconosciuto da numerosi studi, nonché dalle ricognizioni per il rilievo dei danni post-sisma. Sebbene in alcune occasioni la presenza dei tamponamenti abbia effetti positivi sul comportamento strutturale, i muri sono spesso suscettibili di alti livelli di danneggiamento, finanche all'espulsione del pannello, particolarmente pericolosi per l'incolumità a causa della caduta di detriti. Nonostante l'importanza critica dei muri di tamponamento per la salvaguardia della vita, la presenza dei pannelli è spesso trascurata nelle fasi di progettazione e di modellazione numerica, in quanto gli stessi sono formalmente elementi non-strutturali. Inoltre, la maggior parte delle campagne sperimentali e dei modelli numerici riferite ai tamponamenti in muratura si sono occupati principalmente della risposta nel piano dei pannelli: fino a tempi molto recenti la risposta fuori dal piano dei pannelli è stata proposta solo attraverso micro-modellazioni di notevole complessità. Negli ultimi anni diversi ricercatori stanno proponendo macro-modelli semplificati che includano l'interazione tra risposta nel piano e nel fuori piano dei muri di tamponamento, aprendo la strada all'inclusione nella progettazione di questi fenomeni. Tuttavia, solamente in un numero molto limitato di studi questi modelli sono stati applicati all'analisi dinamica non lineare di strutture ed edifici realistici.

In questo contesto, la tesi si occupa di modellazione numerica di pannelli di tamponamento in muratura semplice (non armata), e in particolare della risposta sismica ad azioni combinate nel piano / fuori dal piano dei muri posti in strutture a telaio in calcestruzzo armato.

La prima parte di questa ricerca è dedicata alla disamina degli studi esistenti sul comportamento dei pannelli di muratura semplice, con particolare enfasi alla risposta fuori dal piano. Saranno presentati in questa sede risultati sperimentali significativi, strategie di modellazione, regole di codici di progettazione e osservazioni in scenari post-sisma disponibili in letteratura. Un approfondimento sarà dedicato alla descrizione del macro-modello adottato nelle analisi svolte in questo studio, riferendo

in particolare delle sue potenzialità e limitazioni. Esso consiste in un modello a biella equivalente formato da due elementi allineati lungo la diagonale; nel nodo centrale è concentrata la massa modale del muro. In corrispondenza dello stesso nodo sono localizzate le due sezioni a fibre che garantiscono l'interazione tra la forza assiale nel piano e il momento nel fuori piano. Due domini di interazione limitano la resistenza e gli spostamenti ultimi dei pannelli. Durante un'analisi, quando un elemento esce dal dominio di spostamento del muro di tamponamento, i corrispondenti elementi sono rimossi dal modello, simulando il collasso del pannello.
Successivamente, il modello è stato calibrato in OpenSees confrontando risultati sperimentali già disponibili in letteratura con i risultati numerici. I test utilizzati per la calibrazione comprendono prove cicliche nel piano e successive spinte monotoniche nel fuori piano svolte su telai a una campata tamponati con due tipologie di muratura in laterizio molto comuni in Italia così come in altri Paesi dell'area mediterranea. Il modello così calibrato è applicato all'analisi statica non lineare (*pushover*) di alcune strutture a telaio tamponate, con la contemporanea applicazione di carichi statici in direzione ortogonale ai pannelli.
Il nucleo di questo studio è costituito dall'applicazione del macro-modello calibrato all'analisi dinamica non lineare (*time-history*) di due modelli di telaio piano realistici. Le dimensioni, il numero di piani, i dettagli costruttivi e i materiali degli elementi in calcestruzzo armato dei modelli sono stati scelti per essere rappresentativi dell'insieme degli edifici a telaio presenti in Italia. Le *time history* in accelerazione sono costituite da una serie di registrazioni bi-direzionali registrate in concomitanza di eventi sismici reali, scalate per essere compatibili con spettri elastici da Eurocodice 8. La fessurazione e il collasso dei pannelli sono monitorati durante l'analisi. I pannelli raggiungono gli spostamenti ultimi di collasso per una combinazione di spostamenti nel piano e nel fuori piano, con quest'ultima componente che risulta dominante nella maggior parte di casi. La relazione tra intensità sismica e danneggiamento degli elementi in muratura, nonché i pattern di collasso dei pannelli ottenuti dalle analisi sono consistenti con i danneggiamenti dei pannelli di tamponamento osservati in concomitanza a terremoti recenti in edifici con caratteristiche simili.
Questa ricerca suggerisce che macro-modelli semplificati sono idonei all'impiego in modelli numerici orientati alla progettazione dei pannelli in muratura semplice posti a tamponamento di strutture a telaio in calcestruzzo armato, essendo capaci di coglierne i fenomeni di interazione nel piano/fuori dal piano, senza rendere eccessivamente complessi i modelli stessi.

DEDICATION

This work is specially dedicated to an incredibly courageous young man.
Keep holding on, Loris.

To my Father, Mother, Sister and Brother.
Thank you for your patience, support and love. I feel blessed to have you.

To my wonderful Nonni.
I hope one day to achieve half of what you did. You are an inspiration for me.

To Alessandro and Andrea, my best and most trusted friends.
I relied a lot on you during these years. Thank you for being there.

To my Uncles, Aunts and cousins, in every country and continent.
It's sometimes difficult to stay in touch, but then it always feels good to get together.

To all the incredible people I met during in these three years, and especially,
Gabriele and Lydell. I owe you a lot. Thank you.

To Naoko/Midori, the Yin and Yang of infinite hours, thoughts, words.

ACKNOWLEDGEMENTS

My first and utmost gratitude is to my tutors, Prof. Claudio Modena and Dr. Lydell Wiebe for their supervision, suggestions and support during my PhD, both in Padova and in Hamilton.

Prof. da Porto is gratefully acknowledged for the opportunity to be part of the ReLUIS 2014 and INSYSME research projects that granted me funding during these years.

I also wish to thank my fellow post-graduate Elvis, Fabio Pietro and "Mezzanino" inhabitants, Marco, Giovanni, Luca, Laura, Marco, Alberto, Giovanni, Nicolò, Giulia for their support.

I am grateful to Gabriele Granello, now a PhD student in Canterbury, for his help with coding, figures, papers and for the interesting discussions about our studies.

I am also grateful to the students I met while at McMaster University, for their friendship and welcoming me from my first day in Hamilton, and especially to Yasser Al-Anany, Yasser Khalifa, Michael Kovacs, Changxuan Zhang, Tarek El-Hashimy, Shady Salem, Ahmad Siam, Taylor Steele, Paul Steneker, Daniel Stevens, Niel Van Engelen, Adrian Crowder.

A special thanks to Marina Rogato and the other staff members of the DICAM Secretariat, who have been the fundamental link in Trento during these three years.

TABLE OF CONTENTS

LIST OF FIGURES

LIST OF TABLES

1 INTRODUCTION

1.1 Background

In frame structures, enclosure panels built with clay or concrete masonry units and without steel reinforcement are generally referred to as unreinforced masonry (URM) infill walls. Reinforced concrete (RC) framed structures with URM infill walls are a common building design solution in many countries, especially for low- and mid-rise buildings (Fig. 1.1). Infill walls are used to make the structural frame functional for habitability, providing a physical enclosure from the outside environment. The panels are usually placed on a vertical plane, identified by contiguous pairs of beams and columns. Popular materials used for buildings the walls are burnt clay brick masonry, solid or hollow concrete blocks and hollow clay blocks in cement mortar. The use of tiles with hollows in particular is on the rise across the world.

There are several reasons that explain the diffusion of URM infill walls in many parts of the world. Firstly, since the beginning of the 20th Century, they represented an historical continuity with previous traditional masonry buildings. Previously, masonry constructions were characterized by massive walls. The use of iron rods to clasp masonry units first and the advent of reinforced concrete afterwards, provided the solutions to build more resilient structural skeletons of buildings, enabling thinner masonry sections in the rest of the constructions. Deprived from its structural role, masonry gradually became a “filler” for the void spaces left in structural frames, indeed infills. However, masonry infill walls are still used nowadays not only because of a legacy of the past. On the contrary, they evolved in order to provide many desirable features in modern constructions, especially for human leaving places. Among these properties are durability, reliability against fire and moisture, good performances in terms of thermal and acoustic insulation and low production and execution costs. Finally, masonry units used as external enclosure panels or veneers are very often considered architecturally pleasing (Fig. 1.2).

The widespread use of URM infill walls concerns, with different techniques and materials, both developed and developing countries, temperate and more extreme

climates, and relevantly for this research, both areas that are mostly exempt and susceptible to significant seismic events.

Fig. 1.1 Examples of typical usage of URM infill walls in residential RC frame structures. Showing a six storey condo in Bibione (VE), and low-rise family house under construction in Cusignana (TV).

Fig. 1.2 Architect Mario Botta: La Fortezza, Maastricht, 1991–1999 (left); Chiesa del Santo volto, Turin, 2008.

1.1.1 Terminology note: infilled frames and confined frames

A construction with the exterior appearance of a reinforced concrete frame and masonry infill walls can be classified in two different construction systems depending on the construction sequence. When the structural frame is constructed first and the masonry walls are added at a later stage, the system is classified as an infilled frame. In the opposite case, when the masonry walls are built in first place and the RC frame is cast afterwards, the system is known as “confined masonry”. Confined masonry is particularly diffused in South America and some Asia countries. More detailed description about confined masonry can be found in (Brzev 2007). In spite of similar appearance, the behaviour of these two constructions systems can be quite different, especially under horizontal loads. In this work only infilled frames were considered, even if in principles many modelling aspects could be incorporated even for confined masonry buildings.

1.2 Motivation

1.2.1 Effects of URM infill walls on the seismic behaviour of RC frame structures

Masonry infill walls can have contrasting effects on the seismic response of RC structures, with researchers identifying both positive and negative effects on the global behaviour, in some cases apparently conflicting. Many studies support that, with a regular distribution of the panels in the frame, infill walls provide a structure with extra stiffness and strength during an earthquake (Dolšek and Fajfar 2008), reduce the global displacement demand and increase the energy dissipation capacity (Ozkaynak et al. 2013). Based on these benefits, some researchers support the use of masonry infill walls as “alternative for seismic strengthening for low-rise reinforced concrete building structures” (Pujol et al. 2008). Conversely, other researchers have highlighted both the intrinsic deficiencies of URM infill walls even during minor earthquakes (G Michele Calvi, Bolognini, and Penna 2004) and their detrimental effects on the overall performance of the RC structures (Haldar, Singh, and Paul 2012), consisting of damage and even collapse of both the panels and the RC elements. Some researchers concluded that, when significant seismic action is to be expected, masonry infill walls should not be used unless they are specifically designed to work in conjunction with the frame to resist the lateral loads, or remain

isolated from the frame (Murty et al. 2006), both requirements that are very rarely fulfilled in current practice. In fact, masonry infill walls are frequently excluded from the computational models in contemporary design practice. There are two main reasons for this praxis: panels being considered non-structural elements and complexities related to their inclusion in the models.

1.2.2 URM infill walls in the seismic design of structures

The notion that URM infills are non-structural elements is common to most design guidelines. This allows designers to ignore the contribution of the infills to the strength of a building. Furthermore, as noted by Crowley and Pinho (2010), the contribution to stiffness, which instead should be taken in account, is in many cases ignored as well, because of the lack of practical modelling tools. Additionally, the verifications of non-structural elements such as infill walls, now demanded by modern design codes albeit still far from being harmonized between different guidelines (Kaushik, Rai, and Jain 2006), are based on simplified calculations that do not require the panels to be included as elements in the computational model of the structure. Infill walls are neglected in the design of RC infilled frame buildings also because of the inherent complexities of capturing the seismic response of this typology of buildings. Uncertainty in many of the input parameters of the structural models of infilled RC frames would require the designer to apply preliminary sensitivity analyses (Celarec, Ricci, and Dolšek 2012), which is impractical and expensive for the design of simple buildings. The uncertainties include the properties of the brittle materials (and particularly the URM components), the conditions at the interfaces between the infill walls and structural elements, the stiffness of the bare RC frame relative to that of the infill wall, the size and location of openings within the panels and the rapid degradation of the stiffness and strength of the infilled structure that follow cracking and failures of the URM infill walls (P. G. Asteris et al. 2013).

Despite the difficulty of modelling URM infill walls, neglecting them in the nonlinear analysis of building structures leads to considerable inaccuracy in predicting the lateral stiffness, strength, and ductility of the structures themselves (El-Dakhakhni et al. 2006). Indeed, it is now well recognized that during an earthquake infill walls can behave structurally (Fardis and Panagiotakos 1997; Luca et al. 2013). However, regardless of whether this behaviour is favourable or not, both old buildings, designed only for gravity-loads, and modern ones, in which the RC structure was engineered to resist lateral loads, were designed with little to no consideration of the interaction between masonry panels and the frame members. This contradiction emerged in

many recent earthquakes, where the infill walls have usually been the first elements to be damaged (Tasligedik, Pampanin, and Palermo 2011).

1.2.3 Performances of URM infill walls in recent past earthquakes

The performance of RC framed structures with masonry infill walls under seismic action has been frequently discussed following many past earthquakes: Northridge (1994) in the U.S.A. (Bruneau 1995), Kocaeli (1999) in Turkey (Dolšek and Fajfar 2001), Bhuj (2001) in India (Humar, Lau, and Pierre 2001), Lefkda (2003) (Karakostas et al. 2005) in Greece, L'Aquila (2009) (EERI 2009) in Italy. Images taken in post-earthquake scenario illustrate the vulnerability of infill walls to horizontal dynamic actions, as shown in Fig. 1.3, Fig. 1.4 and Fig. 1.5.

Fig. 1.3 Damage and collapse of infill walls in 1999 Turkey earthquakes. Left: August 17 Izmit (Kocaeli) earthquake. Image credit: NOAA National Geophysical Data Center. (NOAA 2007) Right: November 12 Düzce earthquake. Image credit: NOAA/NGDC, Roger Bilham, University of Colorado, Dept. of Geological Sciences.

Fig. 1.4 Damage to infill walls after 2003 Boumerdes and Algiers (Algeria). Image credit: NOAA/NGDC, Djillali Benour. University of Bab Ezzour, Algeria.

Fig. 1.5 Damage to clay blocks infill walls after 2009 L'Aquila earthquake, Italy. Left: Image from (Scott 2009). Right: Image from (Miyamoto 2013).

In many critical analyses, RC frames with URM panels have been identified as a source of the high economic losses and sometimes connected with the loss of human lives. Damage to this type of structures concerned both the structural RC members and the masonry walls, albeit with very different extents and frequency. In fact, RC elements have generally been less prone to failure and damage compared to the infill walls.

Several failure mechanisms have been observed in URM infill walls under earthquake action, including in-plane (IP) mechanisms and out-of-plane (OOP) collapse. The OOP collapse of masonry panels has been reported in many post-earthquake reconnaissance inspections. In spite of its relevance for earthquake engineering, there are fewer studies dedicated to OOP behaviour of masonry infill walls under seismic action compared to those regarding the IP behaviour, and only a subset has examined the interaction between the IP and the OOP responses of the walls. Particularly, very seldom is the OOP response incorporated in the numerous computational models used to simulate the walls.

1.2.4 Computational modelling of URM infill walls

Since the 1960s, with the aim of correctly simulating the response of structures with masonry infill walls, two main modelling approaches have emerged: macro-models and micro-models (Crisafulli, Carr, and Park 2000). Some researchers (Lourenço 1996) also distinguish between three or more approaches (e.g., detailed micro-modelling), which posses intermediate characteristics between the two aforementioned. Micro-models (P. G. Asteris et al. 2013), involve non-linear finite element modelling of the RC frame, the infill panels and the interface between the

frame and the wall. Even though this type of model can be most accurate, there are several drawbacks to their implementation and use, mainly related to their complexity and the associated computational time needed for the analyses. These features make them more suitable for research applications, rather than design and verification of the many walls typically present in real structures. Macro-models, on the other hand, are relatively simple analytical models that can simulate the overall wall force-deformation behaviour obtained from experimental results (Lam et al. 2003). Macro-models of URM infill walls require less computational power during analyses and are therefore more suitable to represent the global behaviour of structures, an aspect that has received less attention compared to experimental behaviour and modelling of individual infill panels (Fardis and Panagiotakos 1997). (P. Asteris et al. 2011) have presented a general review of analytical macro-models for the analysis of infilled frame structures since their conception, basically dividing them in two categories: single-strut models and multiple-strut models. In single-strut models, each panel is represented with an equivalent diagonal brace. In the most traditional form, it consists of a pin-jointed diagonal strut made of the same material and having the same thickness as the infill panel. Recently, a few macro-models for the three dimensional behaviour of URM infill walls have been developed and shown to be less computationally demanding compared to micro-models. However, very few studies have applied these models to the dynamic seismic response history analysis of realistic structures.

1.3 Objective and methodology of the research

The purpose of this research is to use a numerical model to characterize the seismic response of URM infill walls in realistic RC framed structures by monitoring the development of cracking and collapses induced by a combination of IP and OOP actions on the panels.

The first step is related to the study of the state of the art regarding the out-of-plane behaviour of URM infill walls and IP/OOP interaction, that provides the basis to add a new contribution to the research.

Subsequently, a framework for the computational modelling and analyses is created. In this study, a recently proposed macro-model for masonry infill walls and capable of capturing the interaction between the in-plane and the out-of-plane responses is used to represent URM infill panels in the computational models of infilled frames. The model is calibrated with already available experimental results related to two

types of clay masonry infill walls that are frequently found in Italian buildings, and that are also typical of other Mediterranean countries. The calibrated macro-elements are used in the numerical planar models of RC framed structures, with frame configurations representative of the Italian building stock (number of bays and stories, geometry of the members, materials) and considering both legacy and current design practices. These realistic infilled frames are analysed with a suite of bidirectional ground motions that are scaled to be compatible with Eurocode 8 elastic spectra.
The outputs of the analyses are focused around the response of the infill walls during and at the end of the seismic excitation. More specifically:

1) the IP and OOP forces and displacements of the infill walls are monitored during the time-histories to identify when cracking and collapse occur;
2) the level of damage of the panels in the frames at the end of the analyses is examined to assess which panels are most susceptible to damage.

1.4 Organization

The thesis is organized in 6 chapters, outlining the main steps of the research.

Chapter 2, serves as an overview of the scientific literature relevant to this study. To begin with, the experimental and analytical investigations concerning the out-of-plane behaviour of URM infill walls are presented. Next, the studies concerning the interaction between in-plane and out-of-plane responses of masonry walls are articulated. Of particular interest for the scope of this work are the experimental tests that demonstrated the role of interaction and the representation of the phenomena through interaction curves. The most relevant computational modelling proposals are also reported, focusing on the macro-modeling approaches.

Chapter 3 is dedicated to the specific analytical and computational model used in this research to represent the infill walls considering in-plane/out-of-plane interaction. A detailed description of the model is followed by a discussion of its limitations. Subsequently, the adaptations to the original formulation for the scope of this study are presented. Finally, the procedure used to calibrate the macro-model with experimental data from past experimental campaigns on two common types of clay masonry infill walls is explained.

Chapter 4 relates to the framework of the analyses performed in this study. First, a selection of RC frame buildings is performed considering representative structures of the Italian residential building stock. Then, the RC frame materials and configurations identified as the most common, as well as the infill walls previously calibrated, are incorporated into a set of eight infilled frame models. Lastly, a suite of bi-directional ground motions compatible with the European building code elastic spectrum is assembled to perform non-linear time-history analyses.

Chapter 5 reports the results of the dynamic time-history analyses, which are focused on the response of the infill walls during the seismic excitation at three different intensity levels. The outputs of the analyses are shown with two types of graphic outputs: force and displacement history path and colour maps of the damage sustained by the URM infills. The and frequency of cracked and collapsed walls is also discussed.

Chapter 6, serves as a summary of the study, its conclusions and presents recommendations for future research work.

2 LITERATURE OVERVIEW

2.1 Damage and out-of-plane-collapses of URM infill walls in past earthquakes

Even when a seismic event has a relatively low intensity, the most frequent type of damage that affects RC infilled buildings involves the infill masonry walls (Decanini et al. 2004). The lower stories are often the most affected by infill wall damage (Dolšek and Fajfar 2001), which is reasonable because the highest inter-storey drifts are usually located at the bottom of the building.

In particular, at early stages of a seismic event URM infill walls can detach from the surrounding frame following the IP displacement demand dictated by the frame structure. Unfortunately, the boundary condition between the panels and the surrounding RC frame has long been recognized (West 1973) as one of the paramount parameters that govern the OOP strength of the walls. Once the condition of the connections between the panels and the surrounding frame is compromised, their resistance to OOP loads is significantly reduced. In particular, the component of the seismic excitation acting orthogonally to the panels can lead to brittle failure of the URM infills, also referred as “expulsion” or “overturning” of the walls. This type of failure was widely reported in many damage surveys after the 2009 Abruzzo earthquake in Italy (Braga et al. 2010; Liel and Lynch 2009; Vicente et al. 2010), as shown in Fig. 2.1. URM infill walls are particularly vulnerable to this type of failure, at the point that an on-going research branch is dedicated to the development and application of enhanced construction techniques that can reduce this issue (El-Dakhakhni et al. 2006; Tasligedik, Pampanin, and Palermo 2011; Preti, Bettini, and Plizzari 2012).

Ultimately, OOP failures of URM infill walls in RC frames lead to disproportionate damage to properties, injures or even casualties. As discussed, panel expulsion often arises from a combination of IP and OOP actions on URM infill walls. However, there are the far less studies dedicated to OOP behaviour of masonry infill walls under seismic action, compared to those regarding the in-plane behaviour, and even less take into account the interaction between the IP and the OOP responses of the walls.

Fig. 2.1 Out-of-plane collapses of masonry infill walls. Image from (Braga et al. 2010). Note that the most damaged panels are typically localized at the lower stories, albeit not necessarily at the first storey.

2.2 Out-of-plane behaviour of URM infill walls

The external actions on an infilled frame (Fig. 2.2) can be subdivided between vertical forces (among which gravity loads represent the major contributors), and horizontal forces. Vertical loads seldom cause the failure of the infilled frame because masonry is able to resist relatively high compressive stresses and the sections of masonry units are usually big enough to limit the pressure.

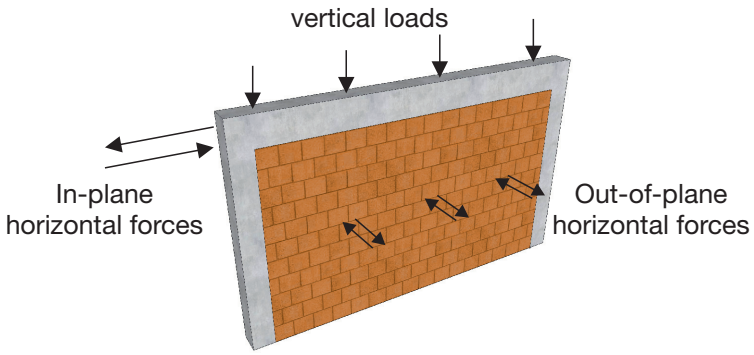

Fig. 2.2 Actions on an infilled frame.

As far as the response to horizontal actions is concerned, the most notable effect of the presence of URM infill walls in a frame structure is the vast increase of its stiffness along the direction parallel to the panels, and therefore the great majority of the studies on masonry infill walls concentrated on the response to actions in the same geometrical plane as the panel, the so called in-plane (IP) direction. However, in general each panel is subjected to forces both parallel and perpendicular to the geometrical plane of the wall. During a ground motion, for example, inertia forces acting orthogonally to the wall, in the so called out-of-plane (OOP) direction, are also present, and they are transferred across the panels to the surrounding frame system. The OOP response of masonry infill panels has been studied both analytically and through experimental tests, albeit with fewer efforts compared to those dedicated to the IP behaviour (Hashemi and Mosalam 2007). As a first step of this work, the most relevant findings and valuable information on the OOP behaviour of infilled frames has been obtained from research performed and published in the last decades.

2.2.1 Experimental studies

Three techniques have been used for the experimental tests on the out-of-plane behavior of URM infill walls.

First, many of the early studies were concerned with the effect of blast loading on masonry walls, therefore panels were subjected to sudden air pressure waves in a wind tunnels or with detonations (Monk 1958; Gabrielsen and Kaplan 1977). In the last years, there has been a renewed interest in the experimental works that involved the out-of-plane response of unreinforced concrete block walls under blast loading (Abou-Zeid et al. 2011; Abou-Zeid et al. 2014).

Second, another type of tests consisted in the application of uniform or concentrated loads perpendicular to the walls with airbags or hydraulic actuators (West 1973; Anderson 1984; Drysdale and Essawy 1988; Dawe and Seah 1989; Hill 1994). The airbag technique continues to be used nowadays (Akhoundi, et al. 2015).

Third, in recent times, experimental tests have been performed with shake table setups, by applying accelerations in the out-of-plane direction of the infill panel (Bennett, Fowler, and Flanagan 1996; Dafnis, Kolsch, and Reimerdes 2002; Klingner et al. 1996; Žarnić et al. 2001; Tu et al. 2010).

Most of the tests were performed on one-bay and one storey full scale specimens, however scaled models have also been used especially for shaking table tests, due to financial and practical restrictions of the test setups. Several findings gathered a strong consensus among the researchers and are herein summarized.

- Compared to cantilevered walls, masonry infill walls that are tightly fitted between the frame supports, or separated from one support only by a small gap, can reach very high resistance to out-of-plane actions.
- The improved load-bearing capacity, or rather stability, results from the development of an “arching action” within the walls.
- Application of repetitive loadings within the elastic region does not affect the stiffness of the specimen.
- Prior to first major cracking, the main OOP resisting mechanism for infilled panels is by flexural action, while in the post-cracking range it is by “arching” action.
- Under seismic excitation, infill panels separate from their bounding frame, and respond at their own natural frequency.
- The OOP strength greatly depends on the slenderness ratio of the panel.
- A major parameter that influence the OOP strength is the condition of boundaries between the infill and the surrounding frame; in particular, the presence or formation of gaps at the upper interface between infill and frame can decrease significantly the ultimate OOP force the wall is able to withstand.
- In particular, when infill panels become separated from their boundary frames, they are more likely to collapse due to the out-of-plane inertial force caused by their self-weight.
- Ultimate OOP loads increase with increasing panel thickness, but decrease with increasing panel length and height.
- Relatively small central openings in the infills do not reduce significantly the OOP strength.

The experimental observations were incorporated in many analytical models to describe the OOP behavior of URM infill panels.

2.2.2 Analytical models

The first and most immediate approach to represent the OOP behavior of the infill panels is the application of the elastic-plate analysis (Timoshenko and Woinowsky-Krieger 1959). Linearly elastic, isotropic, homogeneous material behavior is assumed in this theory. To evaluate the bending moments and associated rotations of the panels, the elastic plate method uses analytically or numerically calculated bending moment coefficients that depend on shapes and restraints of the walls. A limitation of this method is related to the fact that, because a masonry wall is an orthotropic plate,

the ratio of the wall strengths in the two planar directions will be equal to the ratio of bending moments only for a specific geometric aspect ratio. Additionally, the response of any masonry material can be approximated with elastic formulation only for low levels of loadings (Haseltine, West, and Tutt 1977).

Later, the yield line approach, originally developed to be used for reinforced concrete plates, was incorporated into various proposals to predict the OOP of masonry walls. It allows for different strengths on two orthogonal directions, thus reproducing the orthotropic nature of masonry walls. However, the yield line approach assumes that a pattern of yield lines develops with constant moment along each line until failure occurs, which is valid for ductile RC plates but not for brittle masonry panels. This could lead to slightly unconservative estimates of the OOP maximum strength if true yield line behaviour is assumed (Drysdale and Essawy 1988).

Both the elastic-plate analysis and yield line approaches are however affected by the basic assumption that infill walls response is governed by the tensile strength of masonry. This hypothesis is practically valid up to cracking of masonry. However, early tests (Thomas 1953) had already showed that masonry tensile strength reached with walls bending could not explain alone the lateral capacity of the panels beyond first cracking: the panels developed very high resistance to out-of-plane pressure as a result of “arching” effects in the wall (Hendry 1973). When arching is considered, the OOP strength of URM infill wall is governed by masonry compressive strength.

The first analytical models based on arching action considered one-way spanning unreinforced masonry walls (McDowell, McKee, and Sevin 1956). The “one-way” term refers to the ability of the wall to form an arch in one of the two planar directions. Anderson (1984) proposed a theory for horizontal arching walls, which confirmed that infills that develop arching action within their thickness can have a resistance to transverse lateral loading significantly in higher of their strength evaluated as flexural panels, even if fixed edges are assumed. However, he also recommended to account for the extra-strength achieved trough arching only when conditions of the wall/frame system are known and will not be subjected to alterations, particularly in the factors that affect the connection between the wall and the surrounding frame members.

In later works, formulations for arching action were advanced also for two-way spanning panels.

Dawe and Seah (1989) proposed a method based on an empirical relationship to determine cracking and ultimate capacity of a two-way spanning masonry infilled panel confined within a flexible steel frame. They used an elastic finite element analysis for bending of thick plates to predict first cracking strength, and a yield-line technique modified to account for the arching action to estimate the ultimate load.

Angel et al. (1994) suggested analytical method based on arching action in which the infill panel spans between two rigid supports (i.e. fully restrained against translation and rotation.) They observed that, if panels belong to adjacent bays or stories, then by continuity, rotations at boundaries may be considered to be fully restrained. Additionally, they distinguished between two different types of failure modes: the first being crushing along the edges for panels with a low slenderness *(h/t)* ratio, and the other being snap through for panels with large *h/t* ratios (see Fig. 2.3 for notation). They derived an expression for the critical wall slenderness ratio that differentiate between these two failure modes. The model was found to be in good agreement with experimental tests, estimating accurately both the initial stiffness and the maximum strength. Later, this model was adopted by the FEMA-273 guidelines (FEMA 1997), albeit with a correction factor to define lower-bound strength equation and not a mean strength equation. Angel et al. (1994) study will be recalled in section 2.3, related to the combination of IP and OOP actions on infill walls.

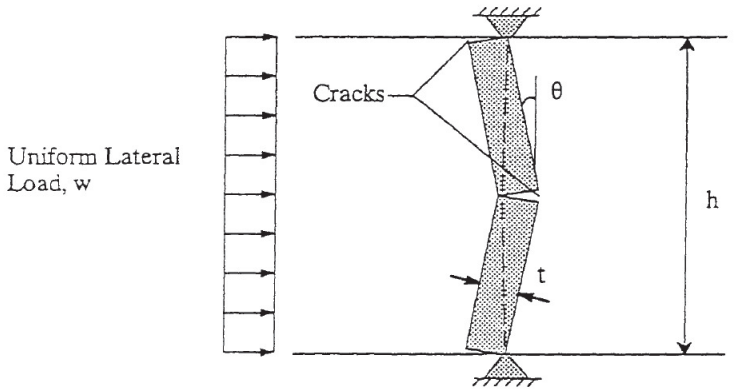

Fig. 2.3 Angel et al. (1994) analytical model for arching action. The infill panel is idealized as a strip of unit width, height h *and thickness* t.

Klingner et al. (1996) proposed another analytical model based on two-way arching action. In their expressions the orthotropic nature of the infill wall is explicitly accounted.

Flanagan and Bennet (1999a) performed a comparison between the analytical models proposed by Dawe and Seah (1989), Angel et al. (1994) and Klingner et al. (1996). They compared the results of the analytical expressions to the experimental results from 36 tests reported in the literature. They found that, based on both the mean and coefficient of variation with respect to experimental tests, Dawe and Seah's method provided the best prediction of uniform out-of-plane capacity of masonry infill

walls due to arching. Noting that this method was also affected by a systematic error which could consistently overestimate the capacity, they proposed a minor correction factor to the original expression. Finally, they also observed that the empirical relationship proposed by Dawe and Seah was the most adaptable to a one-way arching panel, which could develop instead of the two-way arching, if there is a gap at the top of the panel.

More recently, a semi-empirical relationship for predicting out-of-plane resistance of masonry infills due to one-way arching action was advanced by Moghaddam and Goudarzi (2010). Their expression considers the influence of the boundary frame stiffness, the masonry modulus of elasticity and the infill slenderness ratio on the transverse strength. Similarly to the Angel et al. (1994) proposal, they distinguished between two distinct failure modes, boundary crushing and transverse instability.

2.3 In-plane / Out-of-plane interaction in infill wall behaviour

As discussed previously and observed by Maheri and Najafgholipour (2012), most of studies have focused on the in-plane response of masonry walls. Nonetheless, as shown in 2.2, a still substantial number of studies focused on the response of infills under out-of-plane loads, with substantial convergences in the results of both experimental studies and analytical proposals. However, studies on the response of infill panels undergoing a combination of in-plane and out-of-plane loadings have been fewer.

To begin with, it should be noted that, in the field of URM infill walls, the word “combination” of IP and OOP loading (or equivalent expressions, such as “interaction”) has been used by researchers to describe two different phenomena.

1) The first is the modification (usually degradation) of the properties and the response in one of the wall’s planes caused by previously accumulated damage in the orthogonal direction.
2) The second involves the simultaneous loading of infill panels in both the IP and OOP directions.

The two phenomena are distinct, and both can occur during the real seismic loading of a URM infill wall (i.e. an already damaged panel can be subjected to simultaneous IP and OOP loading). However, most of studies considered one of these interaction processes at a time. The following review of published studies on IP/OOP interaction in URM infill walls will be subdivided based on the specific kind of combination phenomena: 2.3.1 will present the works that investigated the effect of previous

damage, while 2.3.2 will concern the studies dealing with simultaneous IP/OOP loading and 2.3.3 will deal with the representation of simultaneous IP/OOP loads with interaction curves.

2.3.1 IP/OOP interaction caused by previous damage

The effect of OOP damage on IP strength of masonry was investigated with experimental tests on URM full-scale infilled steel frames by Henderson et. al (1993). Initially, they loaded the bare frame in order to determine the behavior and stiffness contribution of the frame only. Subsequently, they performed an OOP test of the infilled frame with quasi-static actuators, followed by IP loading up to failure of the structure. They then tested a second, identically constructed infilled frame by loading it only IP, up to failure. In this way, they could compare the IP behavior of the URM infill with and without prior OOP damage. With the results from tests, they concluded that prior OOP damage to the infill reduces the IP initial stiffness, but has limited effect on the IP strength of the wall, which did not deteriorate significantly even after significant cracking in the masonry. They also noted that the IP response of an already damaged wall is notably less brittle than that of an already damaged panel, which develop a sudden diagonal crack. These results were later confirmed in other similar tests (Henderson et al. 2003; Henderson et al. 2006).
Likewise, researchers have studied the complementary situation with experimental campaigns, that is, the OOP behaviour of infills affected by damage caused by previous IP loading (Abrams, Angel, and Uzarski 1993; Angel et al. 1994). These tests comprised full-scale one-storey single-bay specimens of RC frames with infills walls built with both clay bricks and concrete blocks. The specimens were firstly loaded in-plane up to twice the cracking drift, and successively tested out-of-plane by applying a monotonically increasing uniform load on the surface of panel with an airbag. In general, deterioration of the OOP strength resulting from IP damage was found more significant, but greatly dependant on the slenderness ratio (h/t) of the infill wall. Specifically, for infill walls with large slenderness ratios, which therefore could not develop significant arching action, the OOP strength was found to be reduced by a factor as high as two when compared to undamaged panels. In contrast, the influence of IP cracking on the OOP strengths for panels with smaller slenderness ratios were smaller in magnitude. Moreover, for all the walls the reduction in OOP strength was found to increase with the intensity of previously applied IP actions. In fact, for the walls that experienced limited levels of preliminary IP loading and thus maintained good boundary conditions between infill wall and RC frame, the

transverse strength of infill panels was found to be still significant, even though the panel cracked. Based on their observations, the authors concluded that OOP strength and stiffness of the cracked panels were overestimated by the existing analytical models. Therefore, they proposed a new analytical model based on arching action (see section 2.2.2) to evaluate the OOP capacity of virgin or previously damaged infill walls (Angel et al. 1994; Shapiro et al. 1994; Abrams, Angel, and Uzarski 1996).

More recently, Komaraneni, Rai, and Singhal (2011) investigated the effect of IP damage on their OOP behavior, with a series of tests on half-scaled clay brick masonry infill walls, using materials and construction techniques commonly used in India. The panels were subjected to a sequence of slow cyclic IP drifts followed by OOP simulated ground motions on a shake-table apparatus. The authors found reasonable correlation with previous studies. In one case, however, it was observed the infill failed at lower calculated inertial forces compared to the strength after cracking predicted by analytical models. This behaviour was linked to excessive OOP displacements experienced by the walls.

Pereira et al. (2011) performed a series of experimental test on infilled RC frames, comparing the traditional Portuguese construction technique with URM infill walls, to three different enhanced solutions that make use of reinforcements. The tests were carried out by applying IP cyclic load first and then cyclic OOP loads through airbags for slender panels and a rigid concentrated load transmitting system for the strongest wall tested. With reference to the interaction aspects of their findings, the authors noted that as a result of previous IP damage

- the failure mode loaded in the OOP direction of the panel changed due the substantially alteration of support conditions of the masonry.
- the panels resisted a lower out-of-plane load.

Specifically, since the top interface between the wall and the frame was compromised by the IP cycles, during the subsequent OOP cycles a large percentage of masonry units in the upper part of the panel collapsed, as the wall was expelled from the RC frame.

A similar experimental setup was used by da Porto et al. (2013) on one-bay, full scale reinforced concrete frames infilled with two types of masonry infill walls: the first was constructed with thick (300 mm) clay units, the second with thin (120 mm) clay units. Walls with vertical reinforcements and strengthen with a fibre reinforced plaster were also tested in a similar fashion. The OOP strength of the thick masonry infill walls was evaluated after the application of two levels of maximum IP drift achieved under previous cyclic tests, producing two distinct levels of damage in the infill walls. The panels showed high of OOP strength, due to the development of an arch mechanism,

even in the specimens that had attained significant values IP drift. On the contrary, thin masonry specimens developed greater OOP displacements that lead to premature failure, limiting the strength of the wall. Interestingly, the outcome for the thinner wall was the same even for the specimen with fibre reinforced plaster.

2.3.2 Interaction caused by simultaneous IP and OOP actions

Flanagan and Bennett (1999b) studied the interaction phenomena with a comprehensive series of experimental tests, which comprised

- IP lateral load test, carried out with an hydraulic actuator;
- OOP uniform lateral load test tests carried out with air bag pressure loading on panels with different thicknesses (100, 200 single wythe and 330 mm double wythe);
- sequential tests that considered either IP damage followed by OOP loading or OOP damage followed by IP loading;
- OOP drift tests, in which cyclic out-of-plane displacements imposed either at the top or at mid-height of the frame;
- a shake table test to evaluate OOP global (framed infill wall) and infill only frequencies of vibration;
- one combined IP and OOP test with simultaneous loadings.

The simultaneous IP/OOP test was performed through a sequence of loadings. First, progressively increasing IP cyclic forces were applied. Next, at certain points of the IP loading, the beam centerline displacement was fixed while OOP pressure cycles were applied with an air bag. The authors observed that, while the constant IP displacement was held, the IP force needed to maintain the displacement reduced with time and applied lateral pressure.

Most of the tests, and specifically the combined tests, were performed on fully-scaled walls built with structural 200mm thick clay tile units; all the tested panels were square aspect ratio, measuring 2240 mm in length and height.

Results for specimens affected by prior damage confirmed that the primary effect of sequential loading is a loss of stiffness, rather than a loss of strength, particularly at moderate levels of loading. More specifically:

- Prior OOP loadings was found to eliminate the diagonal cracking IP limit state, which resulted in a much less stiff response; however, little effect was observed on the corner crushing limit state.

- Prior IP loading resulted in higher deflections under uniform lateral loads. Some strength decrease was observed, but arching could still form, resulting in substantial capacity.

Instead, simultaneous loading did reduce significantly the lateral pressure capacity of the wall (Fig. 2.4). Nevertheless, the authors observed that the system overall remained stable and did not collapse. However, it should be noted that commonly infill walls have a length to height aspect ratio larger than one, and can be significantly larger than the panels tested by Flanagan and Bennet. As reported in 2.2.1, ultimate OOP loads has been found to decrease with increasing panel length and height.

The observed reduction in peak IP and OOP forces when the loads were applied simultaneously was linked to the concurrence of OOP loads producing thrust forces around the panel perimeter and IP loads producing strut forces along the diagonal, which created high vertical compression near the panel base and caused failure of the bottom course tiles.

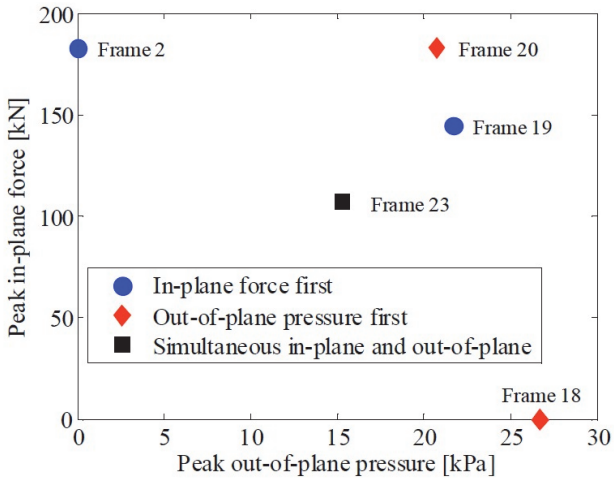

Fig. 2.4 Experimental results reported by Flanagan and Bennett (1999b) on bidirectional testing of clay tile infilled RC frames. Image taken from (Hashemi and Mosalam 2007).

2.3.3 Interaction curves

Hashemi and Mosalam (2007) studied the interaction due to simultaneous bidirectional loading on infill walls with finite element models. In a series of nonlinear static analyses, they were able to replicate the significant reduction of the wall capacity observed in Flanagan and Bennett (1999b) tests. They summarized the

results of the numerical study with an interaction diagram that showed the reduction of IP force capacity of the infilled RC frame for increasing levels of concurrent OOP force acting on the wall. The results they obtained for a specific configuration, geometry, and material properties of the infill are shown in Fig. 2.5.

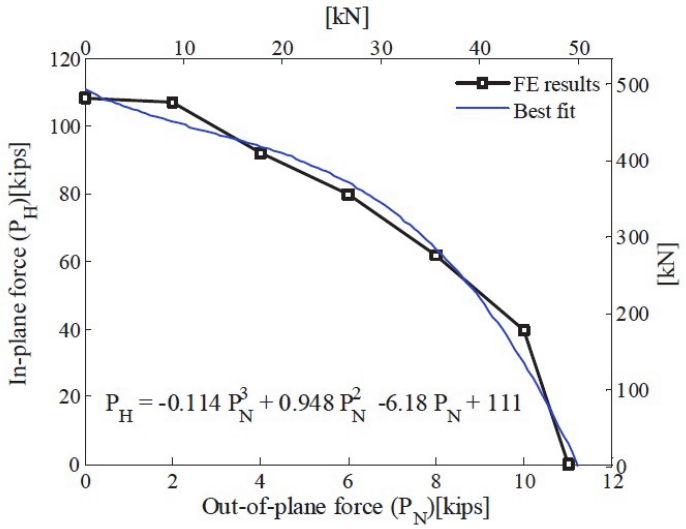

Fig. 2.5 Interaction diagram for URM infill wall obtained with FEM model. Image taken from (Hashemi and Mosalam 2007).

More recently, the interaction curve concepts was investigated more in depth, with both experimental and numerical tests on infill walls and it was also applied to simple URM walls (without frame) (Dolatshahi and Yekrangnia 2015).

Maheri and Najafgholipour (2012) and Maheri and Najafgholipour 2012; Najafgholipour, Maheri, and Lourenço (2013; 2014) carried out experimental investigations addressing capacity interaction in brick masonry infills between the IP shear and OOP bending responses of the walls. The interaction was noted to be particularly strong when one of the load types (IP shear or OOP bending) approaches to the corresponding ultimate capacity of the wall. Based on the experimental results, the authors proposed analytical methods for determining the interaction curves for URM infill walls. As shown in Fig. 2.6, the curves define the maximum combined IP/OOP actions that the infill walls can sustain in terms of simultaneously applied forces or displacements. Several parameters, including aspect ratio, elastic material properties and the inelastic material properties in tension, were found to influence the level of interaction and the shape of interaction curves.

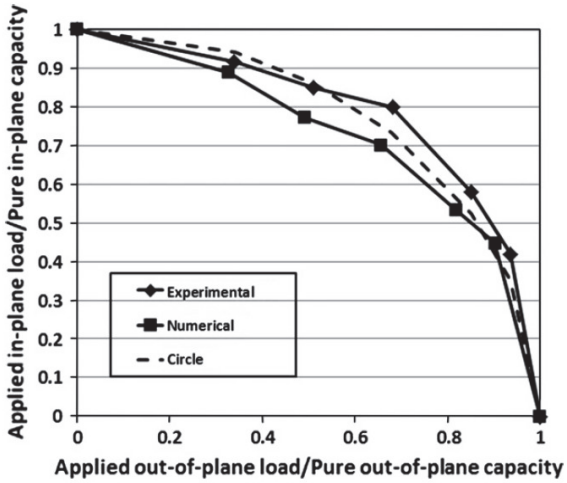

Fig. 2.6 Normalised in-plane/out-of-plane capacity interaction curves for the brick panel. Image taken from Najafgholipour, Maheri, and Lourenço (2013).

2.3.4 Computational models for in-plane/out-of-plane interaction

Recently, many micro-models based on finite element analysis and capable of considering interaction for URM infill walls are being proposed (Yuen and Kuang 2012; Yuen and Kuang 2013a; Yuen and Kuang 2013b; Mohyeddin, Goldsworthy, and Gad 2013a; Mohyeddin, Goldsworthy, and Gad 2013b; Kong, Zhai, and Liu 2015). The paper proposed by Kong et al., in particular, explicitly considers both types of "combined actions", i.e. previous damage and simultaneous loading and is also able to follow the collapse of the panels. In agreement with aforementioned studies, the authors found that peak IP and OOP capacities of the wall are affected markedly when loads are simultaneously applied, and were able to plot an interaction curve with the results from the analyses (Fig. 2.7).

However, the drawback of the micro-model approach is related to the complexity associated with the models and the analyses performed with them being quite computationally complex. In fact, their application is usually aimed to the representation of a single infill wall, especially to match experimental results accurately. In order to apply the interaction concept to structural models of buildings, simplified models are preferred, if not required.

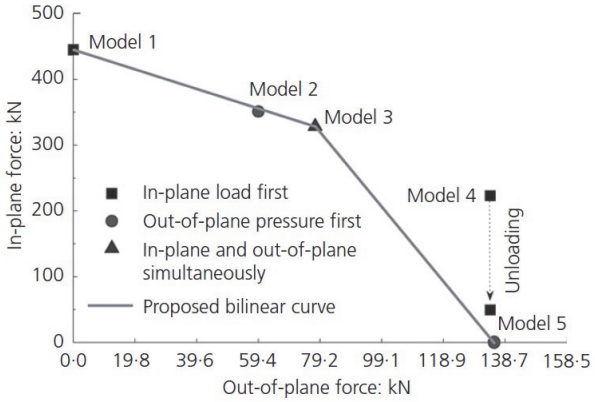

Fig. 2.7 Interaction between the IP and OOP forces by means of 3-dimensional finite element model. Image taken from Kong et. al (2015).

Hashemi and Mosalam (2007) included the IP/OOP interaction in a numerical macro-model based on two equivalent struts. Kadysiewski and Mosalam (2009) discussed this model and proposed a different approach with only one equivalent diagonal to overcome some of its limitations; their macro-model was then refined and implemented by Mosalam and Günay (2014) and will be described in Chapter 3.
Furtado et al. (2015) have recently advanced a similar macro-model expanding an existing two-diagonal infill wall model (Rodrigues, Varum, and Costa 2010).

3 COMPUTATIONAL MODEL

3.1 Overview

In this chapter the analytical and computational model for URM infill walls that has been used to perform analyses on realistic RC infilled frames will be described. The model was chosen because of its peculiar capabilities of considering the IP/OOP interaction that characterize the behaviour of URM infill walls and removing elements during the analysis.
Section 3.2 present a detailed description of the model proposal by Mosalam and Günay (2014) (MG hereafter), with particular emphasis on the in-plane/out-of-plane interaction. The MG model further develops some previous work by Kadysiewski and Mosalam (2009). The analytical model is also implemented (Günay and Mosalam 2010a) in the open source software framework OpenSees (McKenna, Fenves, and Scott 2000). Limitations of the model will be discussed as well.
Subsequently, section 3.3 will present the adaptations that were made to the original MG model for the scope of this study and explain the procedure used to calibrate the macro-model using experimental data from past experimental campaigns on two common types of clay masonry infill walls.

3.2 The Mosalam and Günay (2014) Model

In the MG proposal, infill walls are modelled with diagonal elements capable of simulating the IP/OOP interaction of the panels by following two bi-directional domains that govern the yielding/cracking criteria and the removal algorithm, respectively. In the macro-model (Fig. 3.1), each infill wall is represented with two elastic beam-column elements aligned along one diagonal and with hinges at the extremities. Both elements have a non-linear fibre section at their inner end (i.e. at the central node of the macro-element, where the equivalent mass of the wall is

lumped). At the outer extremities, where the macro-element connects to the RC frame, the hinges are elastic and rotations are left free.
In this section the MG model will be described and discussed more in-depth.

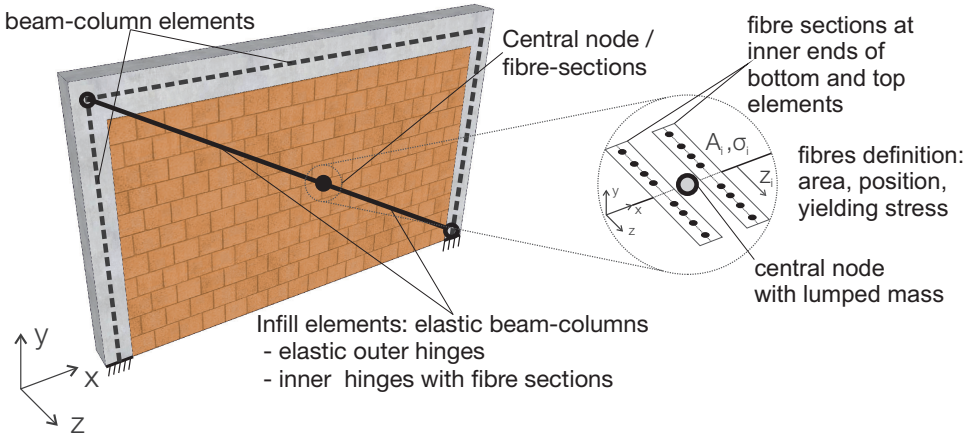

Fig. 3.1 Schematic representation of the MG model for infill walls with In-Plane/Out-of-Plane interaction.

3.2.1 Consideration of In-Plane / Out-of-plane interaction and infill wall removal

In Mosalam and Günay (2014), the authors state the two main objectives of their proposed model:

1) to consider the interaction between in-plane and out-of-plane responses of URM infill walls in a macro-model;
2) to consider the physical collapse of URM infill walls during an analysis by removing the corresponding element from the structural model.

A third modeling aspect, related to the shear failure of RC columns induced by infill walls, is also briefly presented, but it is out of the scope of this work and will not be discussed herein.
The main reason the MG model was adopted for this research is its almost unique capability to include IP/OOP interaction in URM infill walls in a macro-element suitable to perform analyses on computational building-scale macro-models. As noted in section 2.1, the OOP collapse of URM infill walls has been often reported after earthquakes. This type of failure, however, could arise from a combination of IP and OOP actions on the wall.

To justify this statement, assume that a ground motion has equally significant components with respect to the IP and OOP directions of the infill walls of a RC frame building. In most low and mid-rise RC frames infilled with masonry panels, the intensity of the seismic IP demand, which is related to interstorey drift, is highest on the ground stories and reduces along the height of the frame. Conversely, the OOP demand on the infill wall, which is proportional the accelerations applied to the panels, is lowest on the ground storey, and increases along the height of the building. If damage to the panels was governed only by IP action, infill walls at ground floor would almost always be the first to experience damage and, eventually, to collapse. However, results from multiple studies, many of which were reported in section 2.3, point that the behaviour of an URM infill wall is susceptible of interaction between IP and OOP responses, with stiffness and strength of the panel being reduced as a result of combined IP/OOP actions. The interaction is particularly strong when IP and OOP actions are applied simultaneously. Therefore, the effects of IP and OOP actions combined can potentially cause the seismic demand on the panels to be higher on storeys above the first. This kind of outcome has been witnessed after many recent earthquakes (see Fig. 2.1, Fig. 3.2). Additionally, regardless of the storey where infill walls are placed, cracking and failure of the panel will be anticipated by the interaction of forces acting on them.
For these reasons, the inclusion of IP/OOP interaction in computational models of URM infilled RC frames is a step forward and an interesting tool for seismic design of structures.

Fig. 3.2 Collapsed infill walls located at upper-storeys as a result of IP/OOP interaction in L'Aquila 2009 earthquake. Image from Günay and Mosalam (2010b).

The consideration of URM infill wall collapse during the analysis by applying a removal algorithm is the second major modelling aspect of the MG model. The URM panels can contribute significantly to the lateral stiffness and strength of the primary lateral force resisting system, to a degree dependent on the relative stiffness of the walls and the RC frame elements. Brittle failure of the infills at a storey can potentially

transform an originally regular building into a soft-storey building during earthquake excitation (see Fig. 3.3). When infill panels collapse as a result of wall failures, the global response of the structure is affected. Therefore, in order for the analysis to carry on rationally, the elements representing the wall in the computational models needs to reflect the new frame configuration. Since URM infill collapses consist in the physical disconnection and, often, disintegration of the walls themselves, removing the elements from the analysis domain is a coherent choice.

Fig. 3.3 Formation of soft storeys following URM infill wall collapses in 1999 İzmit (Kocaeli) earthquake, Turkey. Image taken from Sezen et. al (2000).

3.2.2 Description of the macro-element

The inertial and mechanical properties of the macro-element are assigned such as they match those of a suitable equivalent strut; in the original MG model, the FEMA 356 (FEMA, 2000) equivalent element is implemented. For the elastic outer hinges and elastic beam-column elements, this is obtained by simply assigning the calculated values of area, second moment of inertia, IP axial strength and OOP bending strength. Similarly, the fibres on the inner hinges, which are aligned along the OOP direction, are specifically modelled to match the same properties;

additionally, however, their area, position and strength are assigned to provide an interaction relationship between the IP and OOP forces.

The relationship proposed by Kadysiewski and Mosalam (2009), based on experimental data and numerical studies (Hashemi and Mosalam 2007), uses a 3/2 power law to link the ratio of the axial strengths of the wall with (P_{IP}) or without (P_{IP0}) OOP force acting on the wall to the ratio of bending strengths with (M_{OOP}) or without (M_{OOP0}) IP force action:

$$\left(\frac{P_{IP}}{P_{IP0}}\right)^{\frac{3}{2}}+\left(\frac{M_{OOP}}{M_{OOP0}}\right)^{\frac{3}{2}}=1 \tag{3.1}$$

The model is also capable of removing equivalent wall elements during the analysis if they reach a user defined envelop combination of IP and OOP displacements. In absence of more specific test data, Kadysiewski and Mosalam (2009) proposed to use the same 3/2 power law to relate IP and OOP displacements (Δ_{IP} and Δ_{OOP} respectively) to the IP and OOP ultimate displacements of the walls ($\Delta_{IP,u}$ and $\Delta_{OOP,u}$ respectively):

$$\left(\frac{\Delta_{IP}}{\Delta_{IP,u}}\right)^{\frac{3}{2}}+\left(\frac{\Delta_{OOP}}{\Delta_{OOP,u}}\right)^{\frac{3}{2}}=1 \tag{3.2}$$

When removal conditions are reached by a combination of simultaneous IP and OOP displacements of the wall, the equivalent elements, their nodes, the wall mass and associated loads are removed from the model; the analysis then continues on the updated model.

Equations (3.1) and (3.2) implicitly assume that the response of the infill wall is symmetric with respect to both IP and OOP behaviour. Therefore, the resulting interaction curves are also doubly symmetric, as shown in Fig. 3.4 and Fig. 3.5, for the force and displacement dimensionless domains respectively.

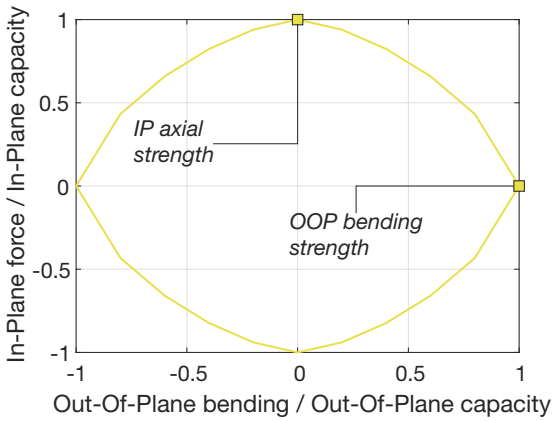

Fig. 3.4 Dimensionless IP Axial force / OOP Bending domain.

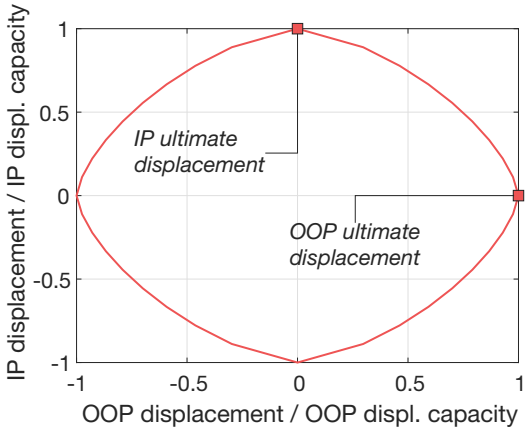

Fig. 3.5 Dimensionless IP / OOP displacement domain.

3.2.3 Model limitations

In general, the aim of infill wall macro-models is to investigate the response of the panels in the framework of the global analysis of the structure. The MG model, in particular, monitors the damage progression of the infill walls, albeit limited to two thresholds: cracking of the masonry and collapse. Therefore, this type of model is intrinsically unsuitable to capture specific types of failure or damage localization of the URM panels, which would involve complex phenomena, such as smeared cracking (Stavridis and Shing 2010), and require specific micro-models as those

named 2.3.4). As previously noted, however, at present macro-models are still the most viable computational tool to represent infill walls for the design of buildings.
A more specific limitation is the lack of consideration of the damage accumulated by the infill walls. In fact, the model accounts for simultaneous IP and OOP actions on the wall, but does not consider degradation of force and displacement capacities due to previous damage accumulated either in the IP or OOP direction. However, Flanagan and Bennett (1999b) have concluded that interaction is considerably less strong when loads (or displacements) are applied consecutively in the two orthogonal directions, that is, when it is due to previously accumulated damage, compared to simultaneous loading. It follows that the MG model is able to catch the main source of interaction between IP and OOP directions. Mosalam and Günay (2014) acknowledge this limitation, observing that it could be possible to define the fibre material to include damage, but given the negative stiffness exhibited by URM infill walls, this would also increase the numerical complexity.
Another shortcoming of the model is related to the representation of the wall with only one diagonal connecting opposite frame nodes. Single-strut or double diagonals models that connect opposite frame nodes are unable to give realistic distributions of bending moments and shear forces of the surrounding RC frame members. However, the focus of this work is on the infill walls response rather than on the frame members, and in this context the MG model is presently one of the very few that consider IP/OOP interaction.
Finally, in its basic formulation, the MG model does not account for openings in the infill walls. In general, the presence of openings decreases the additional stiffness and strength provided by the walls to the frames (Liauw 1979). According to (Mondal and Jain 2008), it is possible to account for the presence of an opening in the infill frames with correction factors applied to the strut-width of equivalent wall elements. The effect of the openings may be ignored if their area is lower than 5% of the area of the infill panel, whereas the infill contribution becomes irrelevant if the opening/panel area ratio exceeds 40%. With this type of modification, the effect of openings could be incorporated in the MG model, however, for the scopes of this work, frame spaces have been considered either fully infilled or without any contribution from the panels.

3.3 Calibration of the model

3.3.1 Adaptations to the original model

The analytical formulation of the MG model uses FEMA-356 (FEMA 2000) as a reference to evaluate design quantities related to the URM infill walls. Furthermore, as in a typical design scenario, material properties are assumed equal to their nominal values. In this work, the design quantities have been adjusted to Eurocode 6 (CEN 2006) where they differ from the American standard. The material properties, instead, were taken from experimental tests on infill wall specimens; the specimens will be described in the section dedicated to the calibration of the model. Hereafter the main differences between the MG model and the adapted one are summarized.
Eurocode 8 does not specify how to evaluate the width of the equivalent single strut element. Therefore, the formulation firstly proposed by Smith (1962; 1967) and currently recommended by the FEMA guidelines was used. These are the same expressions used in the original MG proposal, however here they are given in dimensionless form to avoid conversion between S.I. and U.S. standards. The parameter λ_h, representing the relative stiffness between the infill and the frame columns, and the ratio between the width w and the length r_w of the equivalent strut are defined with:

$$\lambda_h = h_c \cdot \sqrt[4]{\frac{E_m t_w \sin 2\theta}{4 E_c I_c h_w}} \tag{3.3}$$

$$w/r_w = 0.175 \lambda_h^{-0.4} \tag{3.4}$$

In Equations (3.3)-(3.4) E_m and E_c represent the masonry and concrete moduli of elasticity respectively, I_c and h_c the moment of inertia and height to the beam centrelines of the column, t_w, h_w and r_w the thickness and height and diagonal length of the infill wall and θ is the angle whose tangent is the infill height-to length aspect ratio.
The axial force capacity of the infill walls, P_{IP0}, which determines the shear strength of the panel at failure, is estimated in accordance to section 6.2 of Eurocode 6, “Unreinforced masonry walls subjected to shear loading”:

$$P_{IP0} = \frac{f_{vk}\, t_w l_c}{\gamma_M} \frac{1}{\cos(\theta)} \tag{3.5}$$

where f_{vk} is the characteristic masonry shear strength, t the wall thickness, l_c the compressed wall length, γ_M the material safety factor taken equal to 1, θ the angle between the beam and the horizontal direction. For the evaluation of the wall axial capacity, the compressed length of the wall l_c was assumed equal to the wall length l_w, thus assuming that no part of the wall that is in tension. This assumption is reasonable for URM infill walls, because there are no means for the frame to transmit tension forces to panel.

The out-of-plane capacity of the wall M_{OOP0} (Equation (3.6)) is extrapolated from the design lateral strength per unit area of wall, q_{lat}, evaluated as shown in Equation (3.7) (Eurocode 6, Section 6.3.2, "Walls arching between supports"):

$$M_{OOP0} = \frac{q_{lat} h_w^{\,2} l_w}{8} \tag{3.6}$$

$$q_{lat} = \frac{f_k}{\gamma_M} \left[\frac{t_w}{h_w} \right]^2 \tag{3.7}$$

where l_w represents the horizontal length of the infill wall, h_w the wall height and f_k the masonry characteristic compressive strength.

The removal displacement interaction criterion was implemented considering the power curve suggested by Mosalam and Günay (2014). Their approach represents a reasonable compromise in the light of the lacking of conclusive test results concerning the shape of the displacement domains for URM infill walls. In this work, however, the IP and OOP ultimate displacements are also derived from the experimental tests used for the calibration.

3.3.2 Calibration of the macro-element

Model calibration was performed on a 1 bay, 1 floor planar infilled frame, by comparing the numerical outputs to available experimental results obtained on two full scale infilled frames previously tested at University of Padova (PD) (da Porto et

al. 2013) and University of Pavia (PV) (Gian Michele Calvi and Bolognini 2001). The specimens and setups of the test setups were very similar; show the frame dimensions and experimental setup for IP and OOP loading as reported da Porto et. al. (2013).

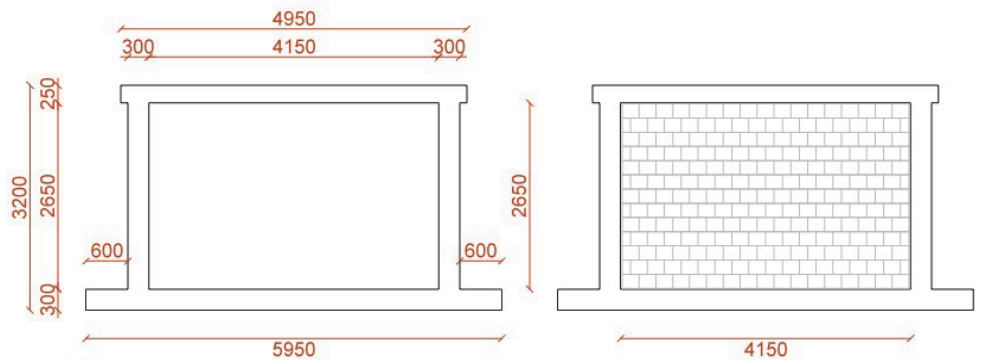

Fig. 3.6 Bare frame and infill wall dimensions tested by da Porto et al. (2013). The infill walls tested by Calvi and Bolognini (2001) were nearly identical. Image from da Porto et al. (2013).

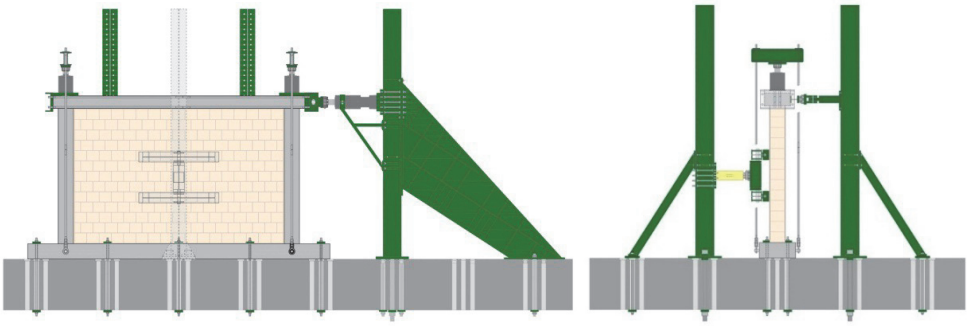

Fig. 3.7 Experimental setup for IP cyclic (left) and OOP monotonic loading used by da Porto et al. (2013). The setup is also representative of the tests described by Calvi and Bolognini (2001). Image from da Porto et al. (2013).

The experimental setups were tested in the IP direction by applying horizontal displacement cycles with increasing target drifts, and subsequently in the OOP direction by applying the load monotonically. The geometric dimensions, detailing and material properties of the two RC frames were almost identical, but the infill walls had significantly different thickness. Both panels were built with perforated clay units that are commonly found in Italy and other Mediterranean countries. The PV walls were representative of slender infill panels, which used to be a typical light enclosure system in the past and are still used as wythe for cavity walls. They were constructed

with masonry units measuring 245×245×115 mm in height, length and thickness respectively, with the holes placed horizontally. The PD URM panels were instead made of thicker clay units with vertical holes, designed to achieve some degree of anti-expulsion resistance even when unreinforced. The masonry units measure 195×240×300 mm (height, length, thickness), dimensions that are representative of URM blocks typologies currently adopted in newly designed infilled frames. The thickness of horizontal joints was about 10 mm for both the experimental setups. Table 3.1 summarizes the geometrical and mechanical properties of the walls that were used for the calibration, as reported in (da Porto et al. 2013) (PD test) and (Gian Michele Calvi and Bolognini 2001) (PV test). Data include the height, length and thickness of the URM infills (indicated with h_w , l_w , t_w respectively), the average modulus of elasticity measured between 10 and 40% of the strength and the average compression strength of the masonry. Both the modulus of elasticity and the compression strength of the masonry were reported both in the direction parallel ($E_{m,//}$, $f_{m,//}$) and perpendicular ($E_{m,\perp}$, $f_{m,\perp}$) to the masonry units holes.

Test	h_w (mm)	l_w (mm)	t_w (mm)	$E_{m,//}$ (MPa)	$E_{m,\perp}$ (MPa)	$f_{m,//}$ (MPa)	$f_{m,\perp}$ (MPa)
PV	2750	4200	115	5646	1873	3.97	1.10
PD	2650	4150	300	4312	1767	4.25	0.85

Table 3.1 Geometrical and mechanical properties from of the walls used to calibrate the MG macro-element.

Reinforced concrete frame members were modelled with force-based beam column elements with fibre section discretization (Neuenhofer and Filippou 1998). Both the beams and the columns were modelled in OpenSees with five integration points. A Kent-Scott-Park constitutive relationship (Kent and Park 1971) with added linear tension softening was used as the concrete material law. Mander's model (Mander, Priestley, and Park 1988) was adopted to evaluate different material parameters for plain and confined concrete. Steel fibres representing the longitudinal reinforcing bars were modelled, using a (Menegotto and Pinto 1973) model to capture elasto-plastic behaviour and strain-hardening.

The concrete and steel strengths of the PV and PD reinforced concrete frames are reported in Table 3.2. Both the nominal and experimental average values measured by means of standard material tests are reported because they were significantly different. In performing the calibration, the measured strengths were tried first, however better results were obtained using the concrete nominal strengths.

Test	Concrete f_c (MPa)		Steel f_y (MPa)	
	Nominal	Average	Nominal	Average
PV	25	29.3 columns 34.6 beams	500	562
PD	30	55.6	450	537

Table 3.2 Concrete and steel strengths of the experimental RC frames descripted in (Gian Michele Calvi and Bolognini 2001) (PV test) and (da Porto et al. 2013) (PD test).

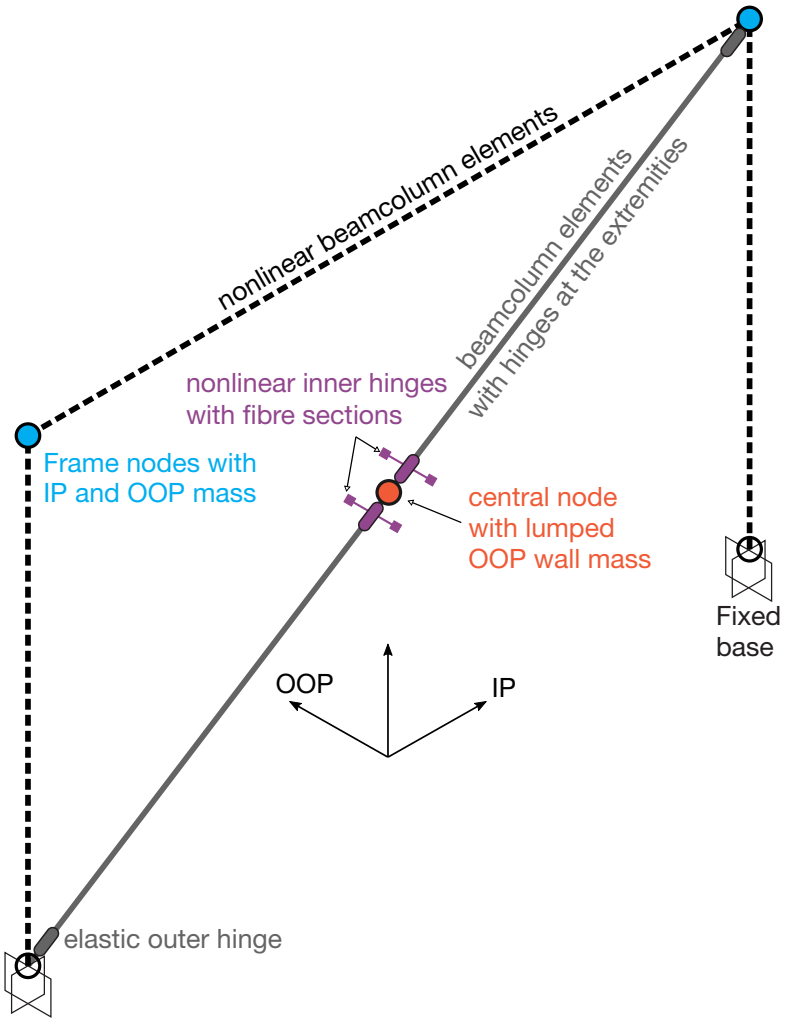

Fig. 3.8 Numerical model of the experimental frames used for the calibration of the infill wall elements.

Since, both the PD and PV experimental campaigns tested the frames with cyclic in-plane loading, the experimental IP pushover envelope was available for both the tests. A numerical model of the experimental frames was created in OpenSees, considering the dimensions and material properties indicated in Table 3.1 and Table 3.2 and tested with a nonlinear static pushover analysis in the IP plane direction. A comparison between the experimental data and the numerical analyses are shown in figures Fig. 3.9 and Fig. 3.10 for the PD and PV experimental frames respectively. The figures compare experimental and numerical data of the IP pushover curves obtained on the bare frame and the infilled frame; the infill contribution to the lateral force is also calculated as the difference between the curves of the infilled and bare frames.

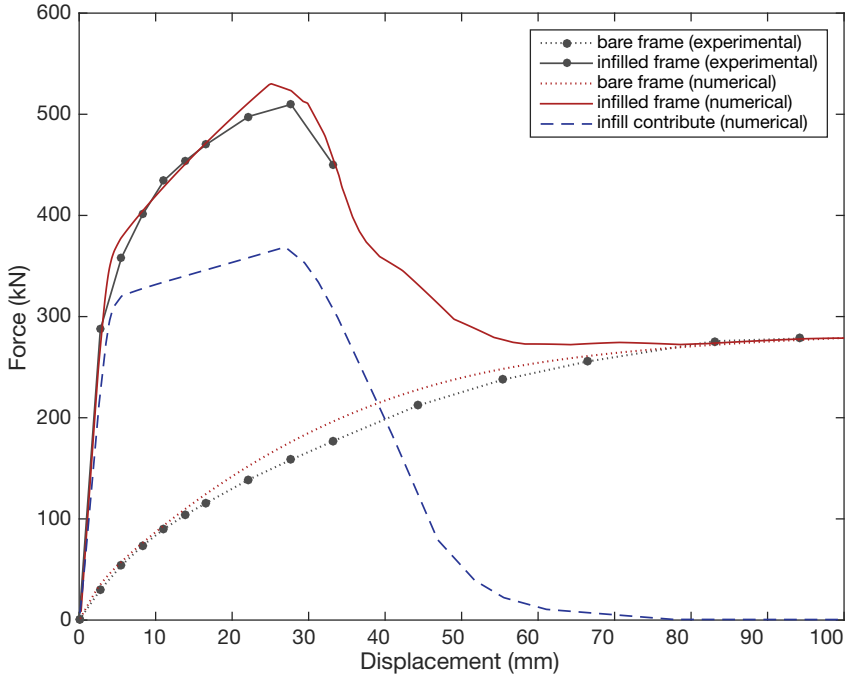

Fig. 3.9 Comparison between experimental (da Porto et al. 2013) and numerical pushover curves for the PD infilled frame.

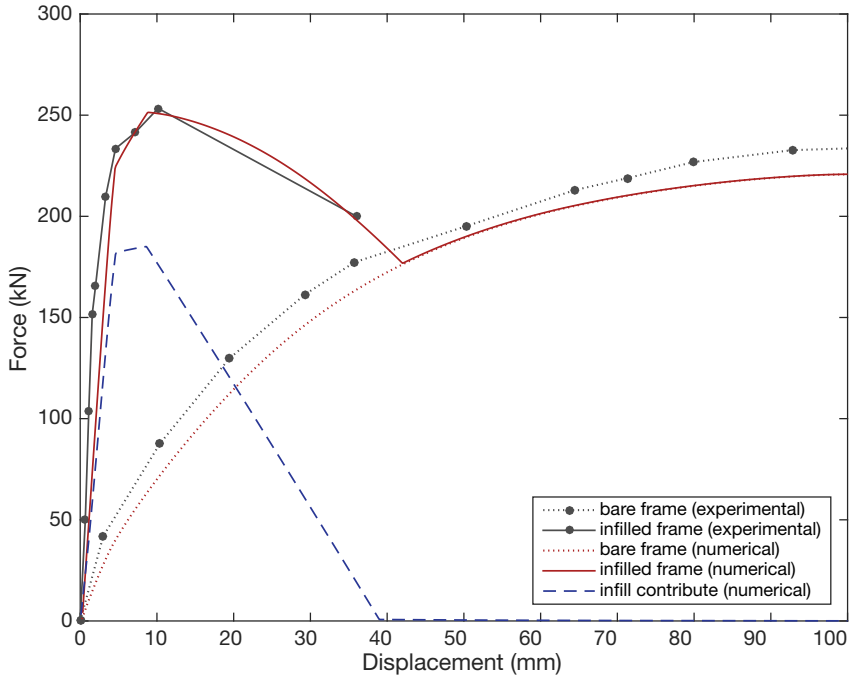

Fig. 3.10Comparison between experimental (Gian Michele Calvi and Bolognini 2001) and numerical pushover curves for the PV infilled frame.

4 ANALYSIS FRAMEWORK

4.1 Overview

This chapter illustrates the framework of the analyses performed for this research. The objectives of the framework are

1) to include the infill wall model capable of IP/OOP interaction into the computational model of realistic RC frames structures;
2) to apply the representative RC infilled frames to a set of nonlinear dynamic time-history analyses that can highlight the seismic performance of the URM infill walls when IP/OOP interaction is considered.

First, in 4.2, a selection of RC frame buildings is performed considering representative structures of the Italian residential building stock. Then, the RC frame materials and configurations identified as the most common, as well as the infill walls previously calibrated in 3.3, are incorporated into a set of eight infilled frame models. Lastly, a suite of bi-directional ground motions compatible with the European building code elastic spectrum is assembled to perform non-linear time-history analyses.

4.2 Planar frame models used in the analyses

4.2.1 Realistic infilled frames representative of Italian residential building stock

As remarked previously, there are a few existing macro-models that consider IP/OOP interaction of masonry infill walls. But there have not been extensive applications of these models to the dynamic analysis of realistic RC infilled frames. On the contrary, results have been shown only for single case-study applications. The primary objective of this work is to apply an infill wall model with IP/OOP interaction

capabilities to the computational models of RC frames with URM infill panels representative of common typologies of structures and analyze the models through dynamic analyses. The frame structures chosen are those representative of the current Italian residential building stock, comprising both existing buildings and buildings that could be realistically built according to current design codes. This class of structures is also representative of other Mediterranean countries that share similar building practices for geographical, cultural and regulatory reasons.

In Italy, residential buildings with five or less stories represent 95% of the total (De Sortis et al. 2007; Bramerini and Di Pasquale 2008); according to the last general census two- and three-stories residential buildings accounted for 73% of the total (ISTAT 2011). Even though these figures are based on the absolute values of buildings and thus accent the relative weight of lower-rise buildings (compared to figures based on construction volumes), they clearly show a predominance of low and mid-low rise buildings in the Italian building stock. Floor surface of residential building is also typically moderate, with sizes from 50 to 200 m^2 accounting for 90% of the total (De Sortis et al. 2007). Additionally, Italian residential building stock is relatively aged, especially considering that the first modern seismic-oriented design code became compulsory in 2003 (OPCM 3274 2003): considering only buildings with a reinforced-concrete structure, 67% were built before 1990, and 76% before 2001 (ISTAT 2011). Therefore, currently the majority of Italian RC residential buildings have not been designed with consideration of seismic action.

4.2.2 Computational models used in the analyses

Since most of the Italian residential building stock is composed of low- and mid-rise buildings, two planar frame configurations with three and five stories were used as analysis models (Fig. 4.1). Both configurations have three bays, with the wider external bays being infilled, and the smaller central one without any panel to represent a bay with a wide opening or a staircase. In the following discussion, the models will be designated with 3×3 and 5×3 labels for the configurations with three and five stories, respectively.

In addition, structural RC elements have been modelled to represent two design approaches: “traditional” (T) and “seismic” (S). The traditional design is representative of most of the existing structures, which were built only accounting for gravity loads. Conversely, the seismic approach is the one currently implemented in the Eurocode 8 (CEN 2013) and in the Italian National code (*D.M. 14.01.2008 ‘Nuove Norme Tecniche per le costruzioni’* 2008), with specific provisions for lateral loads,

ductility and displacement capacity of the elements. The RC frame elements were modelled consistently with the design approach, considering the typical sections of columns and beams for existing or newly designed frames structures. In the simplified beam-column modelling technique adopted for this work, the differences between the design approach were introduced in the fibre sections discretization and materials mechanical properties assigned to the element's sections. Table 4.1 summarizes the dimensions and detailing of the RC frame members.

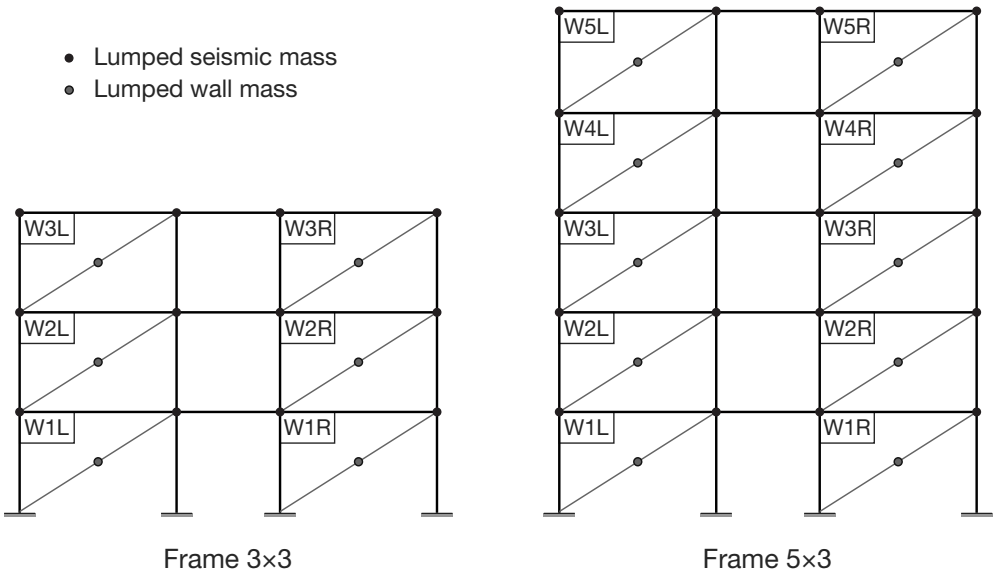

Fig. 4.1 Schematic representation of the infilled RC planar frames models used in the analyses: 3-storeys and 3-bays (3×3) frame (left) and 5-storeys and 3-bays (5×3) frame (right)

The frame models were also analysed with both types of infill panels that were previously calibrated, the "slender" 115 mm thick and the "robust" 300 mm thick. Hence, combining the two frame configurations (designated with 3×3 and 5×3), the two design approaches (labelled with "T" and "S") and two types of infill walls (designated with their thickness, 115 and 300), eight infilled frames models were analysed. Table 4.2 summarizes the labels that will be used to designate the models. The floor height, bay length and infill wall properties were taken close to those of the two calibrated one-bay-one-level laboratory frame because most Mediterranean countries have similar basic building practice rules for infill walls (Luca et al. 2013), so these models are expected to be representative of a wide variety of typical buildings.

Wall thickness	RC design	3 stories and 3 bays	5 stories and 3 bays
135 mm	Traditional	3×3_135T	5×3_135T
	Seismic	3×3_135S	5×3_135S
300 mm	Traditional	3×3_300T	5×3_300T
	Seismic	3×3_300S	5×3_300S

Table 4.2 Summary and designations of frame models.

In order to ensure that the models of the infilled frames had a realistic OOP stiffness, elastic springs with OOP stiffness were placed on the frame nodes where they would connect to beams in the OOP direction (Fig. 4.3). The stiffness values of these fictitious springs were calibrated for each model such that the elastic first period of vibration in the OOP direction was very close to the IP period of the in-filled frame, based on the assumption that the actual building would have a similar natural period in both directions.

Structural masses of the storeys are lumped at the nodes of each floor level. Mass and tangential stiffness proportional Rayleigh damping (5% of critical) is used, with constants calculated using the first- and third-mode periods. Infill walls are typically considered one of the major sources of viscous damping in a RC building; other significant contributes come from finishes, foundations and soil. (Deierlein, Reinhorn, and Willford (2010) recommend the use of less than 2.5% of critical damping (Chopra 2011) as viscous damping in tall buildings, where partition walls, cladding, and foundations contribute less to damping. Because infill walls have a significant effect on the RC frames analysed in this study, the typical viscous damping ratio of 5% was considered here.

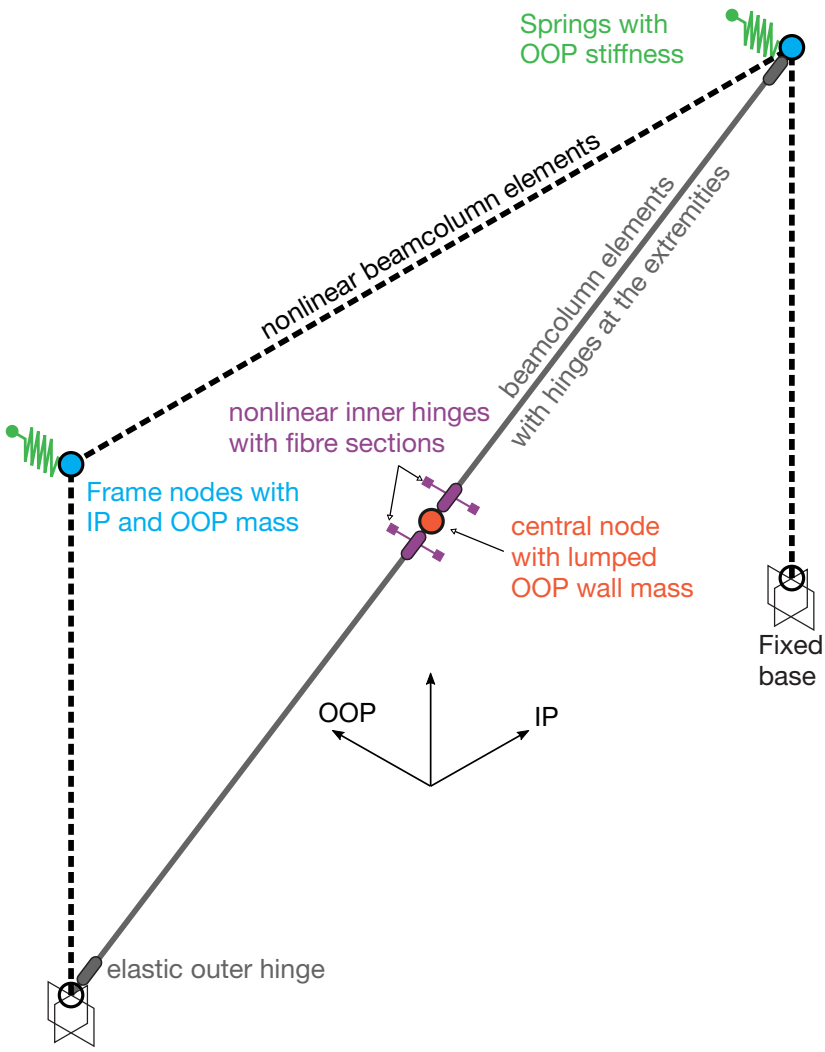

Fig. 4.3 Computational model with OOP elastic springs.

4.3 Definition of a suite of ground motions for bi-directional NLTH analysis

In order to apply simultaneous IP and OOP seismic actions to the models, a bidirectional loading input is required. Specifically, in the case of dynamic time-history analysis, at least the two horizontal ground-motion components should be applied to the model, as the same accelerogram may not be used simultaneously along both horizontal directions. The general problem of selection and scaling of real records for bi-directional analysis of structures has already received numerous contributions

(e.g. Baker and Cornell 2006a; Baker and Cornell 2006b; Beyer and Bommer 2006; Hong and Goda 2007; Grant 2011; Shahi and Baker 2013). Nonetheless, there is not yet consensus about a specific methodology for such task, and existing differences between design codes regulations reflect the openness on this issue (Beyer and Bommer 2007; Stewart et al. 2011). An in-depth analysis for the selection of bi-directional ground-motions is out of the scope of this work; commonly accepted rules were used in order to assemble a suite of bi-directional acceleration time histories. (Iervolino, Maddaloni, and Cosenza 2008; Iervolino, Galasso, and Cosenza 2009; Iervolino et al. 2011) described a comprehensive framework and provided the tools to build sets of natural records for seismic analysis of structures. Among others, (Hak et al. 2012; Hak, Morandi, and Megenes 2013), used this approach to perform dynamic seismic analysis of URM infilled frames, albeit focusing on the in-plane behaviour of the panels and hence selecting sets of one-component records. The same methodology has been used in this work as the basis to build sets of scaled bi-directional acceleration histories derived from real ground motions recordings.

4.3.1 Suite of bi-directional ground motions

Eurocode 8 (CEN 2013) (EC8 hereafter) Type 1 elastic spectra for soil type B (i.e. ground types with shear wave velocity v_s,30 between 360 and 800 m/s) and 5% viscous damping were chosen as targets for the spectra of the ground motion sets. Specifically, the EC8 spectrum was scaled to three intensity levels, namely $a_g S$ = 0.15g·S, 0.25g·S and 0.35g·S, where a_g is the ground acceleration on type A ground (e.g. rock or other rock-like geological formation) and S = 1.20 is the soil factor for Type 1 spectrum and ground type B.

Acceleration time histories and their elastic spectrum were taken from the European Strong-Motion database (ESM working group 2015), which comprises historical ground-motion data recorded in the European-Mediterranean and the middle-East regions. The ESM database provides both the raw (unprocessed) records and processed records; in this work the processed time-histories have been used. All the records that were selected for the assembled suite had been processed in the same batch and details about the procedures applied to the raw data can be found in Paolucci et al. (2011). The sampling interval of the natural records is 0.005 seconds and the same time step has been used for the nonlinear time-history analyses. The database was first filtered to select records that were recorded on sites with a shear velocity within the range of ground type B, with an epicentral distance smaller than 50 km and from earthquakes with moment magnitude M_w > 5.5. This pool of pre-

filtered records was then used to build a suite of 20 records: 2 orthogonal horizontal components, from 10 events, such that the average spectrum of the resulting scaled set was consistent with each EC8 target spectra. According to EC8 3.2.3.1.2 (4), the suite must meet three criteria:

1) a minimum of 3 accelerograms should be used;
2) the mean of the zero period spectral response acceleration values (calculated from the individual time histories) should not be smaller than the value of $a_g \cdot S$ for the site in question;
3) in the range of periods between $0{,}2T_1$ and $2T_1$, where T_1 is the fundamental period of the structure in the direction where the accelerogram will be applied; no value of the mean 5% damping elastic spectrum, calculated from all time histories, should be less than 90% of the corresponding value of the 5% damping elastic response spectrum.

Additionally, in the final suite, no more than two records were allowed for any seismic event (i.e. the two horizontal time-histories streams recorded at a particular station, labelled D1 and D2) in order to avoid very similar acceleration histories.

Table 4.3 present a summarises of the selected 20 records (the 10 events EQ01-EQ10, times two directions D1 and D2), with their general information from the ESM database, including magnitude, type of fault mechanism, and epicentral distance, stream channel of the record, and corrected peak ground acceleration (PGA). The ground motions are shown in Fig. 4.4-Fig. 4.6 scaled at $a_g S = 0.15g \cdot S$, $0.25g \cdot S$ and $0.35g \cdot S$ respectively, mean spectra of the suite and the reference EC8 elastic spectra. Fig. 4.7 compares the three average spectra and the target EC8 elastic spectra.

Suite ID	Event ID	Date	Station Code	M_W	Style of faulting	R epi. (km)	Stream	PGA (cm/s^2)	Scale factor for $a_g \cdot S$ =		
									0.15g·S	0.25g·S	0.35g·S
EQ01-D1	IT-1976-0030	15/09/1976	SRC0	6.0	TF	15.8	HNE	-244.9	0.79	1.32	1.85
EQ01-D2	IT-1976-0030	15/09/1976	SRC0	6.0	TF	15.8	HNN	-128.5	1.51	2.52	3.53
EQ02-D1	IS-2000-0053	21/06/2000	109	6.4	SS	18.5	HN2	426.5	0.45	0.76	1.06
EQ02-D2	IS-2000-0053	21/06/2000	109	6.4	SS	18.5	HN3	688.9	0.28	0.47	0.65
EQ03-D1	ME-1979-0012	24/05/1979	BUD	6.2	TF	8.3	HNE	-260.8	0.74	1.24	1.74
EQ03-D2	ME-1979-0012	24/05/1979	BUD	6.2	TF	8.3	HNN	-116.2	1.67	2.79	3.90
EQ04-D1	ME-1979-0003	15/04/1979	ULO	6.9	TF	22.0	HNE	232.3	0.84	1.39	1.95
EQ04-D2	ME-1979-0003	15/04/1979	ULO	6.9	TF	22.0	HNN	277.0	0.70	1.16	1.63
EQ05-D1	IR-1990-0004	20/06/1990	A6211	7.4	SS	34.4	HN2	573.1	0.34	0.56	0.79
EQ05-D2	IR-1990-0004	20/06/1990	A6211	7.4	SS	34.4	HN3	-504.1	0.38	0.64	0.90
EQ06-D1	IT-2009-0009	06/04/2009	AQK	6.1	NF	1.8	HNE	323.7	0.59	0.99	1.39
EQ06-D2	IT-2009-0009	06/04/2009	AQK	6.1	NF	1.8	HNN	-346.8	0.56	0.93	1.30
EQ07-D1	IT-1980-0012	23/11/1980	STR	6.9	NF	33.3	HNE	309.7	0.63	1.04	1.46
EQ07-D2	IT-1980-0012	23/11/1980	STR	6.9	NF	33.3	HNN	-220.9	0.88	1.46	2.05
EQ08-D1	IT-1976-0002	06/05/1976	TLM1	6.4	TF	23.4	HNE	-309.0	0.63	1.05	1.47
EQ08-D2	IT-1976-0002	06/05/1976	TLM1	6.4	TF	23.4	HNN	339.0	0.57	0.95	1.33
EQ09-D1	TK-1999-0077	17/08/1999	4106	7.4	SS	42.8	HNE	-143.6	1.35	2.25	3.15
EQ09-D2	TK-1999-0077	17/08/1999	4106	7.4	SS	42.8	HNN	255.5	0.76	1.27	1.77
EQ10-D1	TK-1999-0415	12/11/1999	9902	7.0	SS	26.5	HNE	121.0	1.61	2.68	3.75
EQ10-D2	TK-1999-0415	12/11/1999	9902	7.0	SS	26.5	HNN	-156.9	1.24	2.06	2.89

Table 4.3 Suite of ground motions. Mw = Moment magnitude. Style of faulting: TF = Thrust faulting; SS = Strike-slip faulting; NF = Normal faulting. R epi = Epicentral distance.

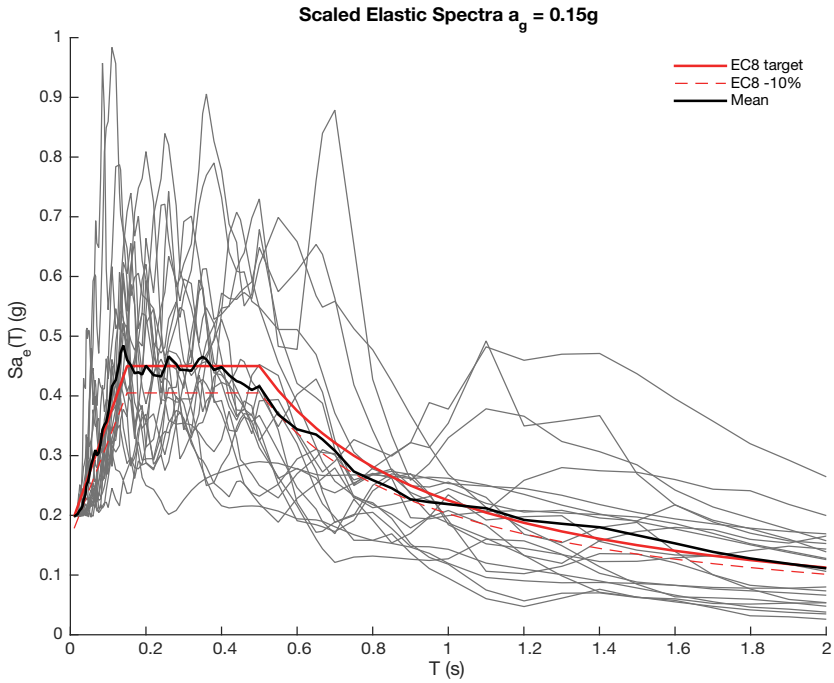

Fig. 4.4 The suite of ground motion record scaled to a_g S = 0.15g·S

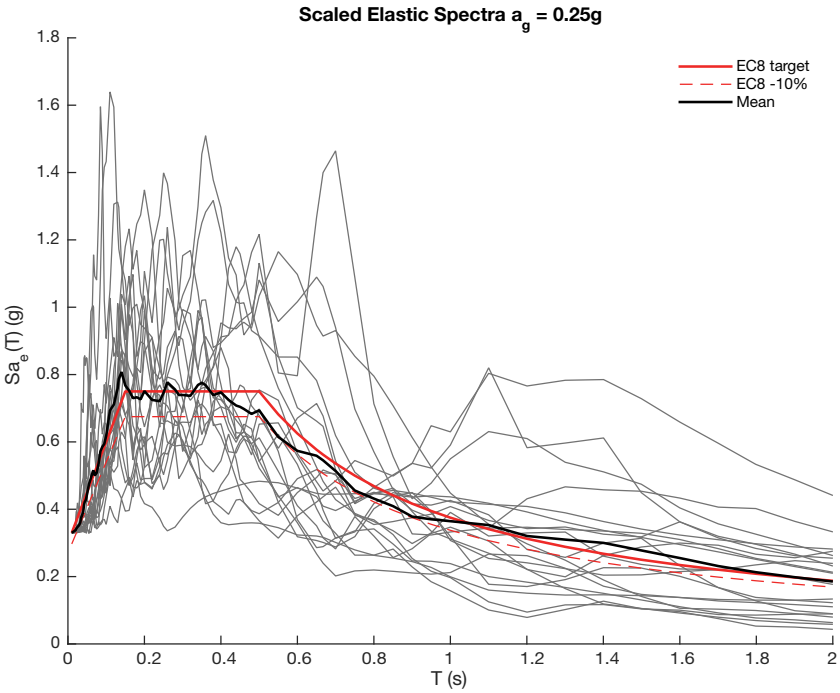

Fig. 4.5 The suite of ground motion record scaled to a_g S = 0.25g·S

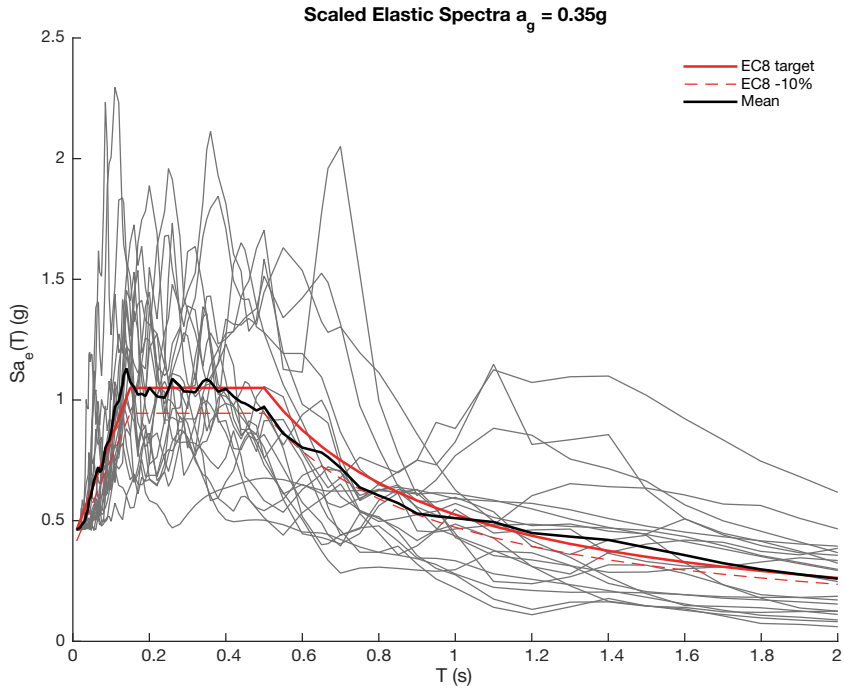

Fig. 4.6 The suite of ground motion record scaled to a_g S = 0.35g·S

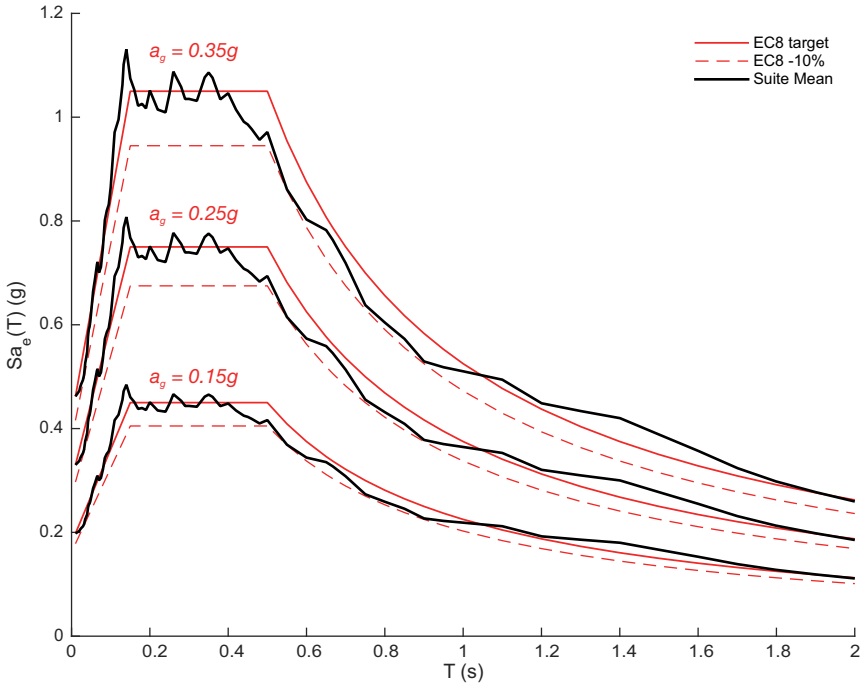

Fig. 4.7 Comparison between average scaled average spectra and reference EC8 spectra.

4.3.2 Scale factors

Even if there is not unanimous consensus around the notion, that scale factors of real ground motions records used for time history analyses should be limited is commonly accepted, or at least considered a positive attribute (Bommer and Acevedo 2004; Watson-Lamprey and Abrahamson 2006). Typical limit values of scale factors have been suggested in the range between 2 and 4.

Therefore, the suite of records was assembled by also aiming to limit the scale factors for the intermediate 0.25*g*·*S* intensity level. The suites for the lower (0.15*g*·*S*) and higher (0.35*g*·*S*) intensity levels comprise the same records scaled to match respective reference spectra, rather than different sets of records with scale factors closer to unity. This was done to ease the comparison of the effects on the infill walls between sets of analyses performed at different intensities of ground motion. As shown in Table 4.4, the mean scale factors for the three intensity levels are 0.83, 1.38 and 1.93 respectively, and range between 0,28 and 3.90 for any single record of the suite.

Mean scale factors of the scaled ground motions for a_g·S =		
0.15g·S	0.25g·S	0.35g·S
0.83	1.38	1.93

Table 4.4 Mean scale factors of the suite for the three intensity levels.

5 RESULTS

5.1 Overview

This chapter is dedicated to the results obtained from the nonlinear time history analyses. The global response in the in-plane direction of the infilled frames was recorded through the analysis; Fig. 5.1-Fig. 5.5 show the hysteretic IP responses of the infilled frames in terms of top-right node displacement against the base shear at the three intensity levels that were chosen as scaling factors. However, the scope of this work, the analytical model and the analysis framework are focused specifically on the seismic response of the URM infill walls under combined IP/OOP actions, therefore only results related to the infill walls will be shown in the next sections.

In section 5.2, the force and displacement history paths of the URM walls will be presented and discussed. This type of representation combines different concepts that were introduced in previous chapters, and in particular the IP/OOP interaction curves and the IP/OOP response of the equivalent element used to represent the panels. Additionally, the series of plots highlights the influence of the modelling parameters (i.e. infill wall type, frame configuration and RC member design) on the panels response. In this section only results from EQ06 analyses are shown, with the plots from EQ10 analyses reported in Appendix A.

In 5.3 the damage sustained by the URM infills by the end of the analyses is shown with coloured grids that represent the infilled frames. These schematic representations will be called “damage grids” and they will provide a visual tool to interpret the results from multiple analyses and sets of analyses.

Finally, in 5.4 the data from all the analyses is aggregated to discuss the frequency of cracked and collapsed walls associated to the frame characteristics and ground motion intensities.

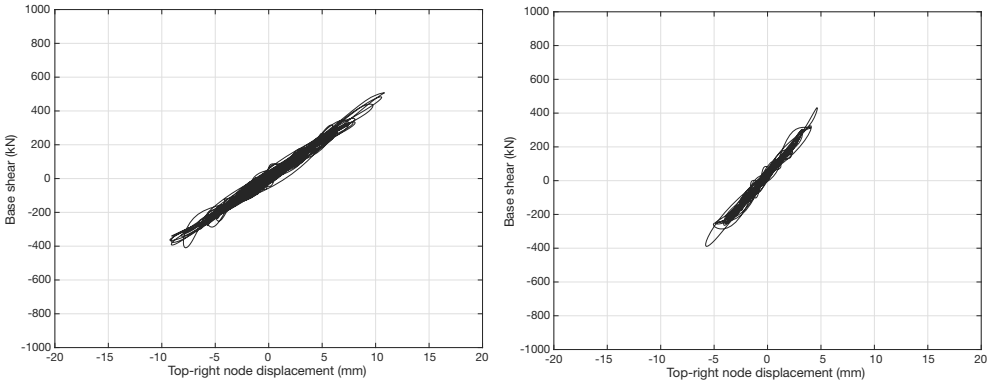

Fig. 5.1 Global base shear / displacement response history of frame 3×3_115S (left) and 3×3_300S (right) for analysis EQ06 scaled to a_g = 0.15g.

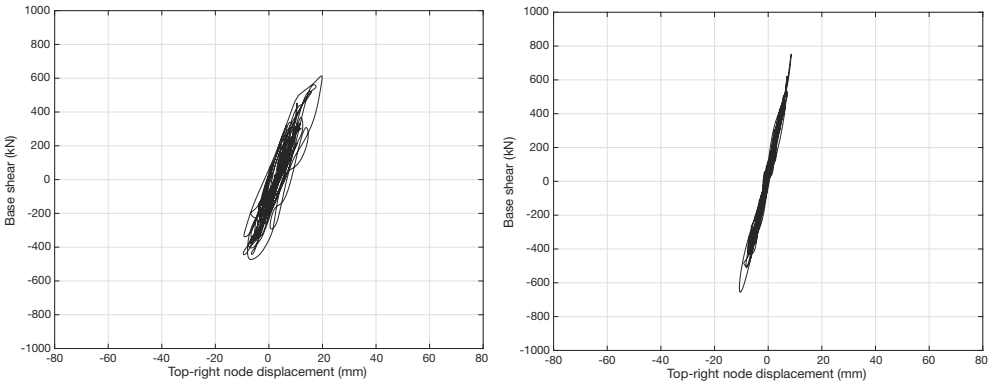

Fig. 5.2 Global base shear / displacement response history of frame 3×3_115S (left) and 3×3_300S (right) for analysis EQ06 scaled to a_g = 0.25g.

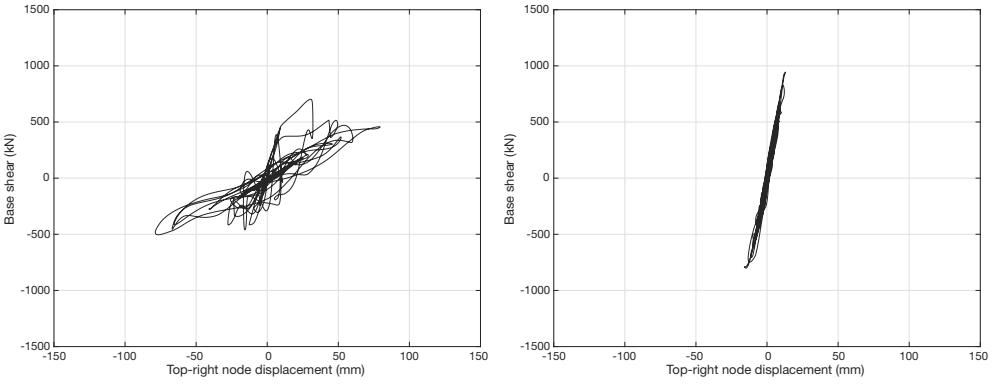

Fig. 5.3 Global base shear / displacement response history of frame 3×3_115S (left) and 3×3_300S (right) for analysis EQ06 scaled to a_g = 0.35g.

5.2 In-Plane / Out-of-Plane force and displacement paths

5.2.1 Description of the plots

During the dynamic bi-directional analyses performed on the infilled frame models, both the IP and OOP forces and displacements of URM infill walls are monitored. In the macro-model, the axial loads and the planar displacements of the URM wall correspond to the IP forces and displacements of the equivalent element; likewise, the bending moment / arching action and deflection of the of the URM wall relate to the OOP bending and displacements on the macro-element. The force and displacement outputs of the element at each time step can be represented inside the corresponding interaction curve of the wall, resulting in a representation of the force and displacement paths histories of the wall during the analysis.

Fig. 5.4 illustrate the graphic layout of the force and displacement paths for a single wall. The label on the top left corner ("W4L" in Fig. 5.4) of each plot designates the position of the corresponding wall on the frame, as previously defined in Fig. 4.1.

Force paths are exemplified by the graph at the top of Fig. 5.4, which plots the response of infill wall W4L for analysis EQ06 scaled to ag = 0.25*g*. The IP and OOP loads of the equivalent wall element are normalized by their respective capacities and plotted on the y- and x-axes, respectively. The IP/OOP force paths are shown inside their corresponding force interaction curves. When an infill wall reaches a combination of IP/OOP forces that yield the fibre sections of the macro-element, cracking is identified and plotted with a dot; the time when this occurred is also registered (T_{crk}), enabling the identification of the sequence in which the walls surpassed their strength limit.

Similarly, the second plot shown in Fig. 5.4 represent the IP/OOP displacement path of infill wall W4L for analysis EQ06 scaled to ag = 0.35*g*. In the displacement paths graphs, IP and OOP are plotted on the y- and x-axes respectively, along with their displacement capacity domains. The displacements of the panels that crack tend to increase due to the reduced stiffness. If the infill wall reaches a combination of IP/OOP displacements that exceeds its ultimate capacity, collapse occurs and the corresponding macro-element is removed from the model for the remainder of the analysis. The failure is identified on the plot with a dot and the time of occurrence is registered ($T_{collapse}$), in order to identify the sequence of collapse.

Model ID	Columns		Beams	
	Dimensions (mm×mm)	Detailing	Dimensions (mm×mm)	Detailing
3×3_115T	350×350	Col350T	500×250	BeamT
3×3_300T	350×350			
3×3_115S	350×350	Col350S	300×350	BeamS
3×3_300S	350×350			
5×3_115T	400×400	Col400T	500×250	BeamT
5×3_300T	400×400			
5×3_115S	400×400	Col400S	300×350	BeamS
5×3_300S	400×400			

Table 4.1 Dimensions of RC frames members.

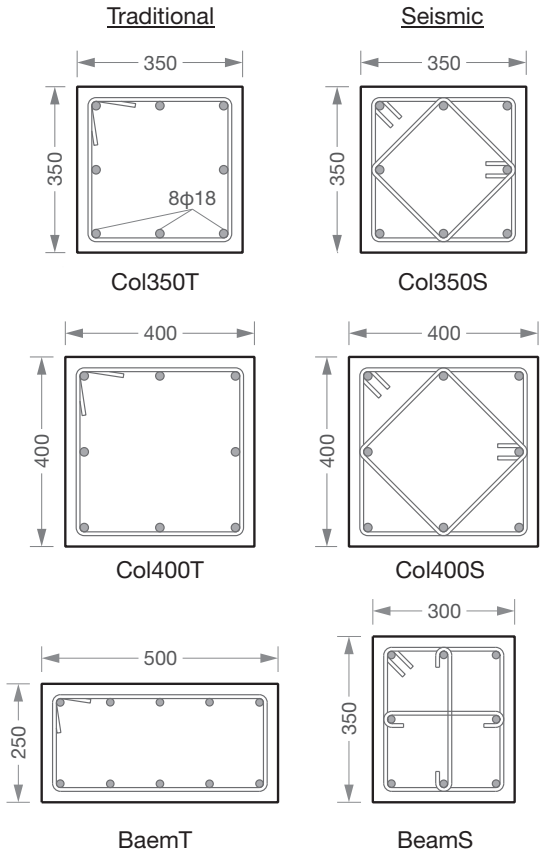

Fig. 4.2 Traditional (left) and seismic designed (right) RC sections of columns and beams used in planar frames models as listed in Table 4.1.

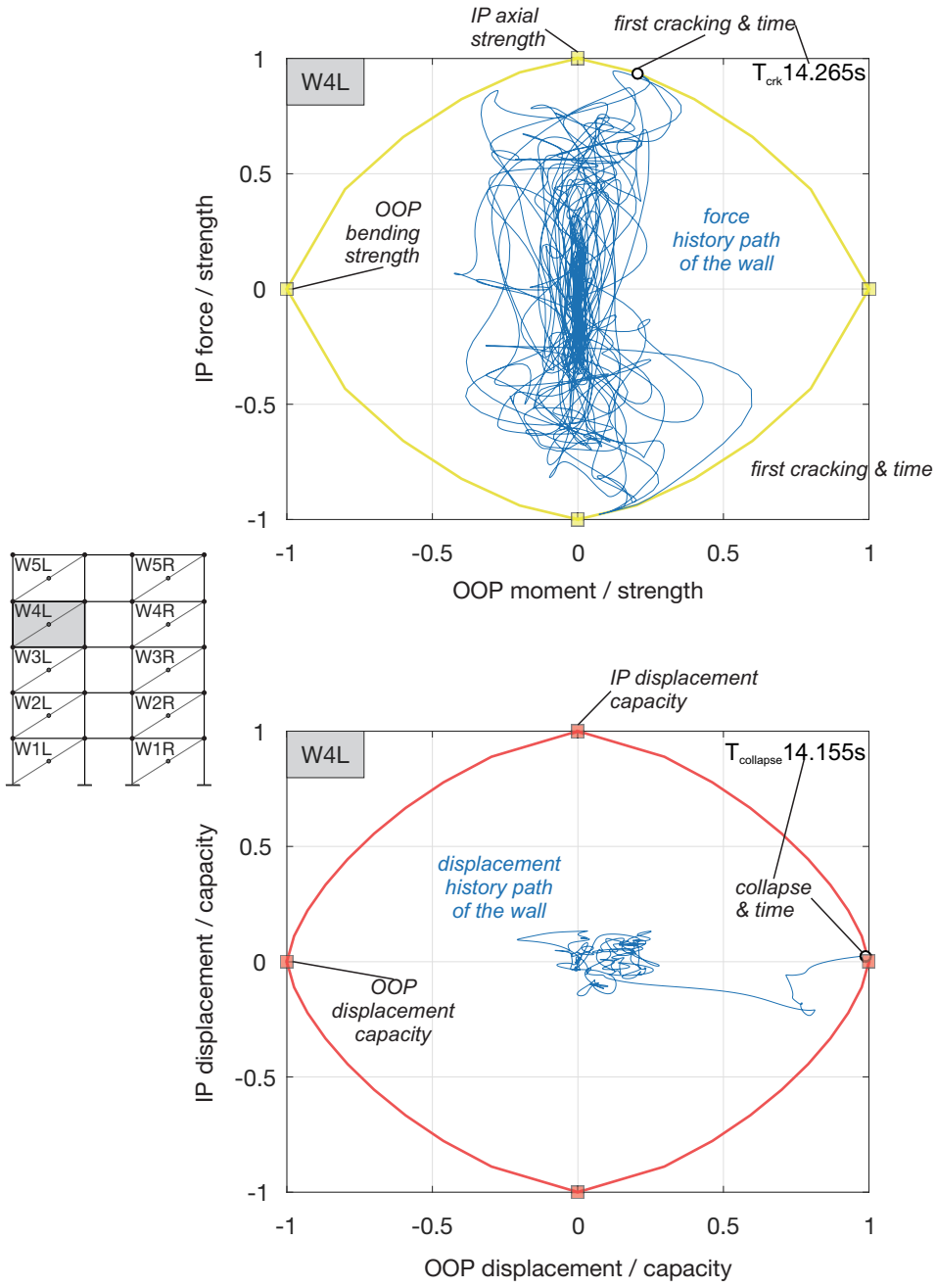

Fig. 5.4 Top: Displacement (top) and force (bottom) history path keys. Paths refer to wall W4L of frame 5×3_115T for analysis EQ06 scaled to a_g = 0.25g (top) and 0.35g (bottom).

In the next pages, figures of the force and displacement paths are grouped based on the wall positions on the frames, as defined in 4.2.2. Specifically, in each figure the plots follow the same arrangement as the infill walls in the planar frames of Fig. 4.1, and are labelled accordingly as well.

In this section, only the paths obtained from the analyses of the EQ06 records and scaled to the three intensity levels defined in 4.3.1 (herein labeled with the ground acceleration a_g = *0.15g, 0.25g, 0.35g* that defines the corresponding scale factor) are shown. Nonetheless, the series reported here is adequately representative of the force and displacement paths resulting from the suite of ground motions. For the sake of comparison, the full series of force and displacement history paths are reported for EQ10 records as well. The EQ06-D1 and EQ06-D2 records are natural records taken in L'Aquila during the 2009 Abruzzo (Italy) earthquake. The EQ10-D1 and EQ10-D2 records are natural records from the 1999 Düzce (Turkey) earthquake.

The IP/OOP force and displacement paths are shown applied to the eight frame configurations defined and listed in Table 4.2. A summary of the infill walls history paths shown in the next pages and Appendix A is reported in Table 5.1.

Frame	*Analysis EQ06 scaled to a_g =*			*Analysis EQ10 scaled to a_g =*		
configurations	*0.15g*	*0.25g*	*0.35g*	*0.15g*	*0.25g*	*0.35g*
3×3_115T	Fig. 5.5	Fig. 5.9	Fig. 5.13	Fig. A 1	Fig. A 5	Fig. A 9
3×3_300T	Fig. 5.6	Fig. 5.10	Fig. 5.14	Fig. A 2	Fig. A 6	Fig. A 10
3×3_115S	Fig. 5.7	Fig. 5.11	Fig. 5.15	Fig. A 3	Fig. A 7	Fig. A 11
3×3_300S	Fig. 5.8	Fig. 5.12	Fig. 5.16	Fig. A 4	Fig. A 8	Fig. A 12
5×3_115T	Fig. 5.17	Fig. 5.21	Fig. 5.25	Fig. A 13	Fig. A 17	Fig. A 21
5×3_300T	Fig. 5.18	Fig. 5.22	Fig. 5.26	Fig. A 14	Fig. A 18	Fig. A 22
5×3_115S	Fig. 5.19	Fig. 5.23	Fig. 5.27	Fig. A 15	Fig. A 19	Fig. A 23
5×3_300S	Fig. 5.20	Fig. 5.24	Fig. 5.28	Fig. A 16	Fig. A 20	Fig. A 24

Table 5.1 Summary and references of the force and displacements paths figures.

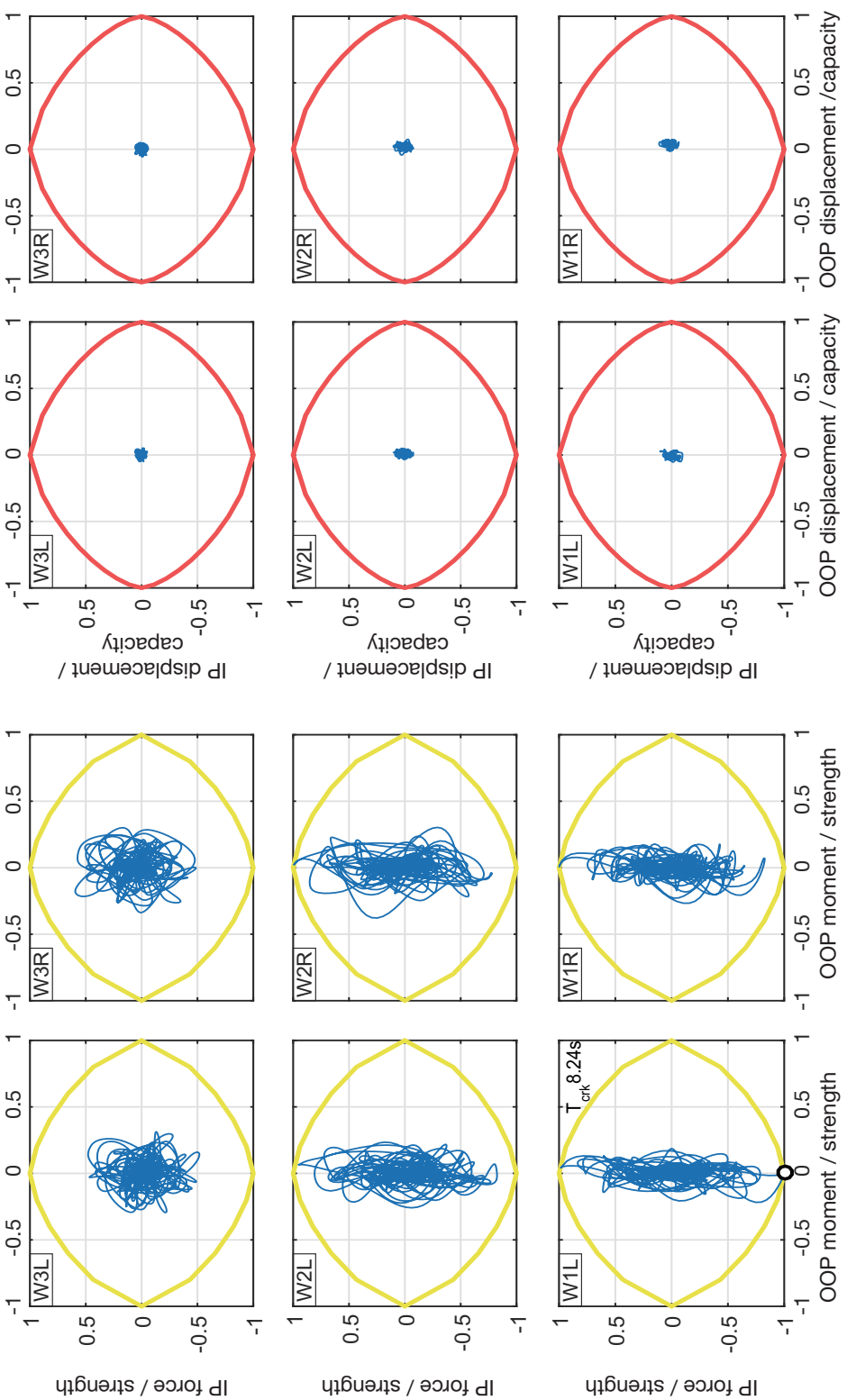

*Fig. 5.5 Force and displacement paths of infill walls in frame **3×3_115T** for analysis **EQ06** scaled to a_g = **0.15g***

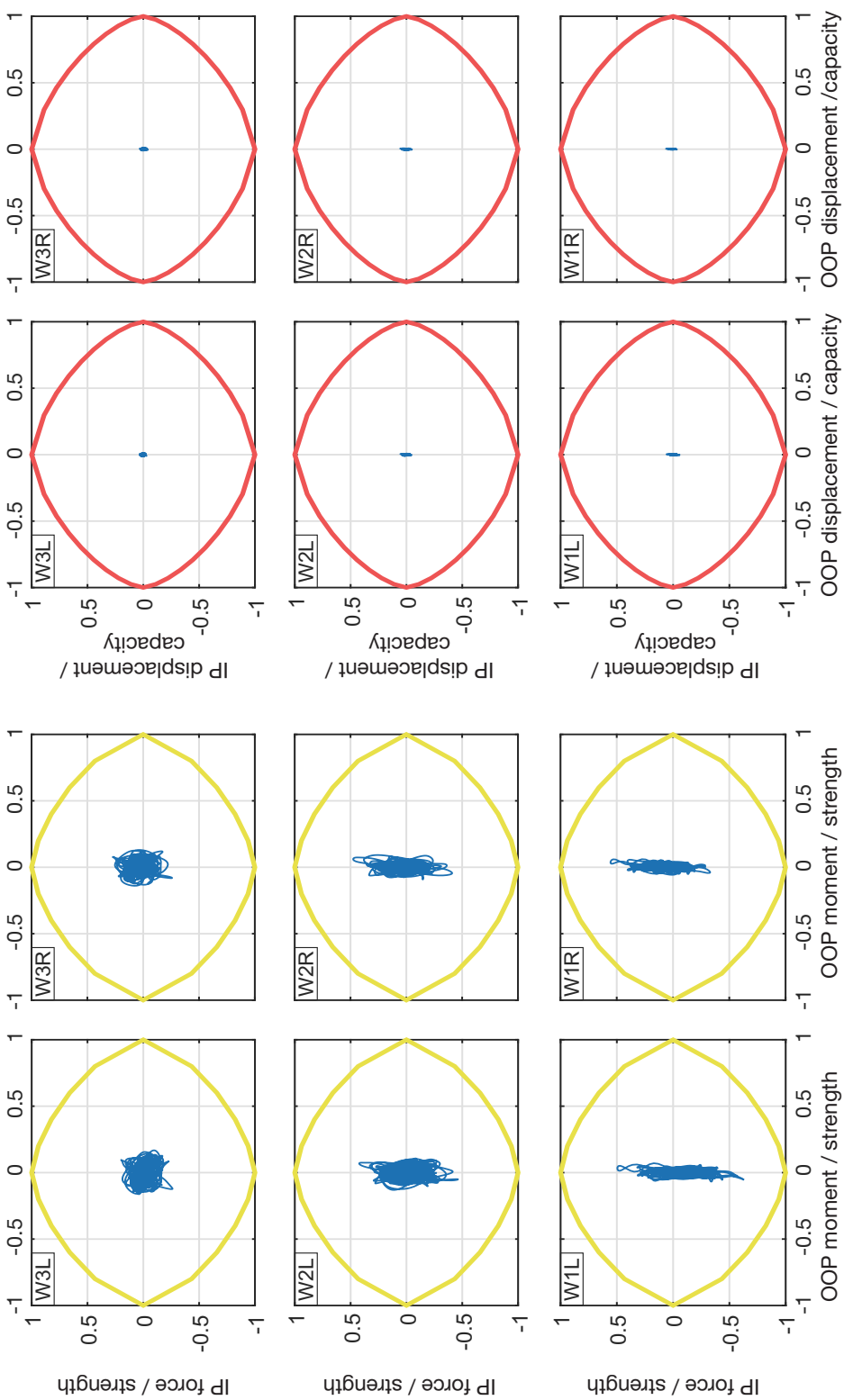

*Fig. 5.6 Force and displacement paths of infill walls in frame **3×3_300T** for analysis **EQ06** scaled to a_g = **0.15g***

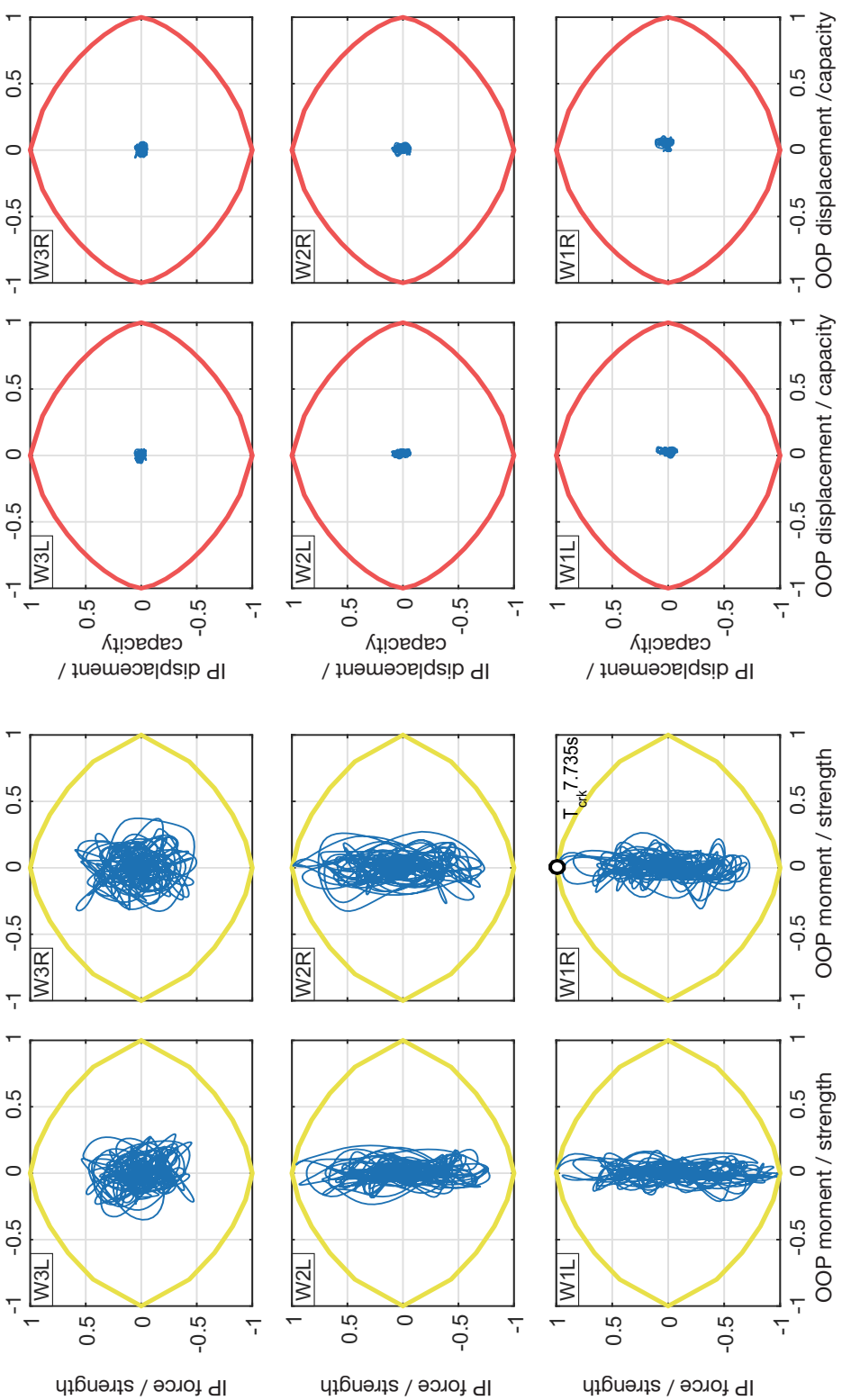

*Fig. 5.7 Force and displacement paths of infill walls in frame **3×3_115S** for analysis **EQ06** scaled to a_g = **0.15g***

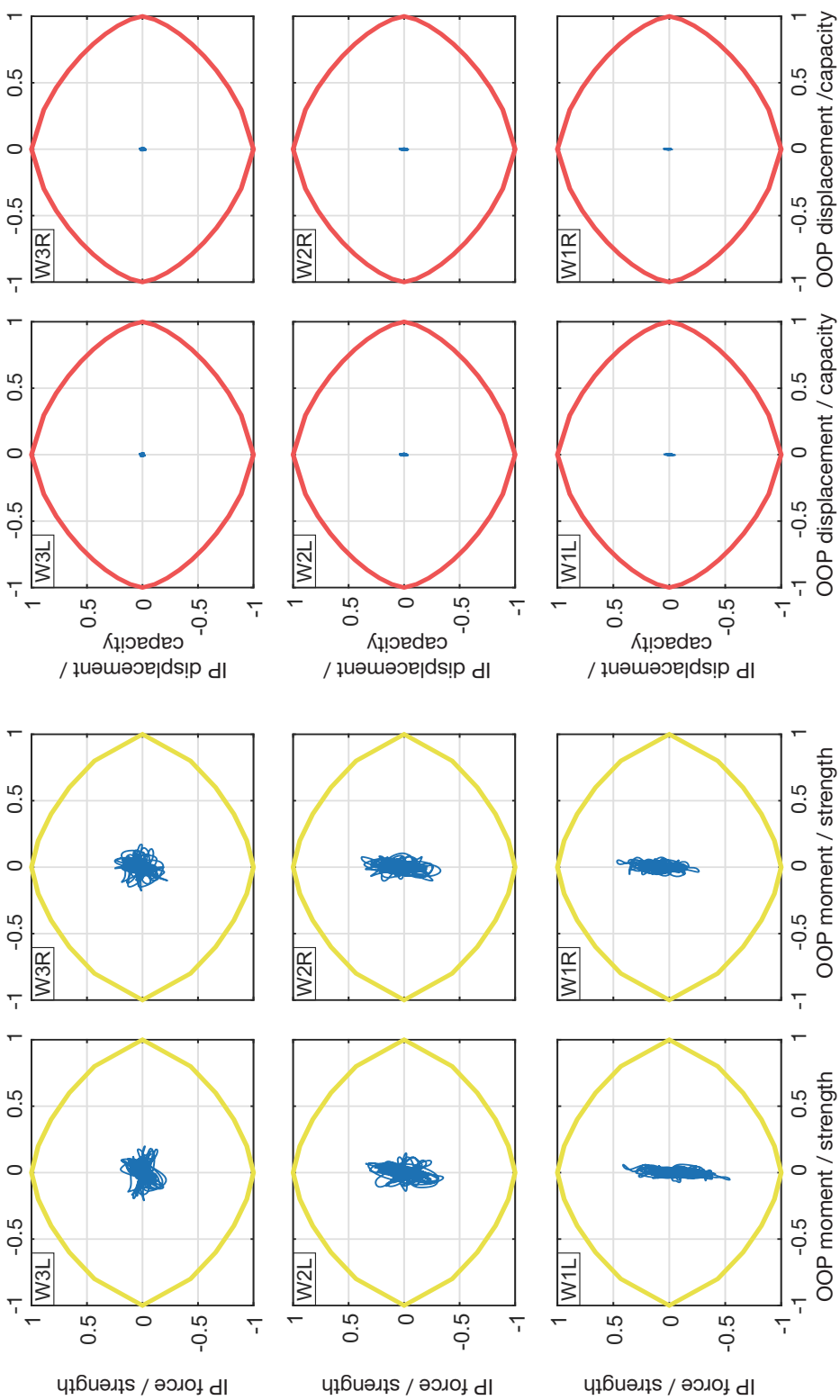

*Fig. 5.8 Force and displacement paths of infill walls in frame **3×3_300S** for analysis **EQ06** scaled to a_g = **0.15g***

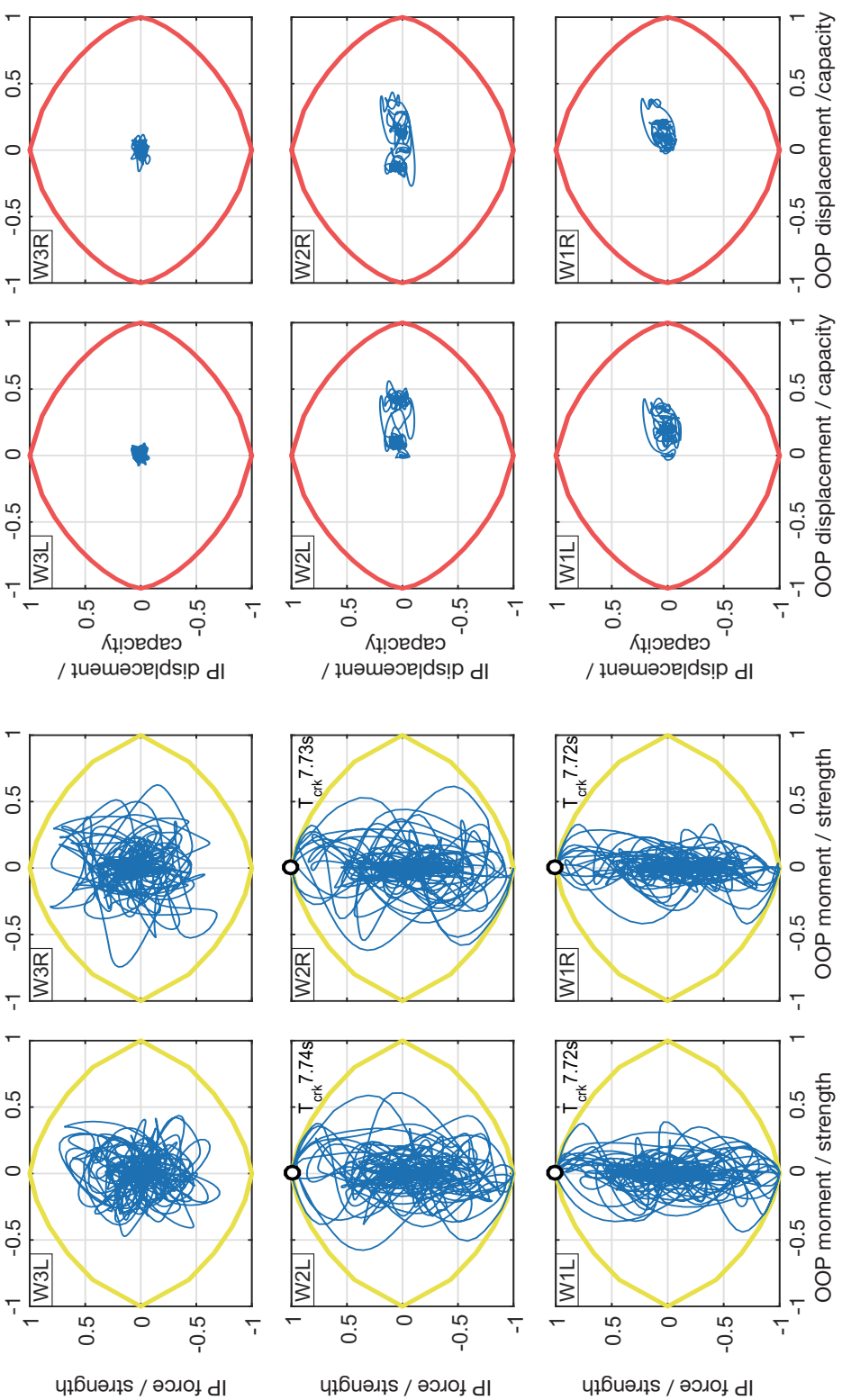

*Fig. 5.9 Force and displacement paths of infill walls in frame **3×3_115T** for analysis **EQ06** scaled to a_g = **0.25g***

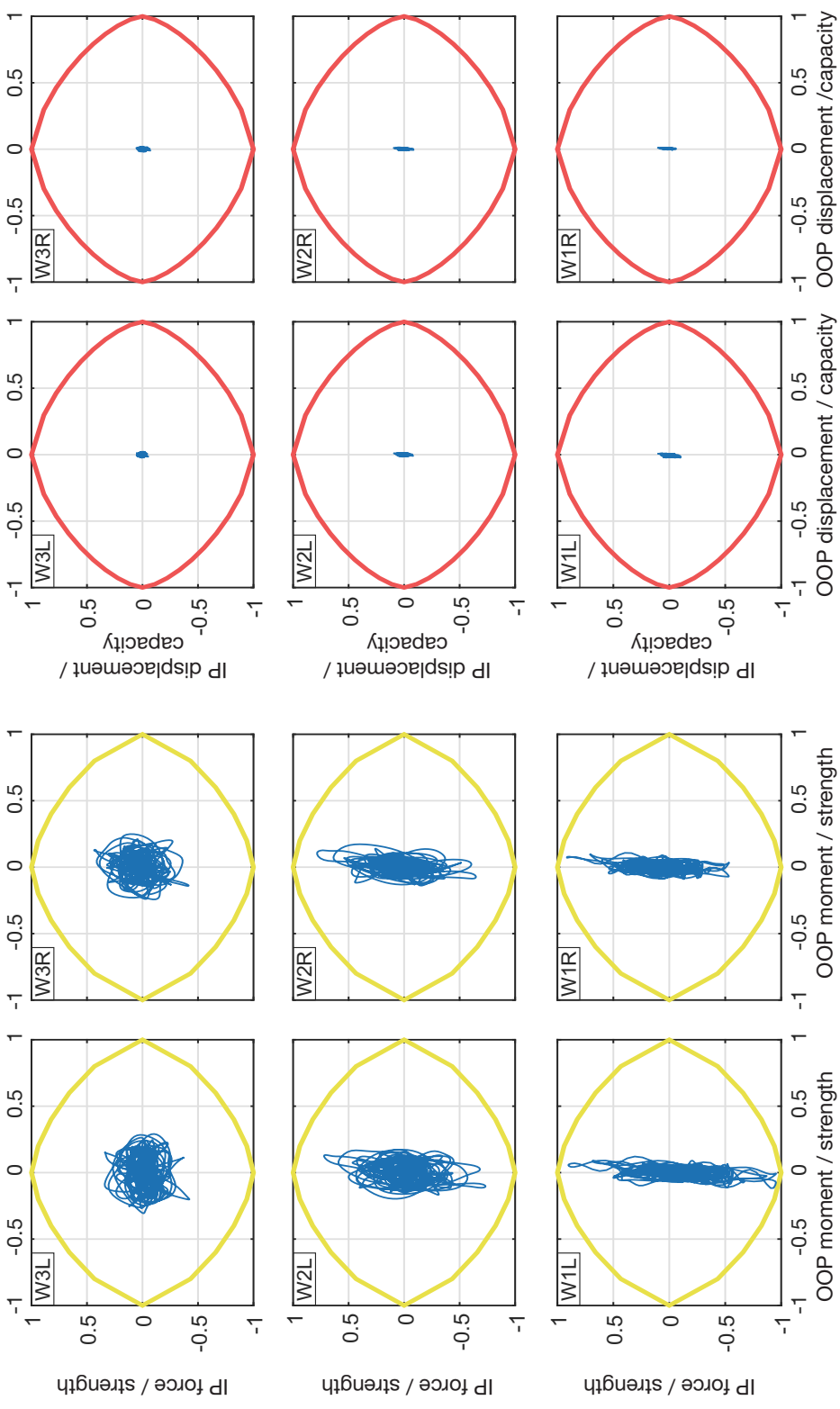

*Fig. 5.10Force and displacement paths of infill walls in frame **3×3_300T** for analysis **EQ06** scaled to a_g = **0.25g***

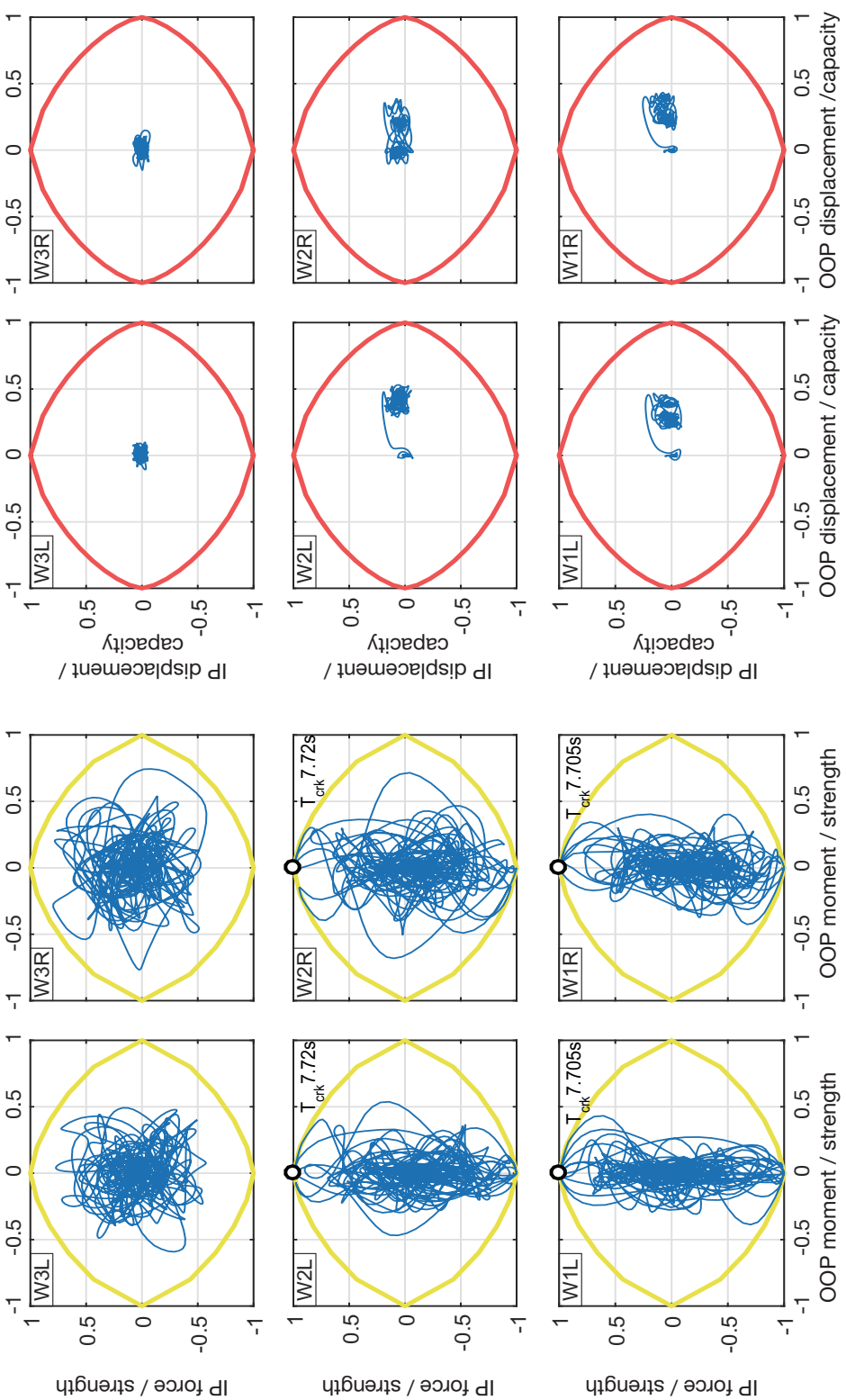

*Fig. 5.11Force and displacement paths of infill walls in frame **3×3_115S** for analysis **EQ06** scaled to a_g = **0.25g***

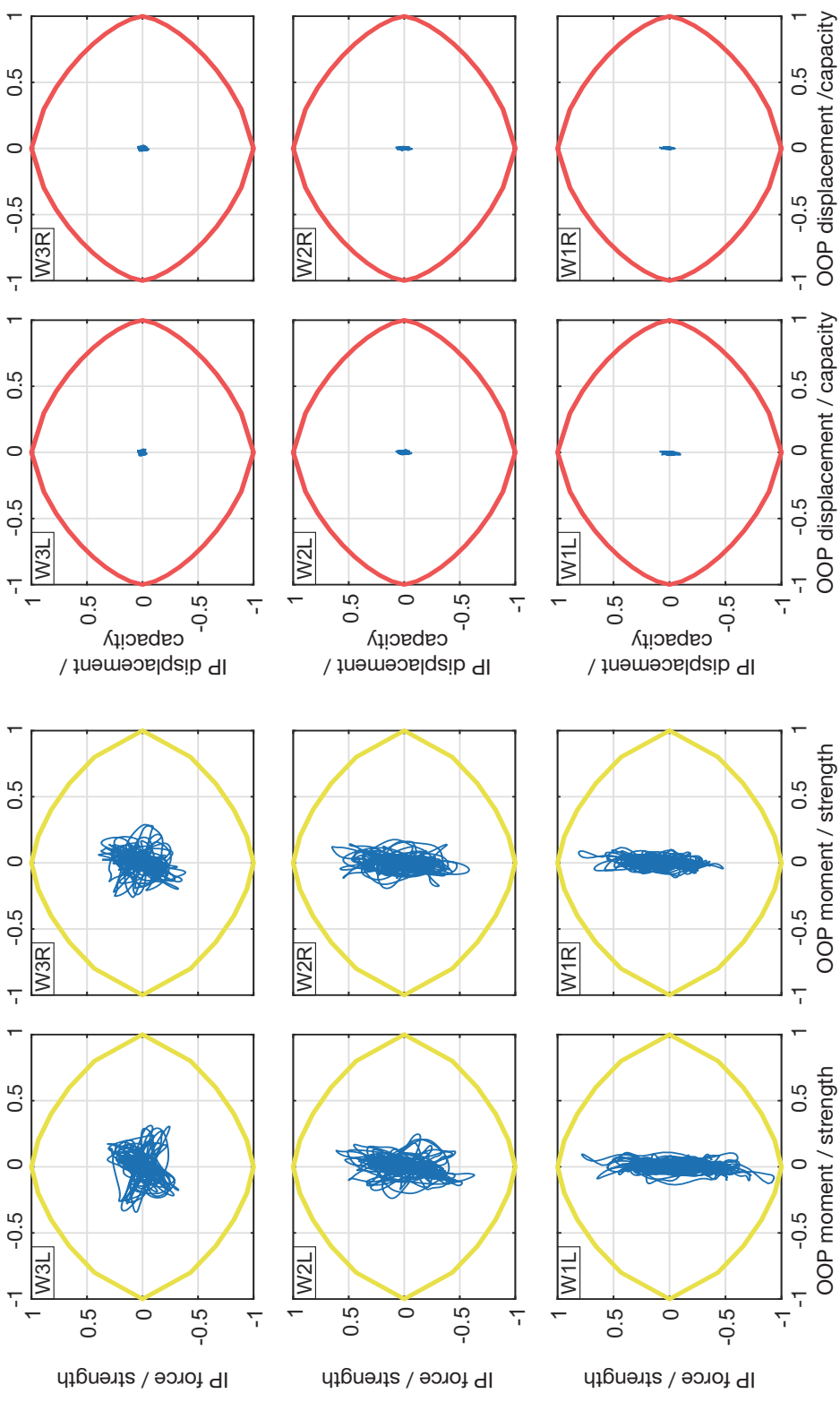

*Fig. 5.12Force and displacement paths of infill walls in frame **3×3_300S** for analysis **EQ06** scaled to a_g = **0.25g***

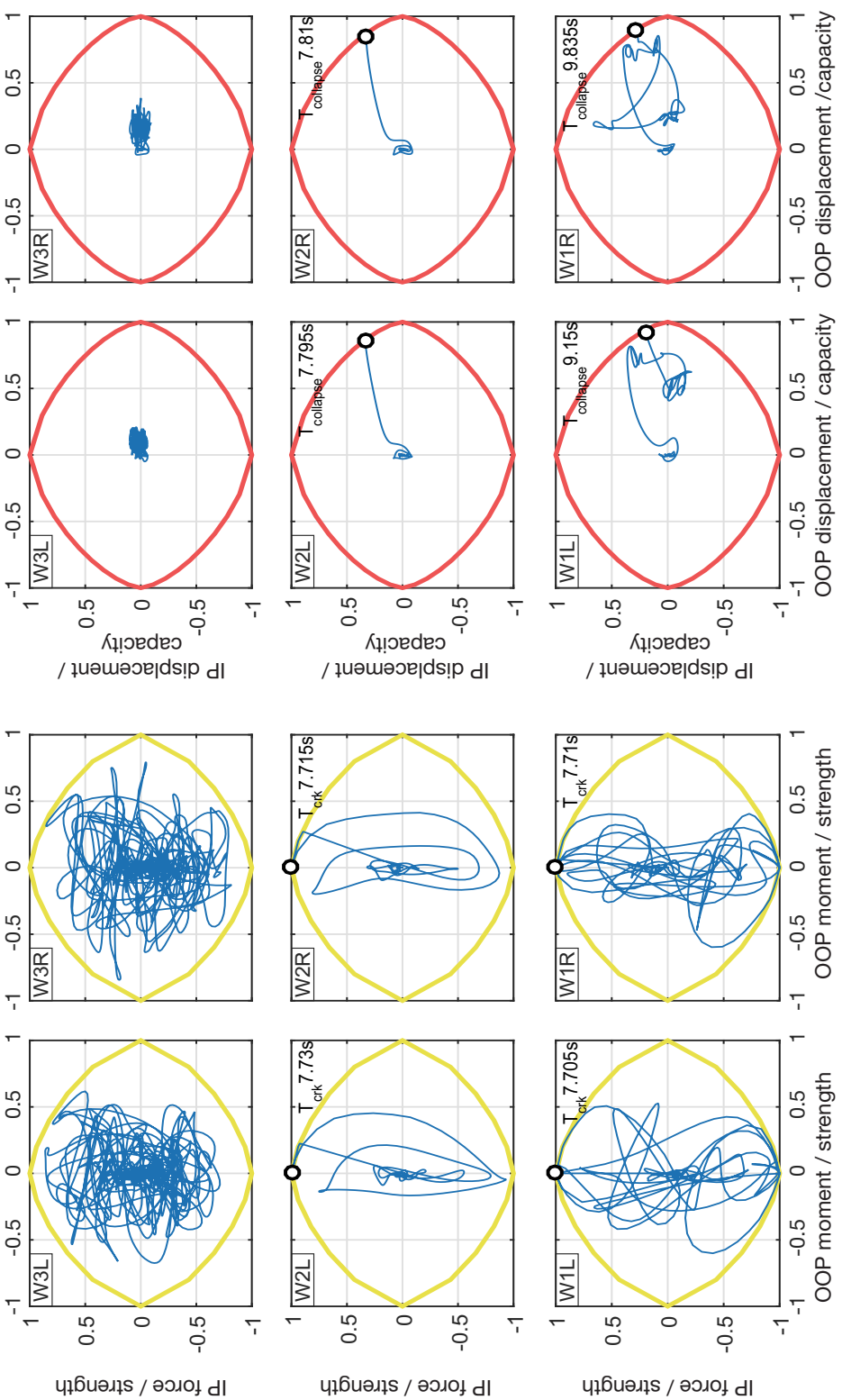

*Fig. 5.13Force and displacement paths of infill walls in frame **3×3_115T** for analysis **EQ06** scaled to a_g = **0.35g***

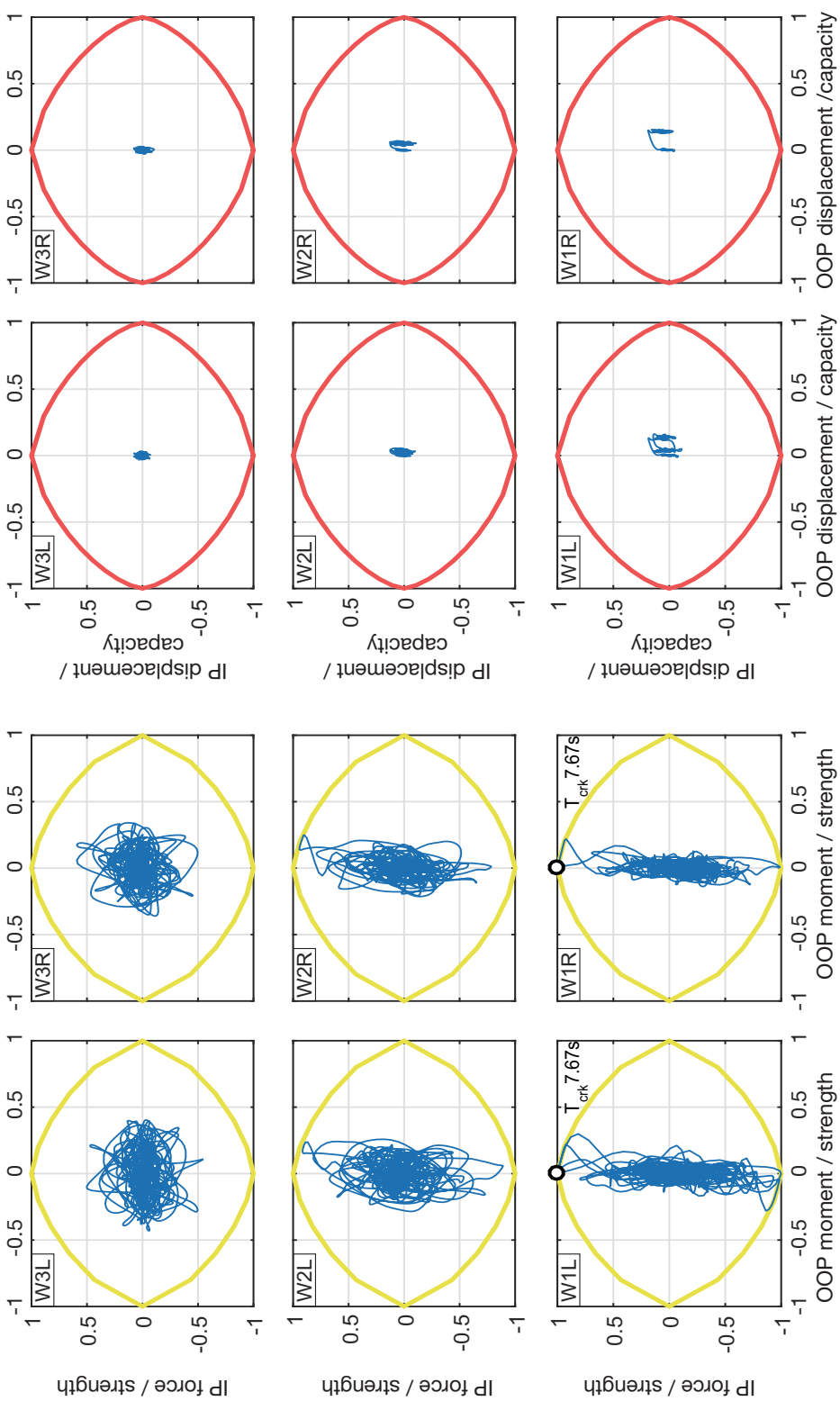

*Fig. 5.14Force and displacement paths of infill walls in frame **3×3_300T** for analysis **EQ06** scaled to a_g = **0.35g***

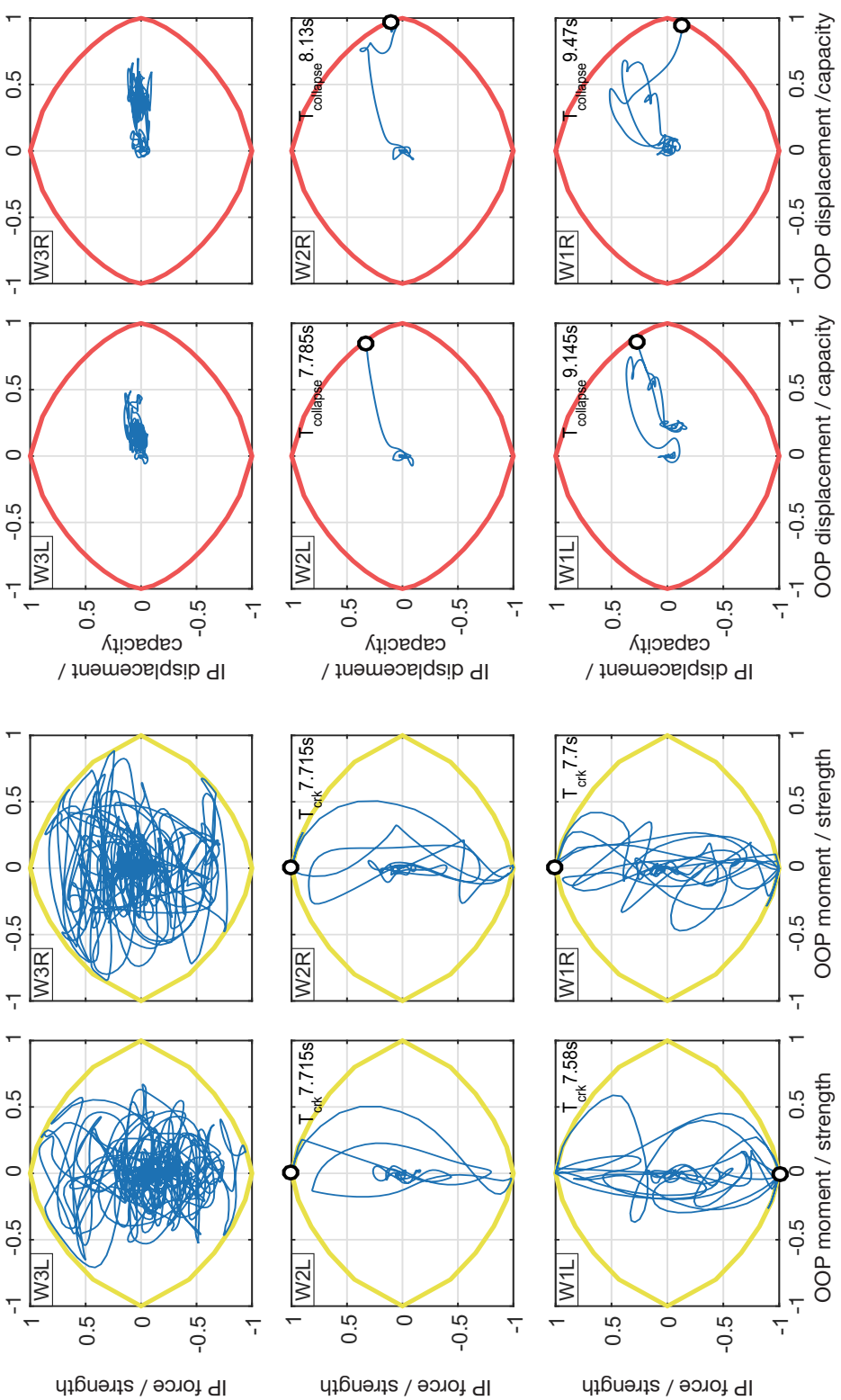

*Fig. 5.15Force and displacement paths of infill walls in frame **3×3_115S** for analysis **EQ06** scaled to a_g = **0.35g***

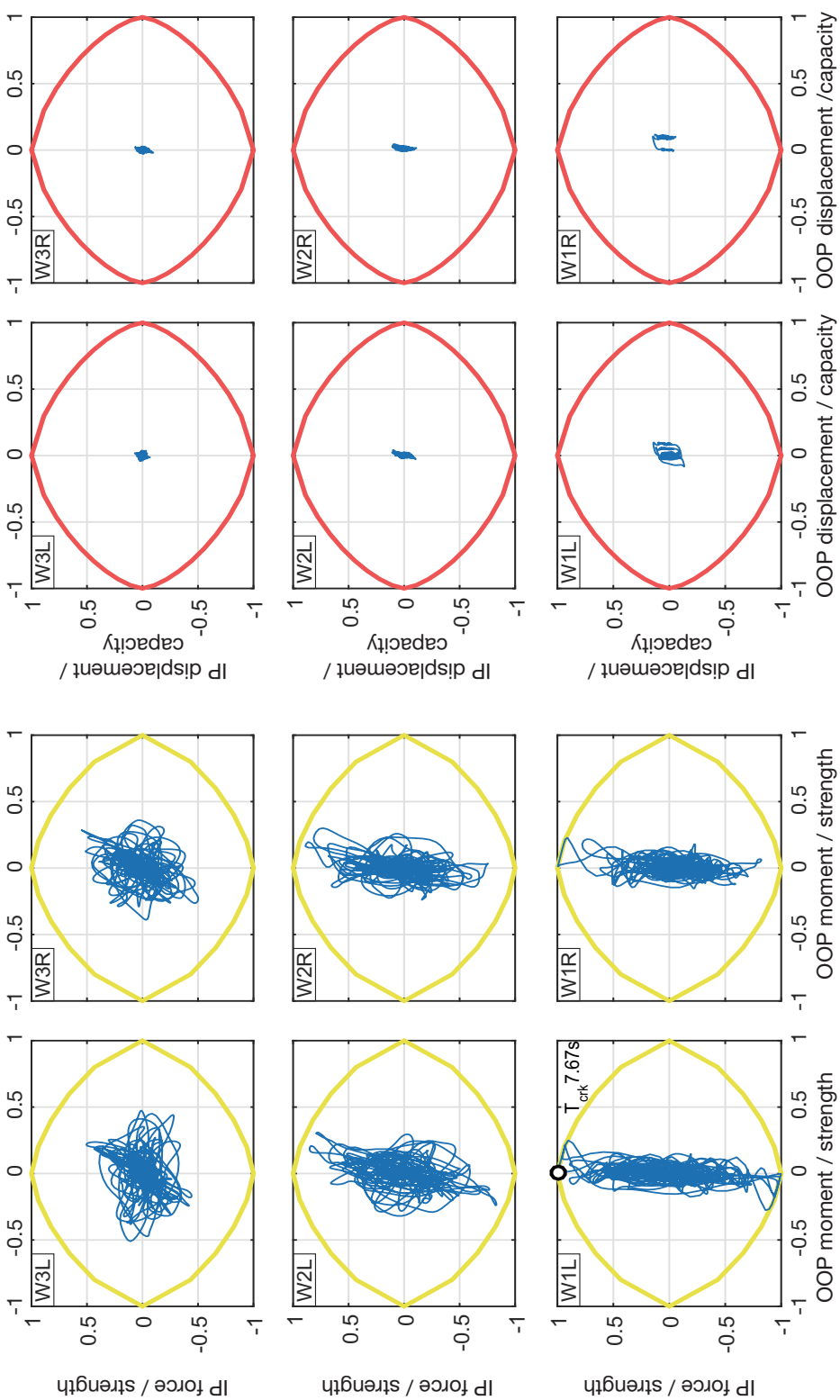

*Fig. 5.16Force and displacement paths of infill walls in frame **3×3_300S** for analysis **EQ06** scaled to a_g = **0.35g***

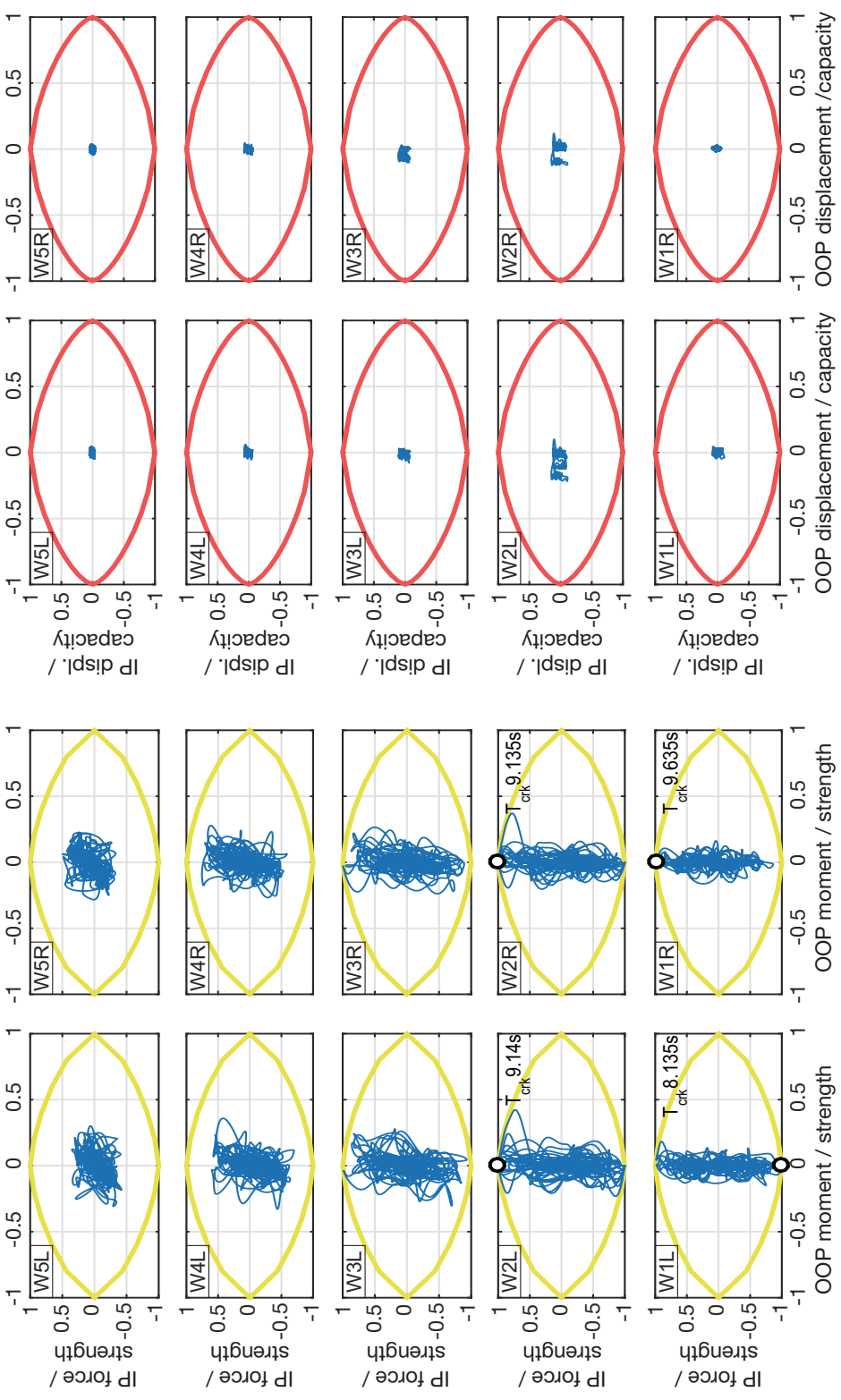

*Fig. 5.17Force and displacement paths of infill walls in frame **5×3_115T** for analysis **EQ06** scaled to a_g = **0.15g***

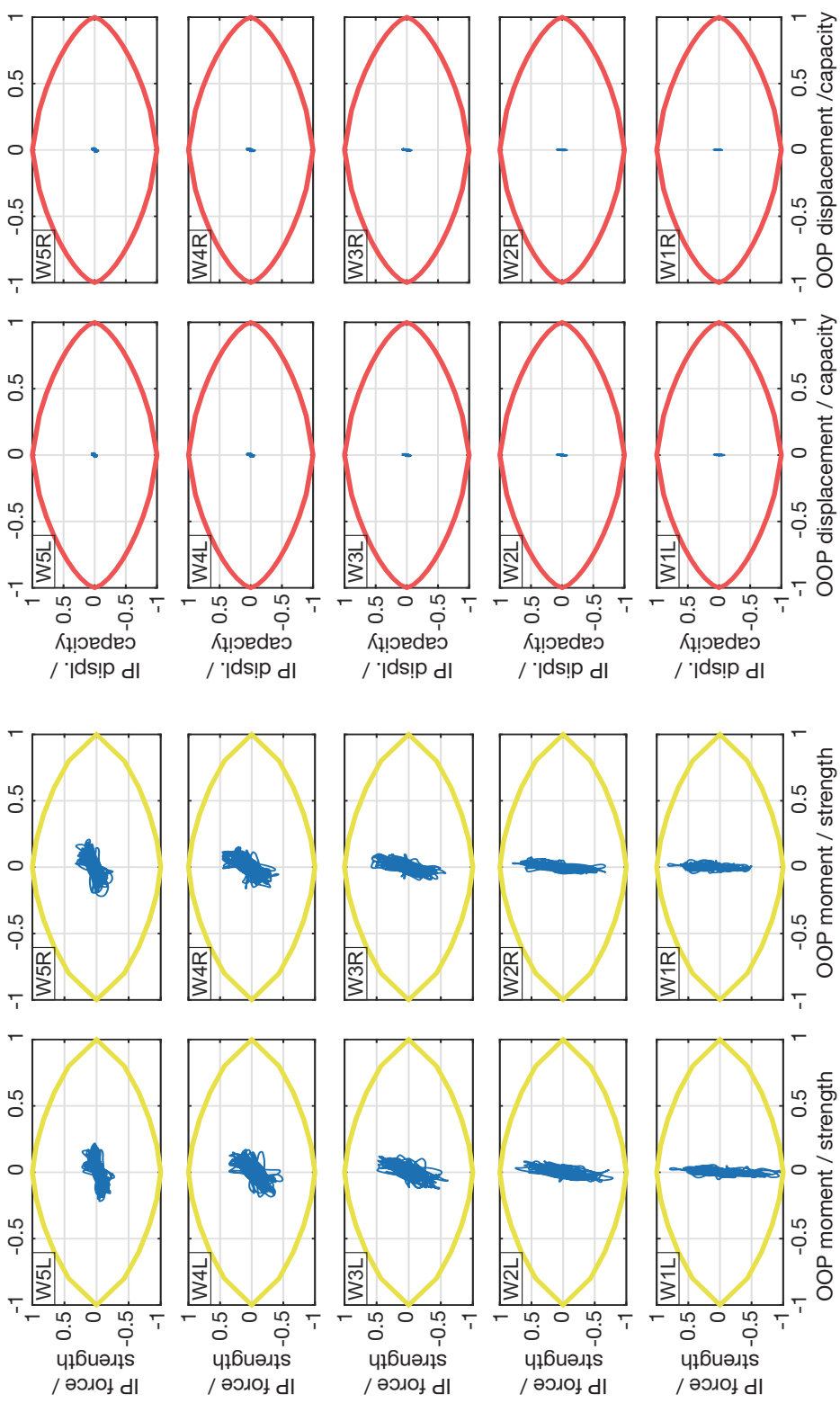

Fig. 5.18Force and displacement paths of infill walls in frame ***5×3_300T*** *for analysis* ***EQ06*** *scaled to* a_g **= 0.15g**

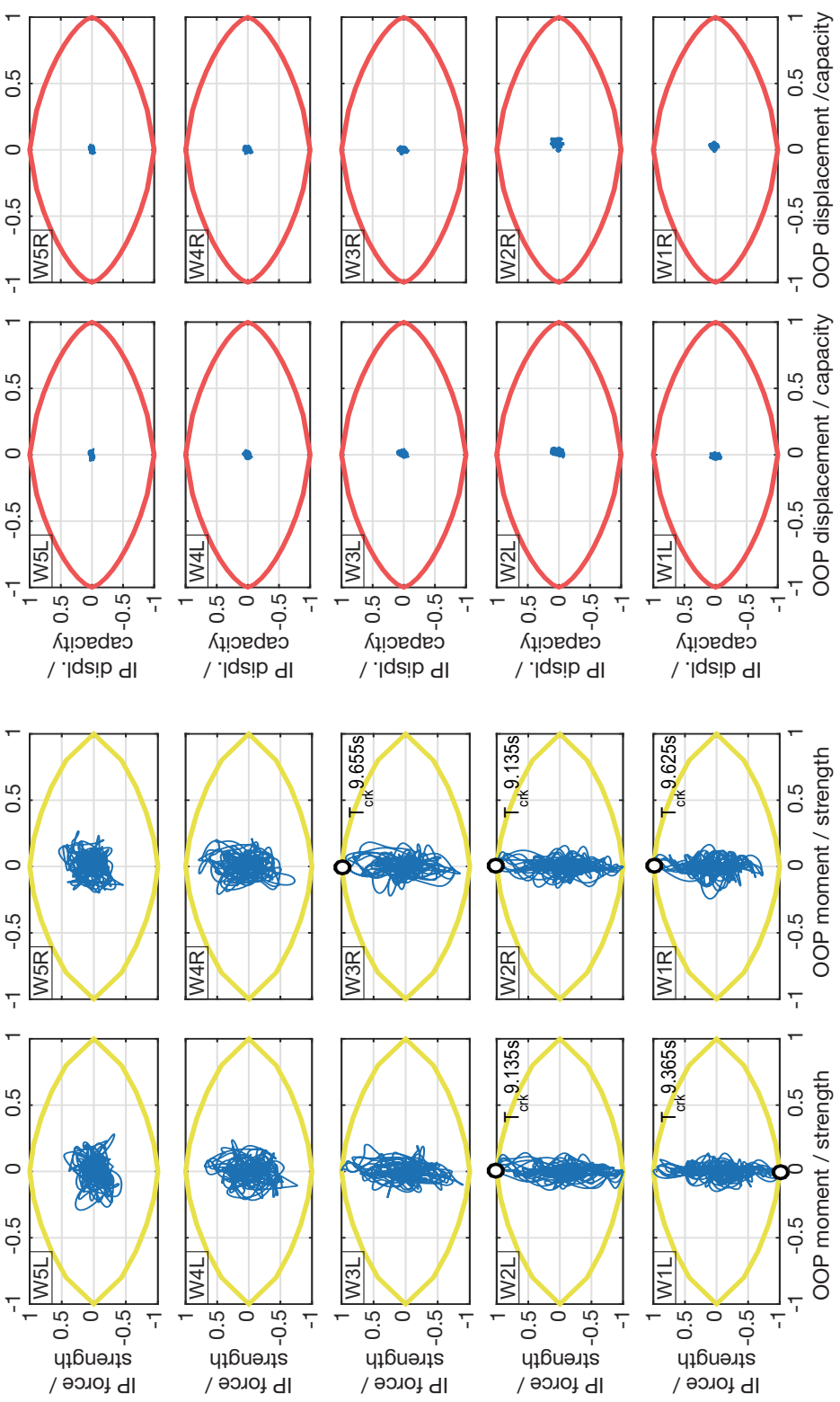

*Fig. 5.19Force and displacement paths of infill walls in frame **5×3_115S** for analysis **EQ06** scaled to a_g = **0.15g***

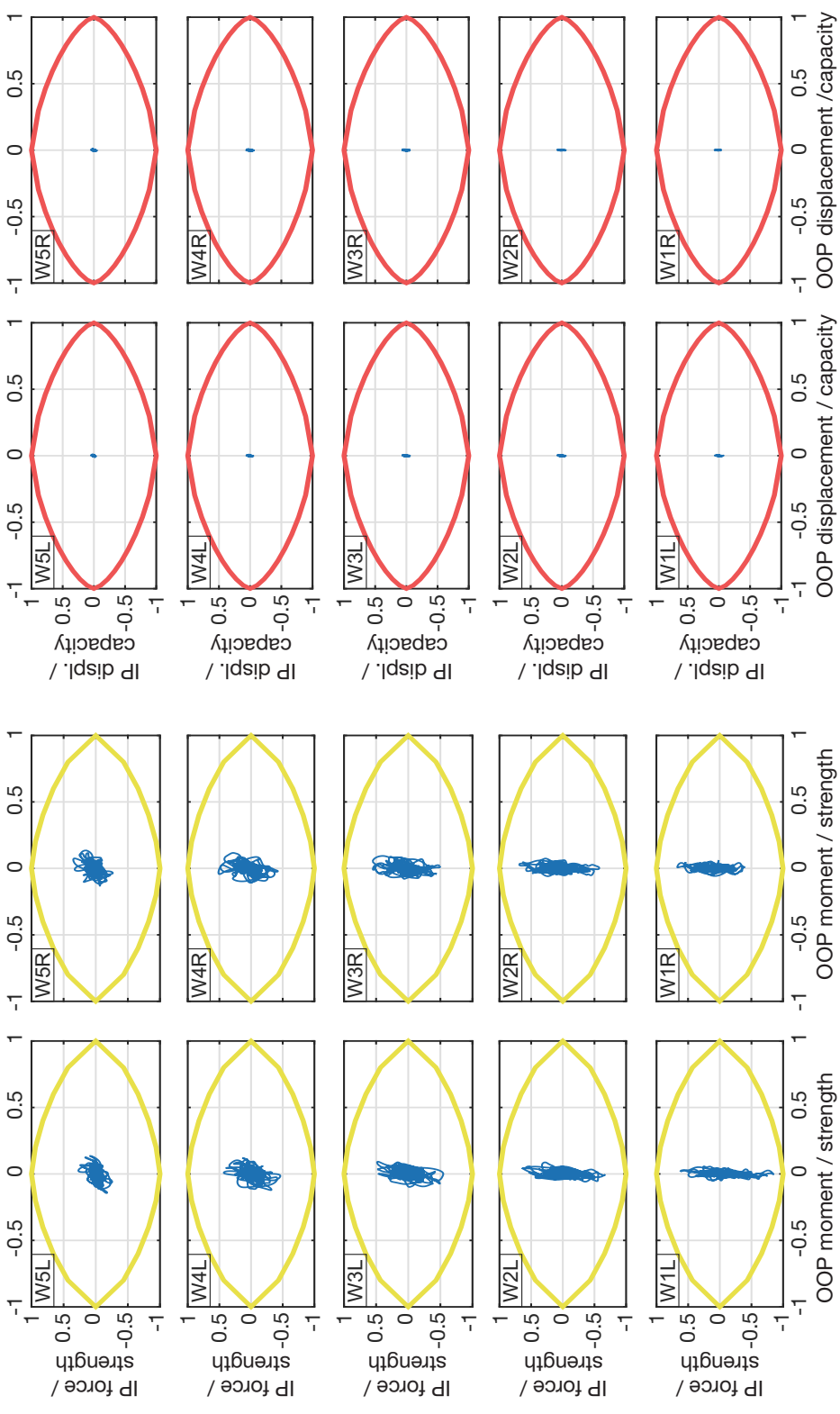

Fig. 5.20Force and displacement paths of infill walls in frame ***5×3_300S*** *for analysis* ***EQ06*** *scaled to* a_g **= 0.15g**

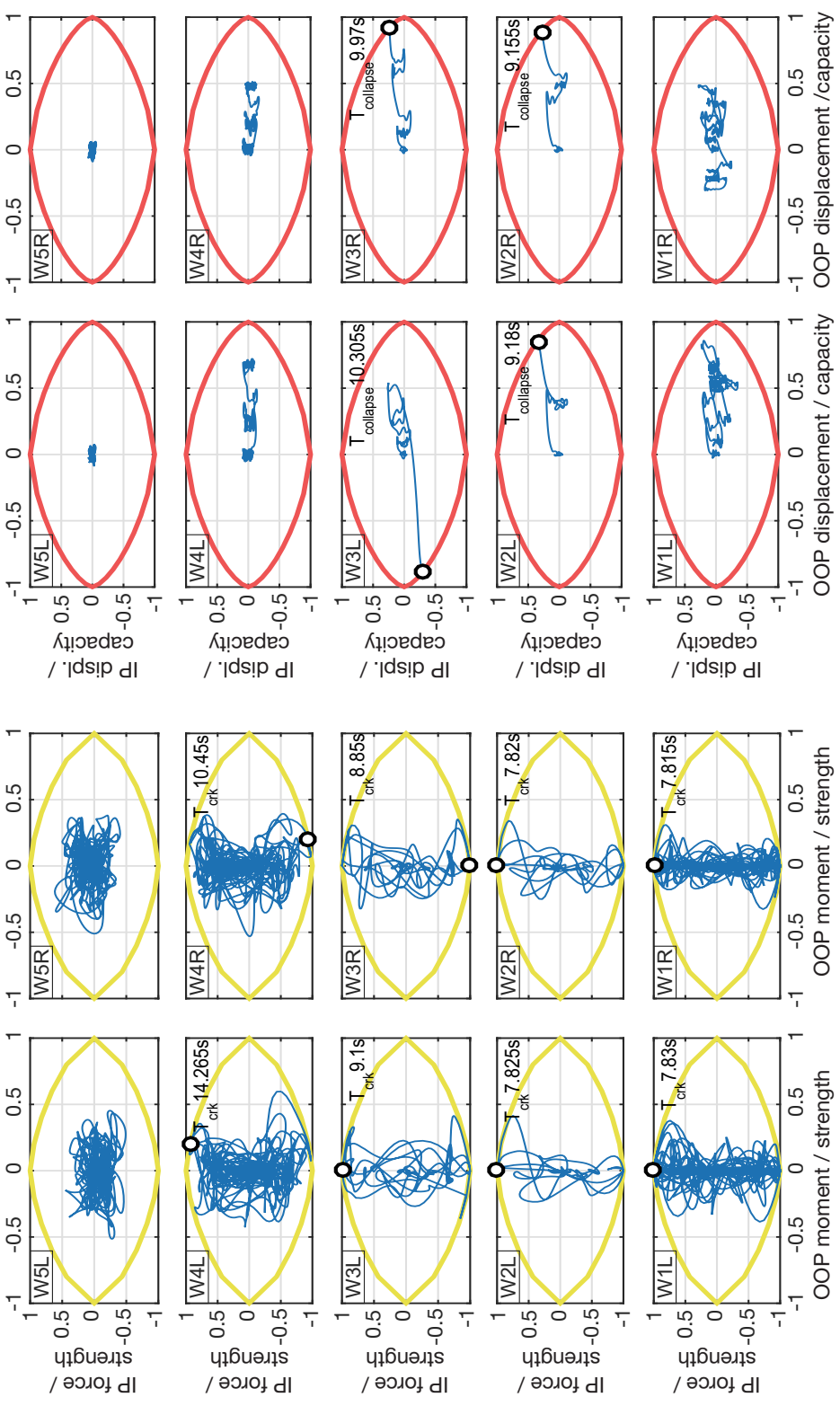

Fig. 5.21Force and displacement paths of infill walls in frame ***5×3_115T*** *for analysis* ***EQ06*** *scaled to* a_g **= 0.25g**

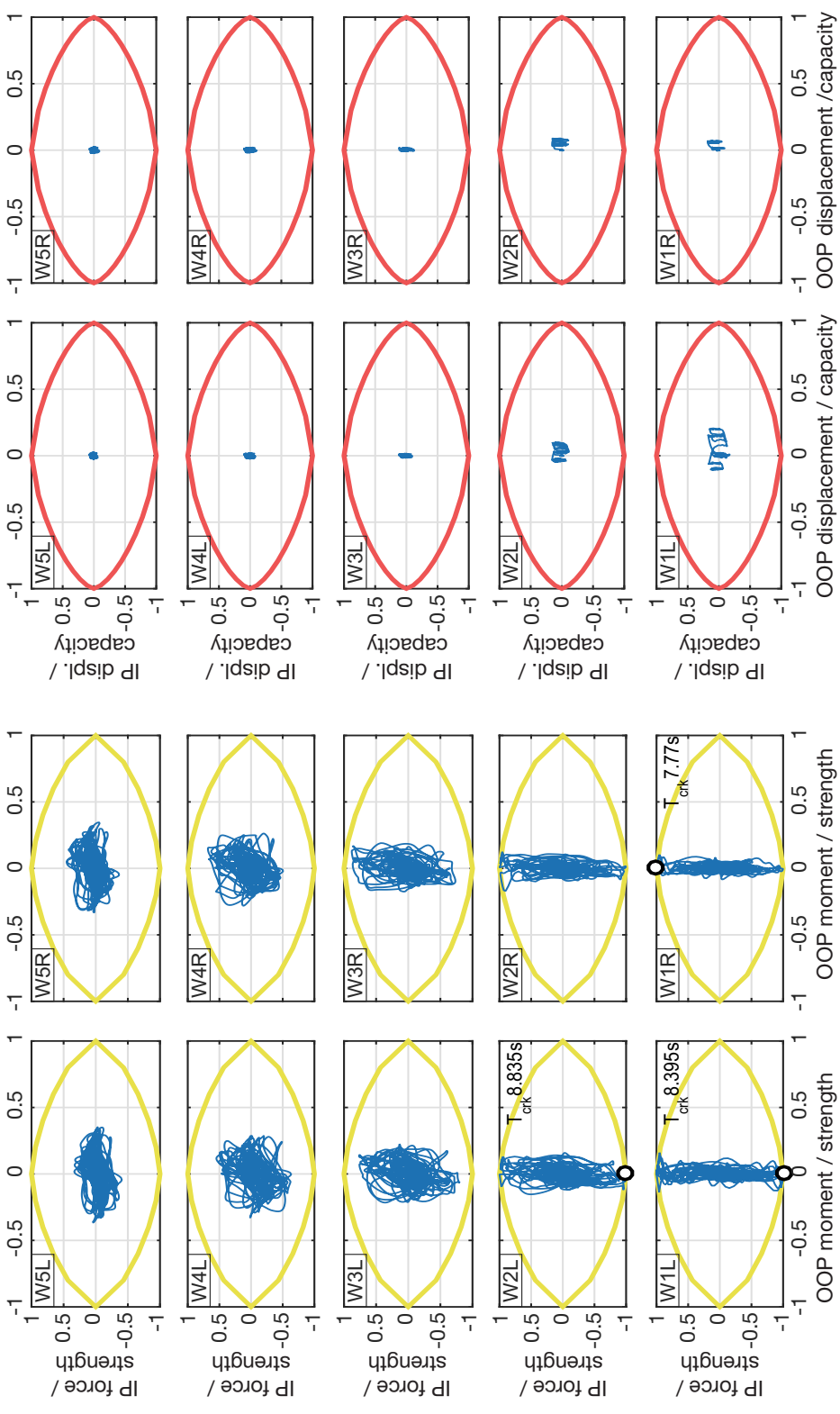

*Fig. 5.22Force and displacement paths of infill walls in frame **5×3_300T** for analysis **EQ06** scaled to a_g = **0.25g***

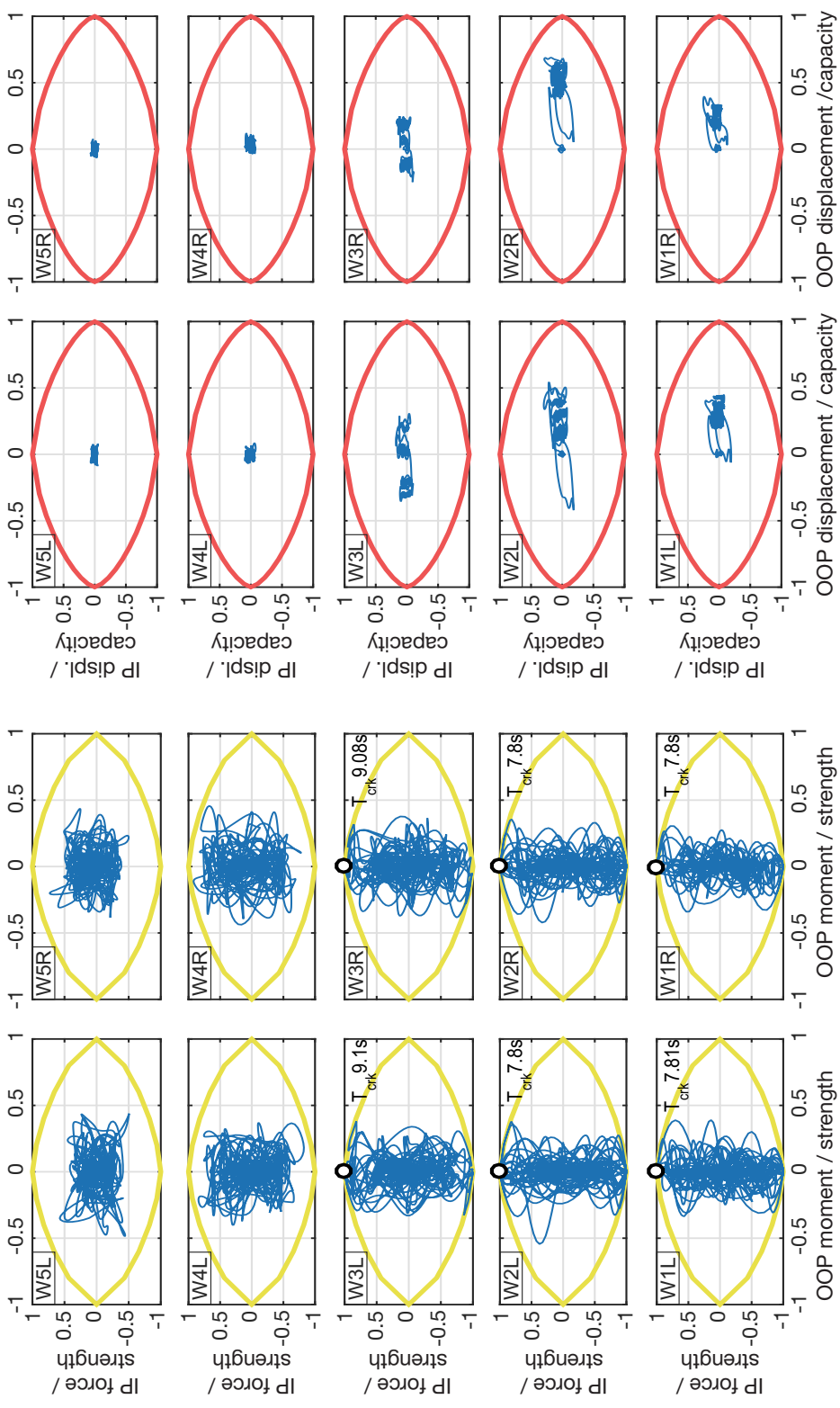

*Fig. 5.23Force and displacement paths of infill walls in frame **5×3_115S** for analysis **EQ06** scaled to a_g = **0.25g***

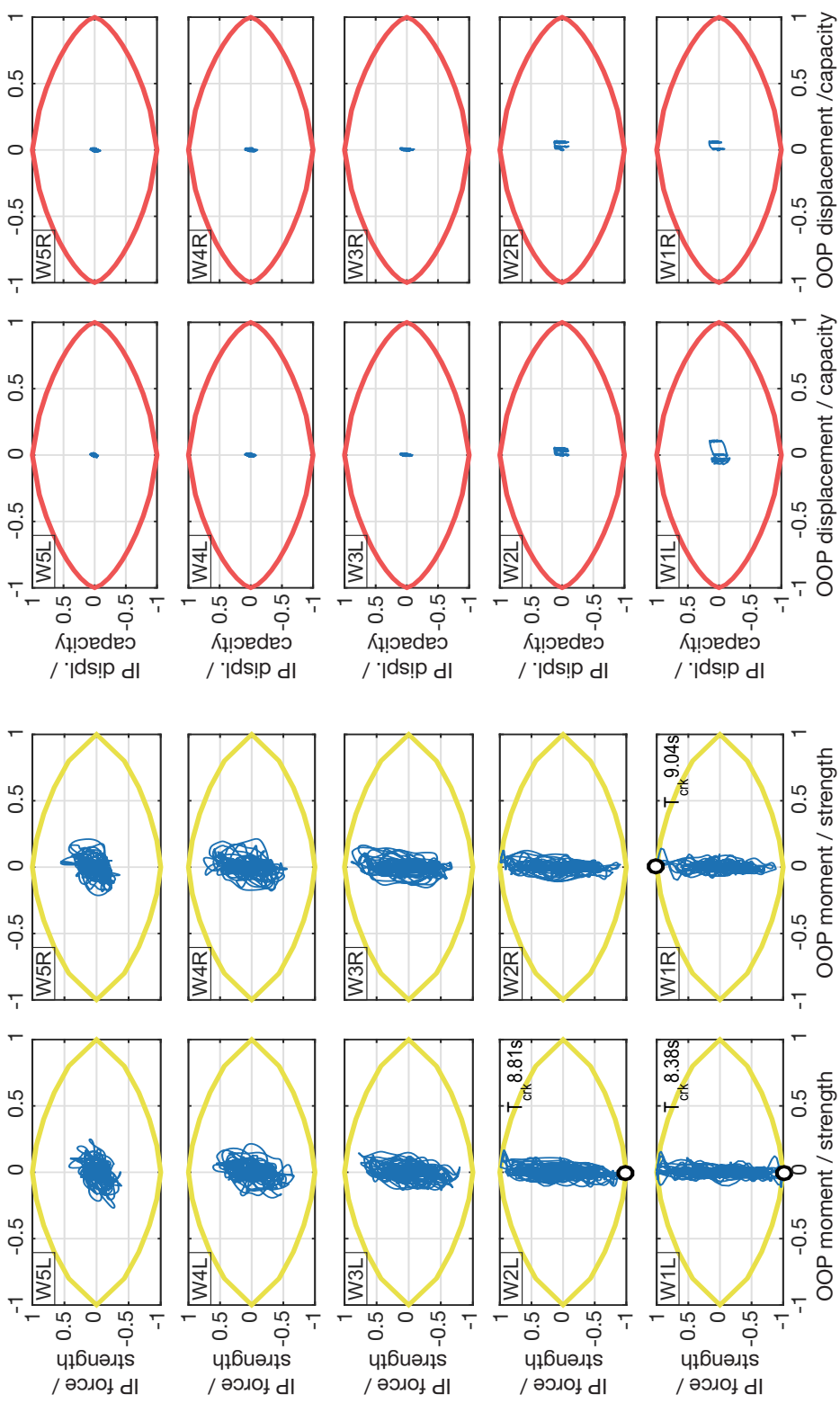

Fig. 5.24Force and displacement paths of infill walls in frame ***5×3_300S*** *for analysis* ***EQ06*** *scaled to* a_g **= 0.25g**

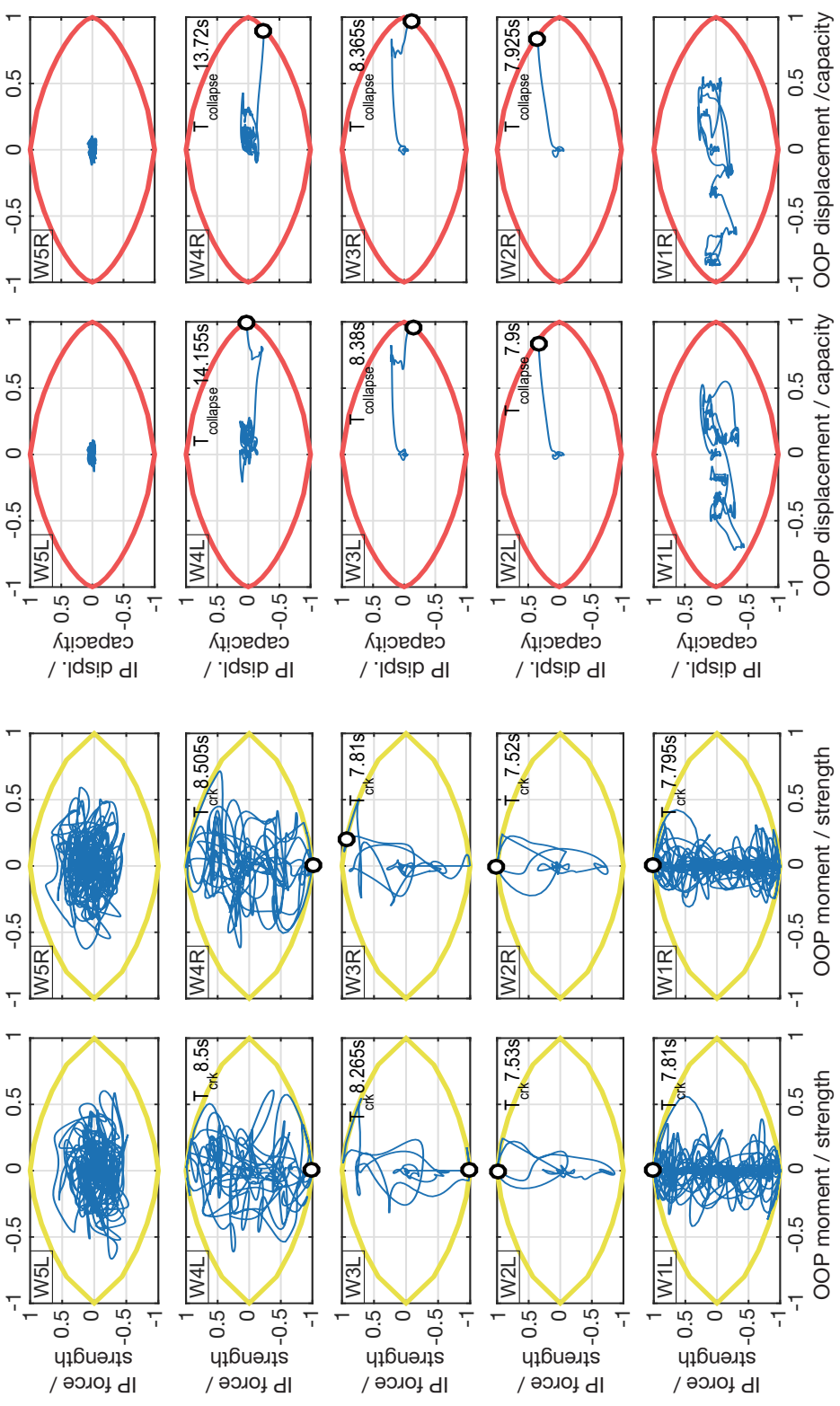

Fig. 5.25Force and displacement paths of infill walls in frame ***5×3_115T*** *for analysis* ***EQ06*** *scaled to* a_g **= 0.35g**

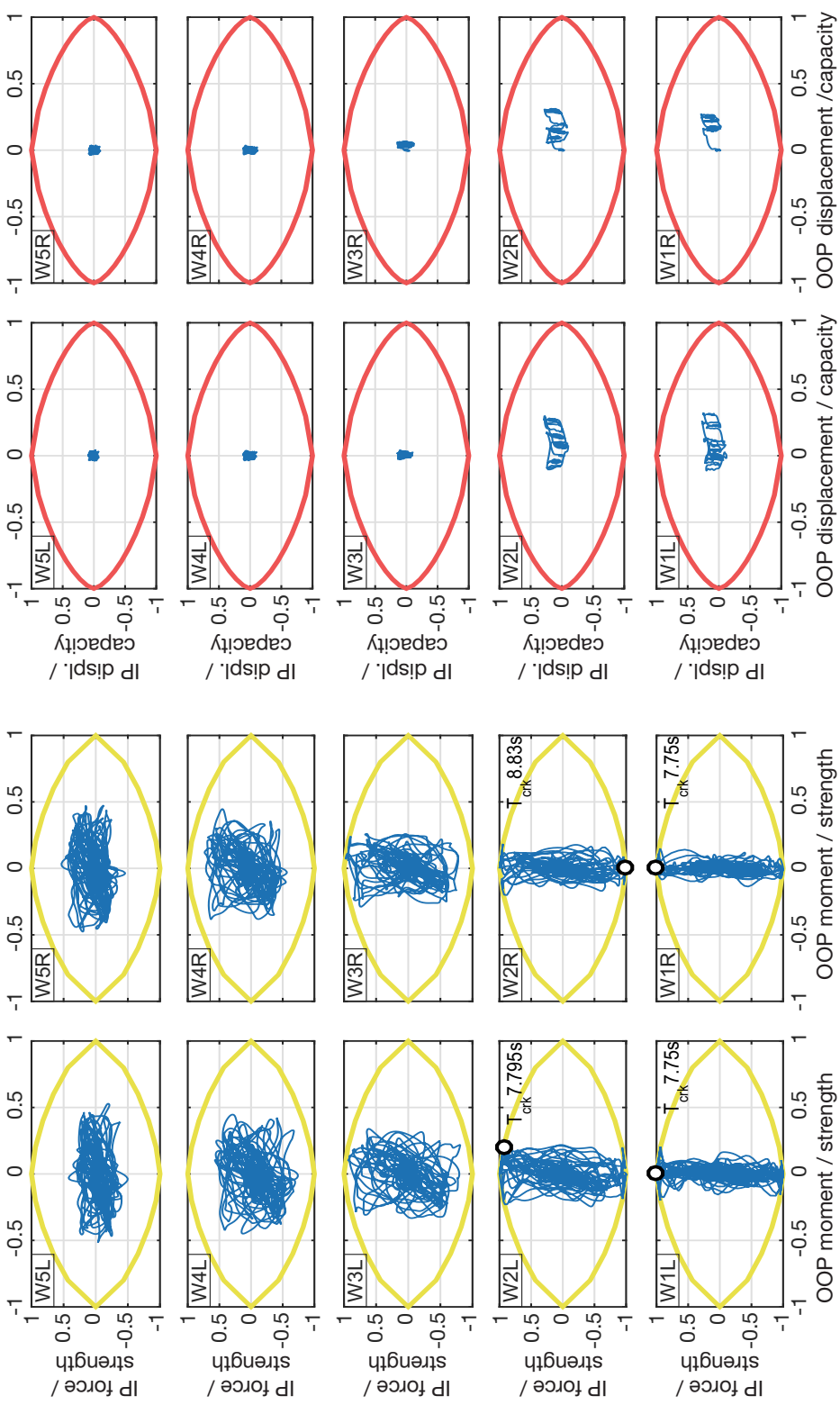

Fig. 5.26Force and displacement paths of infill walls in frame ***5×3_300T*** *for analysis* ***EQ06*** *scaled to* a_g **= 0.35*g***

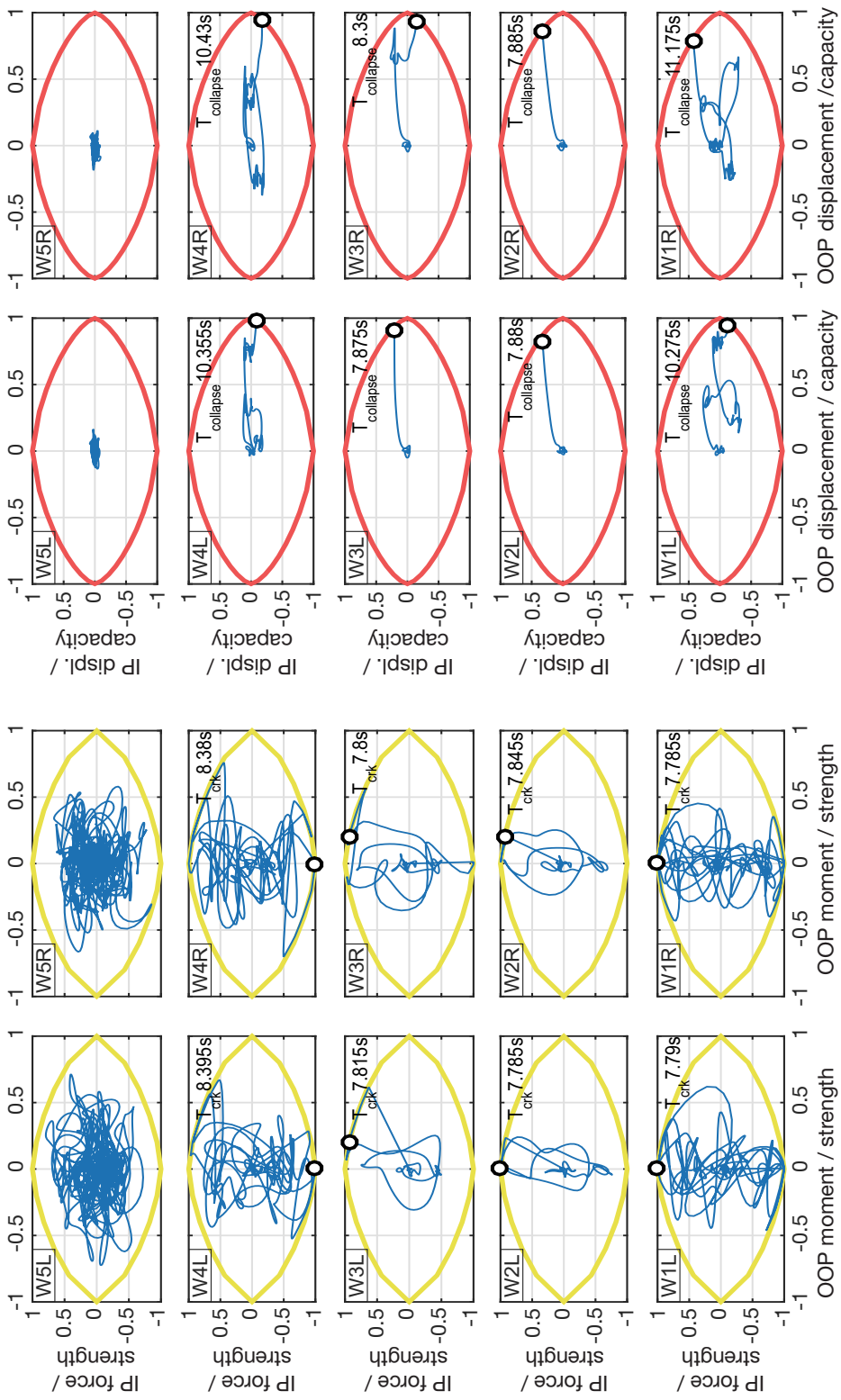

Fig. 5.27Force and displacement paths of infill walls in frame ***5×3_115S*** *for analysis* ***EQ06*** *scaled to* a_g **= 0.35g**

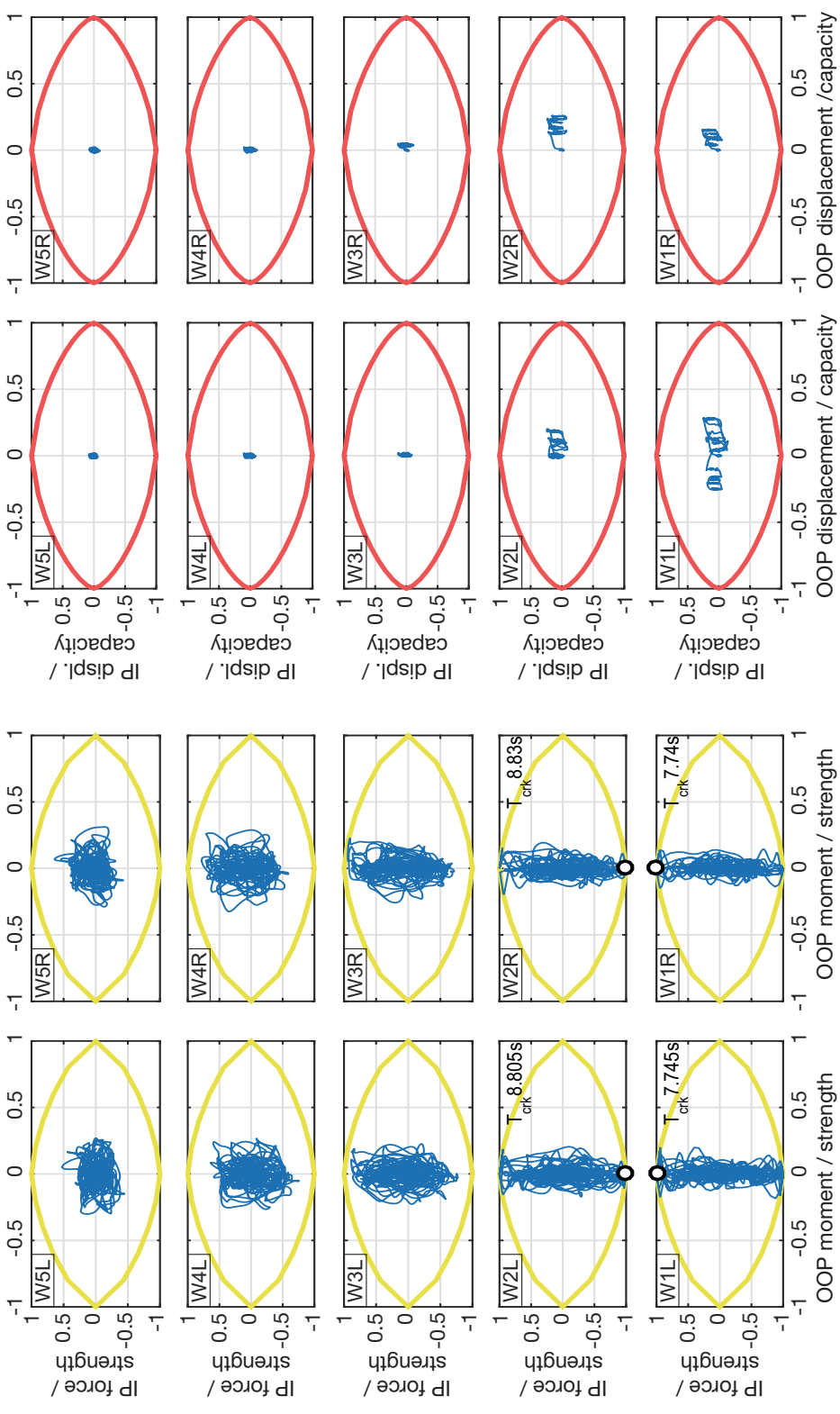

Fig. 5.28Force and displacement paths of infill walls in frame ***5×3_300S*** *for analysis* ***EQ06*** *scaled to* a_g **= 0.35g**

5.2.2 Discussion of the force and displacement history paths

When a force history path does not reach the force interaction domain, the wall can be considered to be undamaged or to have sustained very light damage (below major cracking) through the analysis. This state can be observed on most of the walls for the analyses at the lowest scale factor, a_g = *0.15g* (Fig. 5.5-Fig. 5.8). The force path series show that undamaged walls are generally loaded to a higher proportion of their in-plane strength compared to their OOP strengths. This is visualized by the concentration of the force paths along the vertical line at the center of the force domains, and is particularly evident at the first and second stories. This observation applies to both panel thicknesses, albeit to a different extent. In fact, this trend is stronger for the 300 mm thick walls, which, having a considerably greater OOP stiffness, are subject to smaller OOP displacements, leading to lower forces. This remains also true in spite of the greater mass of the thick walls, which, conversely, tend to increase the OOP forces. The thinner 115 mm infills reach a more similar proportion of their strengths in the IP and OOP directions, with the upper stories force paths occupying almost uniformly the force interaction domain.

As a direct consequence of the pre-cracking behaviour observed in force paths, the actual cracking of the panels is dominated by in-plane forces caused by the lateral drift of the frame at the lower stories, with the dot indicating panel yielding normally located almost exactly at the IP strength limit without any OOP effects. The only exceptions to this tendency can be seen in the force paths related to the 5×3 frame configuration at the highest scale factor (a_g = *0.35g),* where a few walls at the second and third storeys exhibit a modest OOP bending component at cracking (Fig. 5.25-Fig. 5.27). This is in good agreement with many experimental remarks of the high OOP strength demonstrated by intact (non-cracked) URM panels (Angel et al. 1994; Abrams, Angel, and Uzarski 1996; Flanagan and Bennett 1999b).

No cracked panels were detected at the top storey of the 3×3 frames and at the top two storeys of the 5×3 models. No substantial differences in the force paths and cracking point are observed between traditionally (_T) and seismic (_S) designed RC members. However, these preliminary observations will be discussed more in depth in section 5.3, where the results from more analyses will be included.

Comparing the force path histories with their corresponding displacement counterparts, it can be seen that panels that do not reach yielding, mostly located at the top stories, maintain low displacements through the analysis, well below their ultimate displacement limits and concentrated in the inner part of the displacement domain. Conversely, infills where cracking occurs have in most cases much larger displacements both IP and OOP, and those that reach their ultimate displacement

capacity do so by a combination of IP and OOP displacements, with the OOP component playing the dominant role. For example, this can be seen observing in Fig. 5.21 and Fig. 5.25 that usually the dot representing collapse has a greater OOP displacement component than IP.

Wall collapses for the 3×3 frames were detected only at the highest scale factor (a_g *= 0.35g)* and the 115 mm thick URM walls (Fig. 5.13 and Fig. 5.15), involving all the infill panels at the first and second storeys, with no evident differences between traditionally and seismic designed frames. In the 5×3 configurations, collapse involved the 115T walls at the second and third storeys for the ground motions scaled at a_g *= 0.25g* (Fig. 5.21); displacements of the walls of the 115S frame were near the ultimate capacity, with high OOP components, but did not reach the displacement interaction curve. At a_g *= 0.35g,* the walls collapsed on all but the top storey in the 115T frame (Fig. 5.25), and on 2nd, 3rd and 4th storeys in the 115S frame (Fig. 5.27), with the displacements of walls at first storey just short of reaching failure. As expected, the thicker panels, which have significantly higher OOP stiffness, have much smaller displacements and are much less prone to collapse during a given ground motion.

Concerning the registered time of cracking (T_{crk}), in most cases both walls on a given time storey reach cracking at the same time step or, when one wall reaches cracking first, the other panel follows very shortly after (1-4 time steps). A few exceptions were observed where the second wall collapsed many time steps after the first (e.g. as in Fig. 5.17 and Fig. 5.21), or only one wall in a storey cracked during the analysis (e.g. as in Fig. 5.7 and Fig. 5.19). The time of collapse ($T_{collapse}$) is recorded very shortly after the T_{crk} in a few cases, especially for the first walls to experience cracking on the frame (e.g. Fig. 5.25, walls W2L/W2R and W3L/W3R), but more commonly collapse occurs a few seconds later than the cracking, as in Fig. 5.21, and the hysteresis of the wall displacements is appreciable on the corresponding displacement path plot. This results matches well to the notion that infill walls provide a significant source of energy dissipation in buildings during ground motions (Ozkaynak et al. 2013).

The fact that in some instances the response of the infilled frames is not perfectly symmetric at any given storey with respect to the infilled outer bays is not abnormal because, even if the planar frames considered are conceptually symmetric, their computational model is not, with just one diagonal representing each wall. However, the differences between same-storey walls observed in the force and displacement paths and in the resulting cracked and collapsed panels are overall quite minor, as it should be expected for symmetric structures.

Similar results were obtained for most records that were analysed. However, displaying the results from all the analyses with the wall history paths would have been repetitive without providing additional general conclusions. Therefore, the results were condensed in a more compact graphic representation, as presented in the next section.

5.3 Damage patterns of URM infill walls

5.3.1 Description of the damage grids

In order to show efficiently the results on the infill walls from all the analyses (EQ01-EQ10) and frame configurations, a compact graphic representation is suitable. The URM infill walls were categorized in three classes based on the damage sustained by the end of each analysis: undamaged / light damaged, cracked and collapsed walls. This data is visualized on the damage grids shown in Fig. 5.29 for the 3×3 frame models and in Fig. 5.31 for the 5×3 frame models. Each grid schematizes a planar frame, with the tiles representing the walls and their colour identifying the damage status at the end of one analysis. The grids are subsequently grouped in blocks of grids based on the Model ID (as listed in Table 3.1), with each block comprising 30 grids from the ten bi-directional ground motion inputs and the three scale factors.

The natural ground motion recordings used in the analyses produce quite variant outcomes in terms of damage to the walls. For example, for a given scale factor and frame configuration, EQ02 and EQ05 analyses cause a smaller amount of cracked and/or collapsed walls compared to EQ04 and EQ10. In this regard, scaling the natural GM records to match the PGA is not providing a particularly good indication of damage levels, but the trends of damage patterns are still clear. Moreover, given the bidirectional nature of the seismic input, the results are also influenced by the orientation of the components in the IP and OOP directions. In order to partially deal with this aspect, all the analyses were repeated inverting the D1 and D2 components of each ground motion of the suite as listed previously in Table 4.3. The series of analysis with the original IP/OOP orientation of the ground motion components is labelled with “Or1”, while the series with the components reverted is designated with “Rev”. The damage grids for the “Rev” analyses are shown in Fig. 5.30 for the 3×3 frame models and in Fig. 5.32 for the 5×3 frame models. Compared to Fig. 5.5-Fig.

5.28, the results of the “Rev” analyses, even if different on an analysis by analysis comparison, did not alter the general trends observed in the force and displacement history paths of the URM infill walls.

Table 5.2 summarizes the orientation of the ground motion (GM) components used in the “Or1” and “Rev” series of analyses and points to the corresponding damage grids figures. Aggregating the blocks of grids, there are 120 damage grids per Figure. Combining the analyses obtained with both the orientations of the components, 240 grids are related to both the 3×3 and 5×3 configurations, with 120 grids for each panel thickness and RC frame design typology.

Orientation	Ground motion components		Damage grid figures	
series	IP	OOP	3×3 frames	5×3 frames
“Or1”	-D1	-D2	Fig. 5.29	Fig. 5.31
“Rev”	-D2	-D1	Fig. 5.30	Fig. 5.32

Table 5.2 Summary of the orientation of the GM components applied in the series of analyses and corresponding damage grids figures.

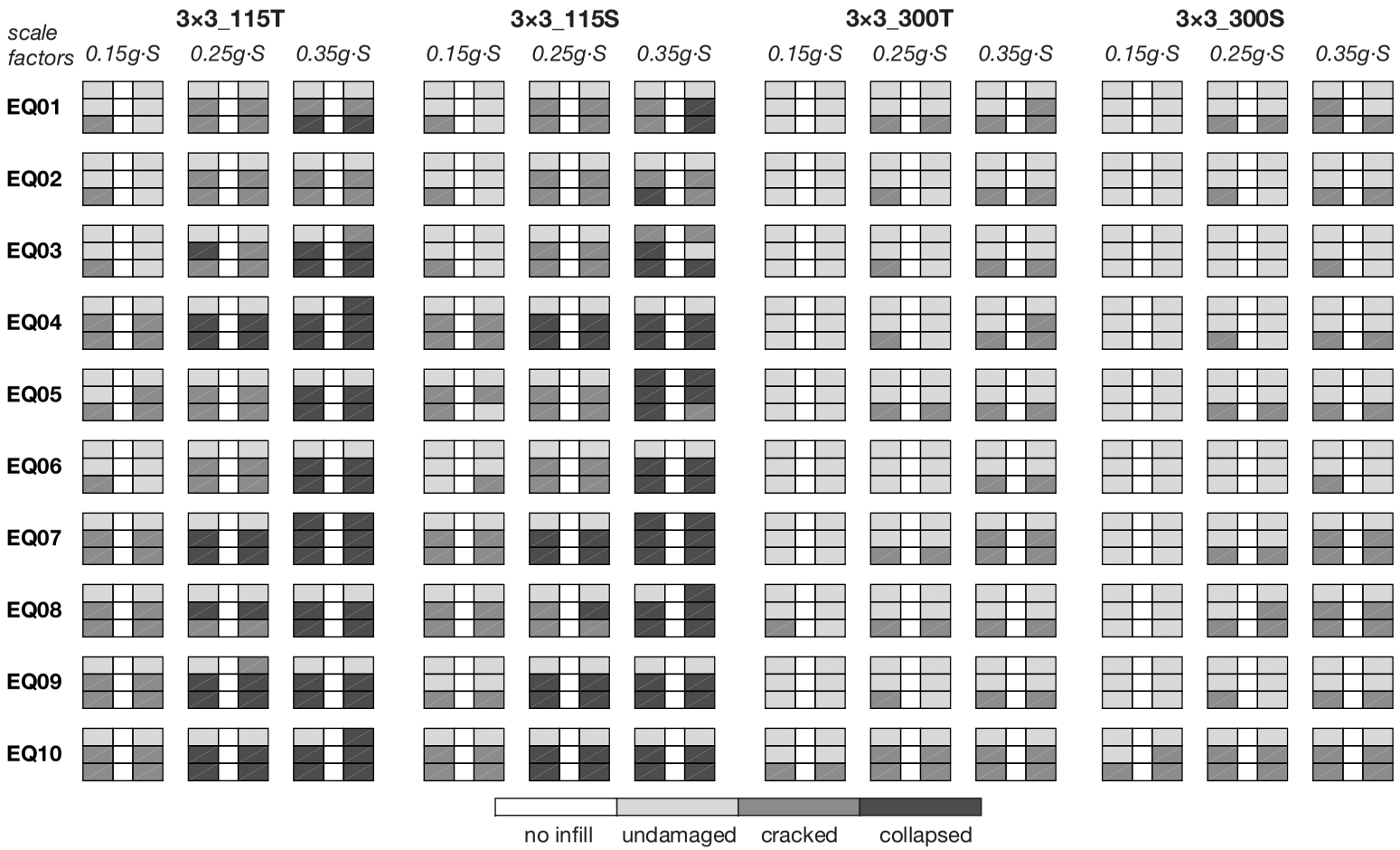

*Fig. 5.29Damage of the infill walls in the **3×3** frame models at the end of the bi-directional analysis with **Or1** orientation of the GM components.*

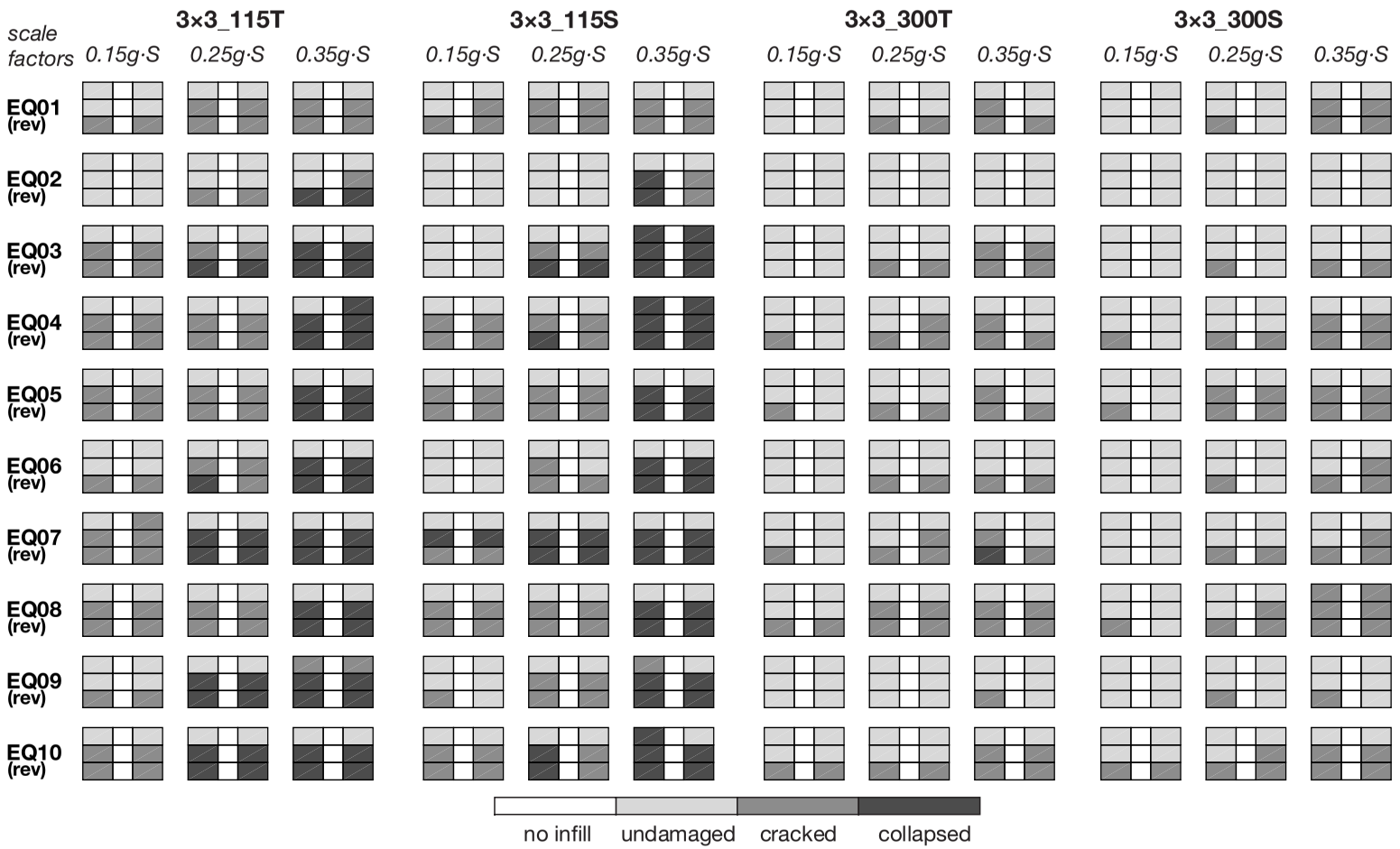

*Fig. 5.30Damage of the infill walls in the **3×3** frame models at the end of the bi-directional analysis with **Rev** orientation of the GM components.*

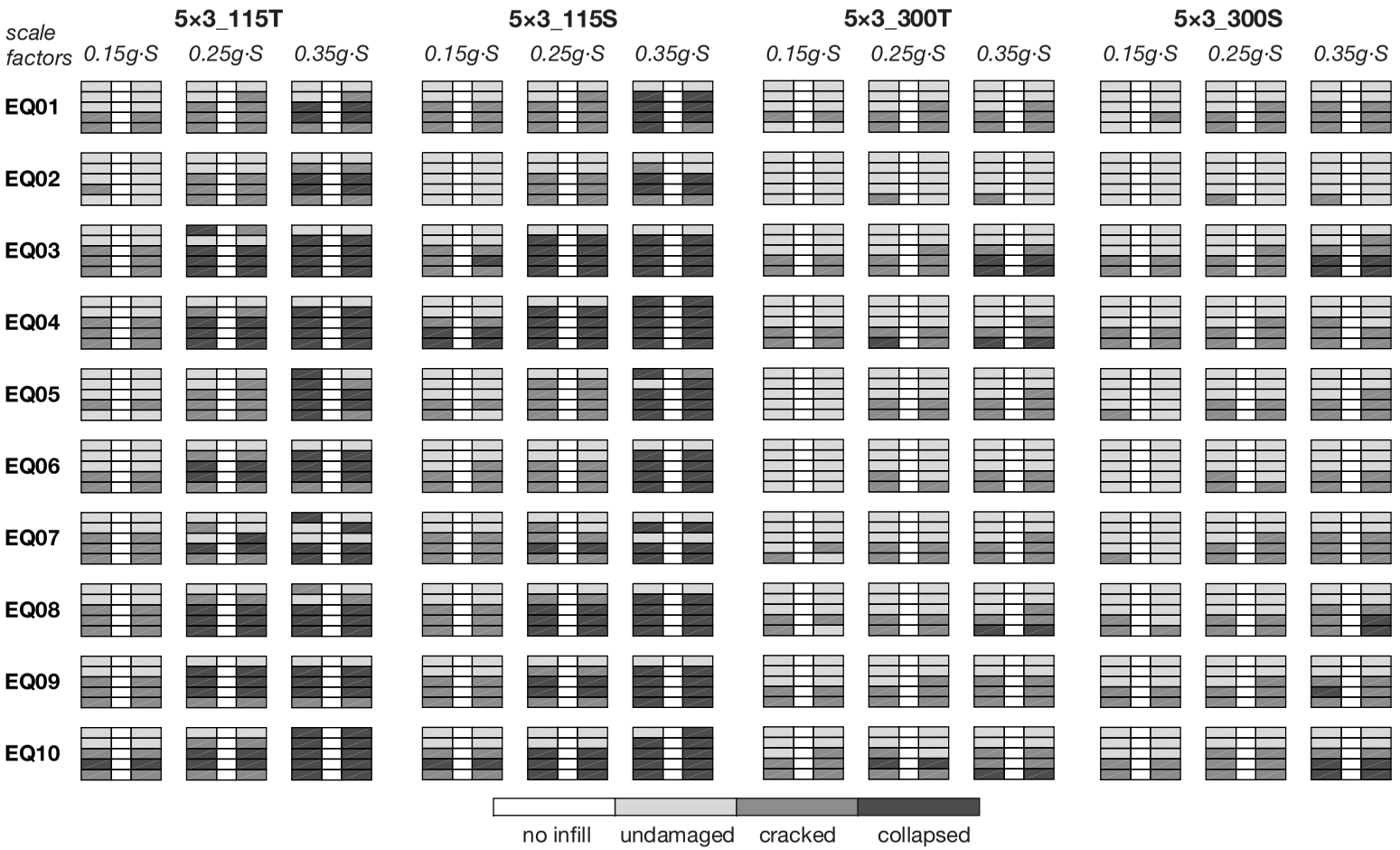

*Fig. 5.31Damage of the infill walls in the **5×3** frame models at the end of the bi-directional analysis with **Or1** orientation of the GM components.*

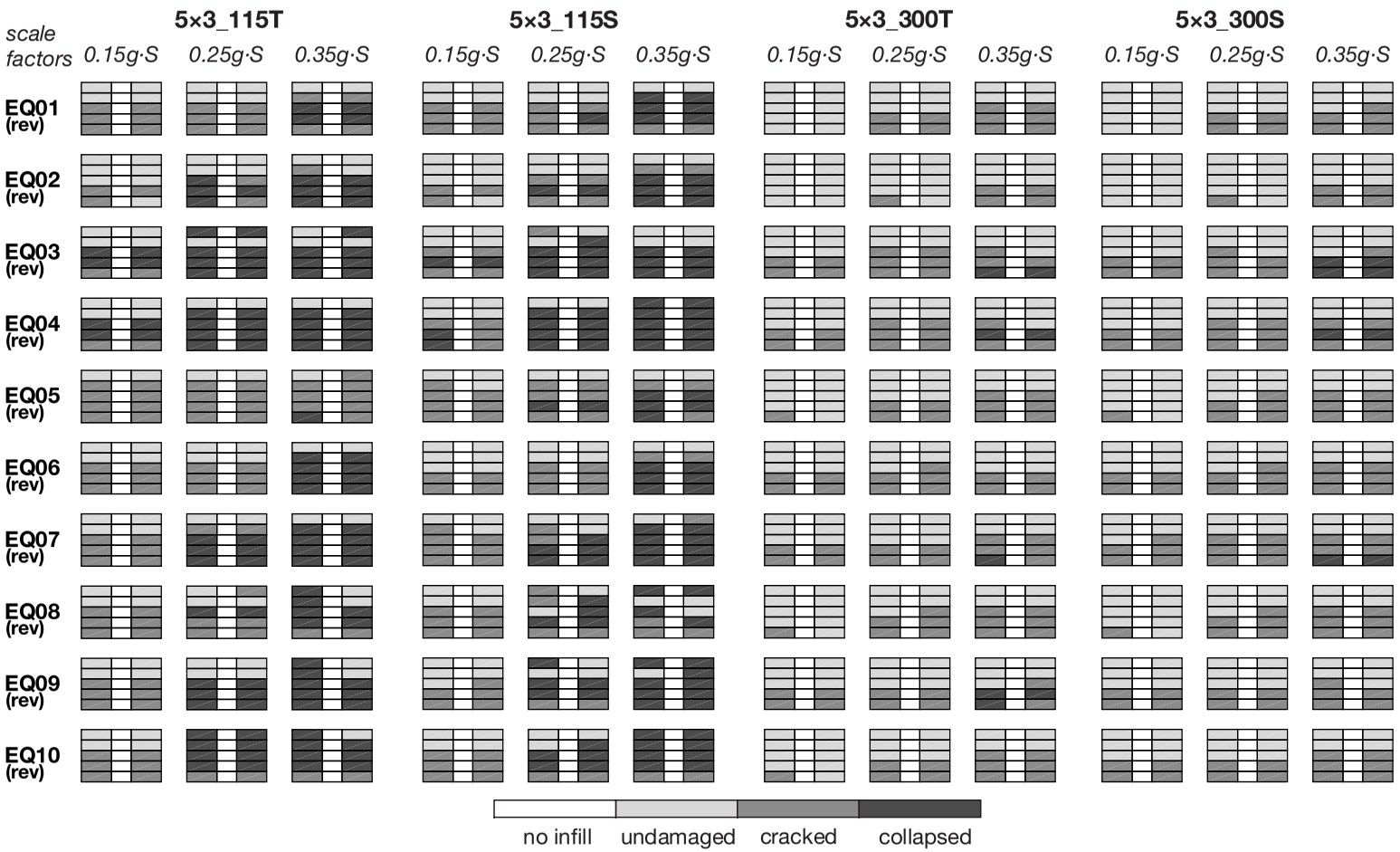

*Fig. 5.32Damage of the infill walls in the **5×3** frame models at the end of the bi-directional analysis with **Rev** orientation of the GM components.*

5.3.2 Discussion of the damage patterns

As noted previously for the history paths related to EQ06 analyses, damage to infill walls is notably higher for the thinner URM panels in all the analyses (EQ01-EQ10, and repeated for the reversed orientation of the components) and scale factors. This generalization, can be particularized for cracking and collapsing occurrences.
Frames without any infill wall reaching cracking by the end of the analyses comprise only six buildings infilled with the 115 mm panels (subdivided in five 3×3 and one 5×3 configurations), and 45 buildings infilled with the 300 mm panels (partitioned between 36 3×3 and 9 5×3 configurations). Additionally, with the only exception of analysis EQ08(rev) scaled at a_g = *0.35g*, no wall reached cracking in the top storey of frame configurations 3×3_300; similarly, there are not any cracked walls in the top two storeys of frame configurations 5×3_300. The same outcomes do not occur in the 3×3_115 (e.g. EQ09(rev) scaled at a_g = *0.35g*) and 5×3_115 (e.g. EQ08 scaled at a_g = *0.25g* and a_g = *0.35g*).
Table 5.3 reports the number of damage grids with at least one collapsed tile. Each entry on the rows with a single orientation of the GM components ("Or1" or "Rev") is related to 10 analyses (EQ01-10 and the EQ01(rev)-EQ10(rev)), therefore the rows that sum both the orientations are associated with 20 analyses.

$a_g \cdot S$ =	Components	3×3				5×3			
	Orientation	115T	115S	300T	300T	115T	115S	300T	300S
0.15g·S	Or1	0/10	0/10	0/10	0/10	1/10	3/10	0/10	0/10
	Rev	0/10	1/10	0/10	0/10	2/10	2/10	0/10	0/10
	Or1+ Rev	0/20	1/20	0/20	0/20	3/20	5/20	0/20	0/20
0.25g·S	Or1	6/10	5/10	0/10	0/10	7/10	6/10	2/10	0/10
	Rev	5/10	4/10	0/10	0/10	7/10	9/10	0/10	0/10
	Or1+ Rev	11/20	9/20	0/20	0/20	14/20	15/20	2/20	0/20
0.35g·S	Or1	9/10	10/10	0/10	0/10	10/10	10/10	4/10	4/10
	Rev	9/10	9/10	1/10	0/10	10/10	10/10	4/10	3/10
	Or1+Rev	18/20	19/20	1/20	0/20	20/20	20/20	8/20	7/20
All	Or1	15/30	15/30	0/30	0/30	18/30	19/30	6/30	4/30
	Rev	14/30	14/30	1/30	0/30	19/30	21/30	4/30	3/30
	Or1+ Rev	29/60	29/60	1/60	0/60	37/60	40/60	10/60	7/60

Table 5.3 Number of frames with at least one collapsed wall.

Collapses occur almost exclusively with the thinner infill panels. In fact, no collapses happened on the 3×3_300 configurations even for the highest scaled ground motions

(with the only exception of one collapsed wall for EQ07(rev) scaled at a_g = *0.35g)*, and only few failures interested the 5×3_300. On the contrary, on the 3×3_115 and 5×3_115 configurations collapse involve a good number of panels at a_g = *0.25g*, and a majority of them at a_g = *0.35g.* Grouping together the results of both _T and _S designed frames, collapse occurred in 58 and 77 out of 120 frames for the 3×3_115 and 5×3_115, respectively, and in only 1 and 17 out of 120 frames for the 3×3_300 and 5×3_300, respectively.

The propensity of lower storeys to sustain damage first, already shown for the path histories of EQ06, is also confirmed throughout the ground motion suite and inverting the ground motion components, by considering the damaged wall patterns on the frames the at the end of the analysis. Interestingly, even though damage is clearly concentrated in the lower storeys, the most damaged walls are not necessarily at the lowest levels. This numerical result is seen most clearly in the five-storey frames, in which, out of 94 frames with at least one collapsed wall, 33 have both the panels at the first storey that did not reach collapse. Additionally, in the three-storey frames, the same happened in 4 out of 59 frames with collapsed walls. This result is also consistent with observed damage during previous earthquakes (e.g. Fig. 2.1). An explanation for this behaviour is linked to the combined IP/OOP interaction on the walls. The IP plane forces are proportional to the building lateral drift and therefore generally decrease with increasing frame height. However, the OOP actions on the equivalent elements are proportional to the inertia forces on the walls, which increase with the height of the panels on the building. Therefore, the effects of the combined actions on the walls can be maximised on a storey higher than the first, even though IP actions would usually dictate the failure of the walls at the base level of the building. Moreover, if the combined actions trigger the first collapse on the second-storey walls, the panels at the ground level are even more likely to avoid collapse during the rest of the analysis because a soft storey is created above the first level, which prompts a significant reduction in the lateral drift of first storey. The damage grids show the formation of a soft storey at the second level in several cases (e.g. analyses EQ08 scaled to 0.25*g*·*S* on frame 5×3_115S and EQ06 scaled to 0.25g·S and 0.35*g*·*S* on frame 5×3_115T) and, in one instance (EQ08(rev) scaled to 0.25*g*·*S*), at the third storey of the building.

In very few cases, (4 three-storey and 3 five-storey frames) all the walls of the building reached collapse for the highest scaled ground motions; all instances related to 115 mm thick panels. More general and aggregated statistics about the number of walls that cracked or collapsed during the analyses will be presented in section 5.4. In general, it can already be said that the suite of scaled ground motions showed realistic levels of damage to the URM infill walls on the frame structures when

compared with observations of damage to URM infill panels after recent seismic events.

The apparent small influence of RC members design on the damage sustained by URM infill walls, already observed in the damage paths related to analyses with EQ06, is confirmed on the larger pool of data represented in the damage grids. When comparing the damage grids resulting from a given analysis/scale factor applied to a frame models differentiated only by the RC design of the beam and columns, the results can be different on a wall-by-wall basis, but are very similar (and in some cases identical) when considering the whole planar frame. Aggregating the data from multiple analyses reinforce this observation. For example, as reported in Table 5.3, there is no strong influence on the number of frames with at least one collapsed wall between traditionally (_T) and seismic (_S) designed RC frames. Compared to (_S) designed RC members, (_T) RC members cause a few more occurrences of frames with collapses when 300 mm infill walls are considered; however, such relation does not hold, and is in fact reversed in few cases, when 115 mm walls are considered. More analyses would be needed to confirm these slight correlations. Particularly, more conspicuous differences between the designs assigned to traditional and seismic RC members should be taken into account, but this kind of parametric study is outside the scope of present work.

5.3.3 Discussion on the influence of ground motions orientation

In 5.3.1, it was already anticipated that different pairs of ground motions, even when scaled at the same intensity level, can have significantly different outcomes on a given infilled frame model. This remark is however true in all applications of dynamic time-history seismic analysis by means of natural or artificial records, because the great variability of the inputs is an intrinsic feature of ground motions. In fact, this is also the main reason why dynamic seismic analyses should comprise sets of dynamic inputs to perform multiple analyses, as suggested by the authors referenced in 4.3.1 (e.g. (Beyer and Bommer 2007; Iervolino, Maddaloni, and Cosenza 2008)) and was done in this research. Notwithstanding the influence of dynamic properties of the input ground motions (e.g. frequencies, elastic spectra, soil amplification, etc.) on the damage sustained by the walls, studying these aspects would require many more analyses and is beyond the intended scope of this work. However, considering the analyses performed with the whole suite of ground motions that was built in this research, and comparing the data from multiple analyses, the results are tangibly consistent with experimental results and post-earthquake damage surveys about

URM infill walls response. Moreover, the full set of results shown in this section enables to draw a few noteworthy observations from the comparison of analyses with ground motion components switched between IP and OOP directions. Fig. 5.29-Fig. 5.30 for the 3×3 frame configuration and Fig. 5.31-Fig. 5.32 for the 5×3 frame configuration are compared paralleling the result of each EQxx (“Or1”) analysis and its EQxx(rev) counterpart. In the three-storey frames, 4 EQ analyses with “Or1” orientation (EQ01, EQ04, EQ08 and EQ09) have more frames with at least one collapsed wall compared to the matching “Rev” analysis with switched IP/OOP components, 3 (EQ02 EQ06 and EQ07) have an equal number and 3 (EQ03, EQ05, EQ10) have less. Comparing the results for the five-storey-frames likewise, 4 EQ analyses with “Or1” orientation (EQ05, EQ06, EQ08 and EQ10) have more, 1 (EQ09) has equal and 5 have less (EQ01, EQ02, EQ03, EQ04 and EQ07) frames with at least one collapsed wall compared to the matching “Rev” analysis with switched IP/OOP components. Firstly, it is worth noting that the D1 and D2 components of the suite of natural ground motion were arbitrarily assigned to the IP and OOP directions of the planar frame for the “Or1” analyses and at the opposite for the “Rev” analysis. Additionally, the directions of the horizontal components of the natural records are randomly rotated with respect to the principal directions of the seismic event. The dependency of ground motion representation on the orientation when bi-directional analyses are performed has been the subject of in-depth studies (Hong and Goda 2007), but is outside the scope of this work. However, the fact that the effects on the URM infill walls are overall equally distributed between the “Or1” and “Rev” sets of analysis suggest that the number of ground motion selected for the suite is adequate. This observation will be recalled also in 5.4.2, where the data from the two sets of analyses is presented both separately and aggregated in bar plots. More specifically, EQ08 causes consistently more damage to the infill walls than EQ08(rev), and the same is true for EQ02(rev) and EQ07(rev) versus the “Or1” oriented EQ02 and EQ07. For the other ground motions, differences are less marked overall, but can be still significant on a single RC frame with URM infill walls. Therefore, the repetition of the analyses with the ground motion components inverted appears to reduce significantly the chance of overlooking specific combinations of IP/OOP actions that cause more damage to the infill walls. In any case, further studies are required to investigate the influence of the ground motion components applied to the IP and OOP directions of infilled frames in bi-directional dynamic analyses.

5.4 Frequency of damage

5.4.1 Description of the bar plots

In this section bar plots are used to summarize the results from all the analyses performed, and in particular the data previously displayed with the damage grids. Fig. 5.33-Fig 5.36 mirror the results from damage grids shown in Fig. 5.29-Fig. 5.32, considering the “Or1” and “Rev” series of analyses separately. Fig. 5.37 and Fig. 5.38, instead, aggregate the results from both the series, for the 3×3 and 5×3 frame configurations respectively.

Each stacked bar displays the damage condition of all the walls in the frame models at the end of the analysis. Since the discussion of the results focuses on the damage of URM infill walls, the bars representing the collapsed panels are placed at the bottom, followed by the walls that cracked in the middle, and the undamaged/lightly damaged infills counted on the top.

To compare the results between different batches of analyses, the bars are normalized by the total number of walls they comprise, resulting in a dimensionless frequency of damage. The total number of walls represented by each bar is different between the bar plots, depending on the frame configuration and number of analyses. The bars that refer to the 3×3 models (6 walls per frame) and to the results of the EQ01-EQ10 analyses taken with just one orientation of the input ground motions (“Or1” or “Rev”) comprise 60 walls (Fig. 5.33-Fig. 5.34); consequently, the plot for the same frame configuration and the aggregated data for both orientations (Fig. 5.37) comprise 120 walls per bar. Similarly, in the 5×3 models (10 walls per frame), that sum up to 100 and 200 walls per bar for single (Fig. 5.35-Fig. 5.36) and aggregated (Fig. 5.38) orientations, respectively.

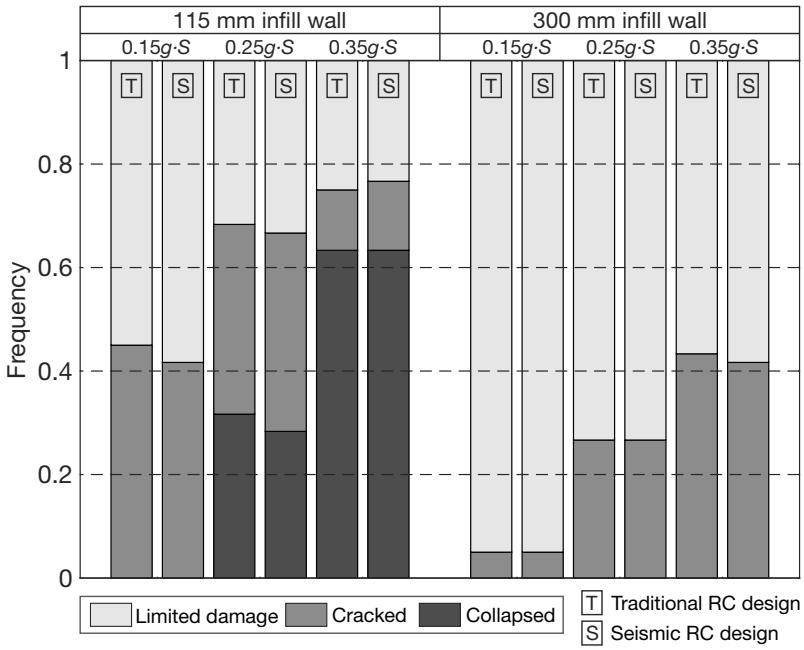

*Fig. 5.33Frequency of damage to the infill walls at the end of the analyses for **3×3** frame configurations. Aggregated data from EQ01-10 ground motions with "**Or1**" orientation of the ground motion components.*

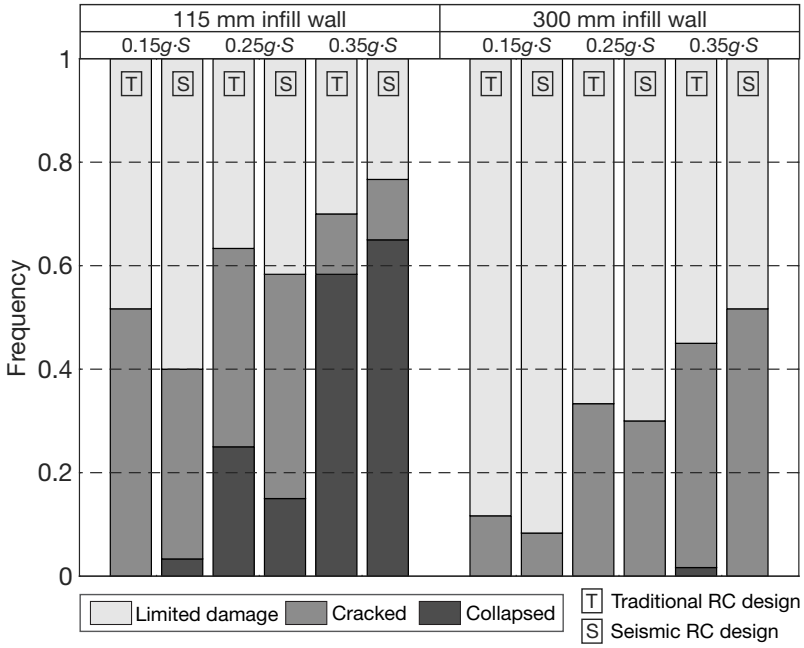

*Fig. 5.34Frequency of damage to the infill walls at the end of the analyses for **3×3** frame configurations. Aggregated data from EQ01-10 ground motions with "**Rev**" orientation of the ground motion components.*

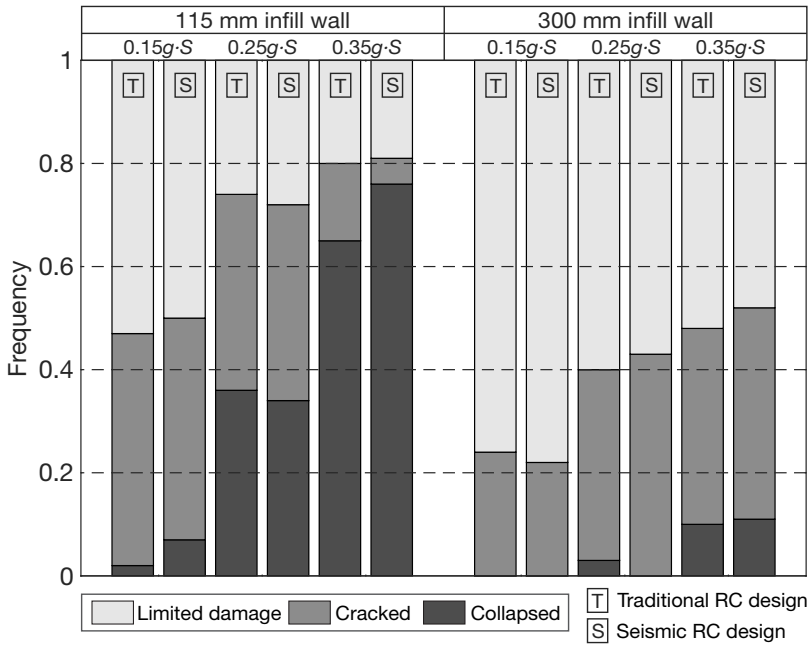

*Fig. 5.35Frequency of damage to the infill walls at the end of the analyses for **5×3** frame configurations. Aggregated data from EQ01-10 ground motions with "**Or1**" orientation of the ground motion components.*

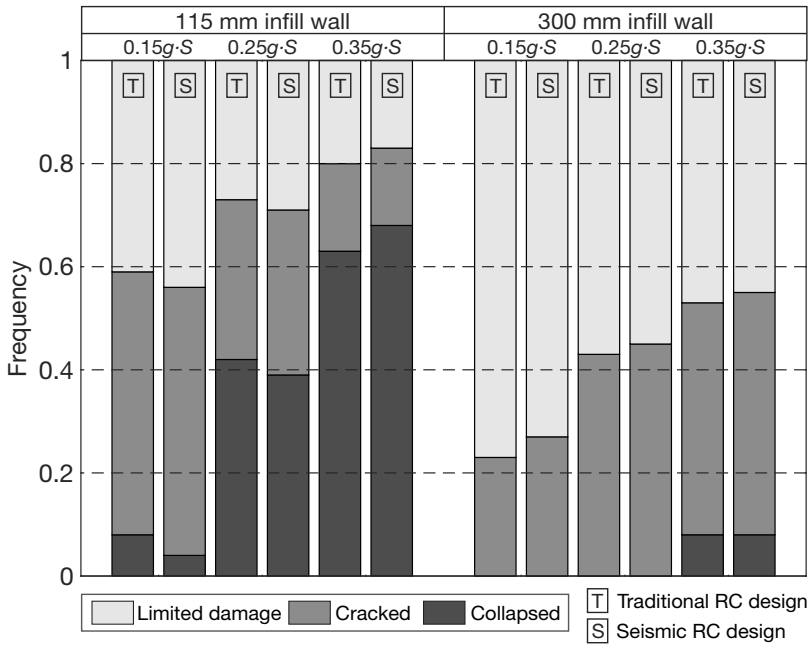

*Fig. 5.36Frequency of damage Frequency of damage to the infill walls at the end of the analyses for **5×3** frame configurations. Aggregated data from EQ01-10 ground motions with "**Rev**" orientation of the ground motion components.*

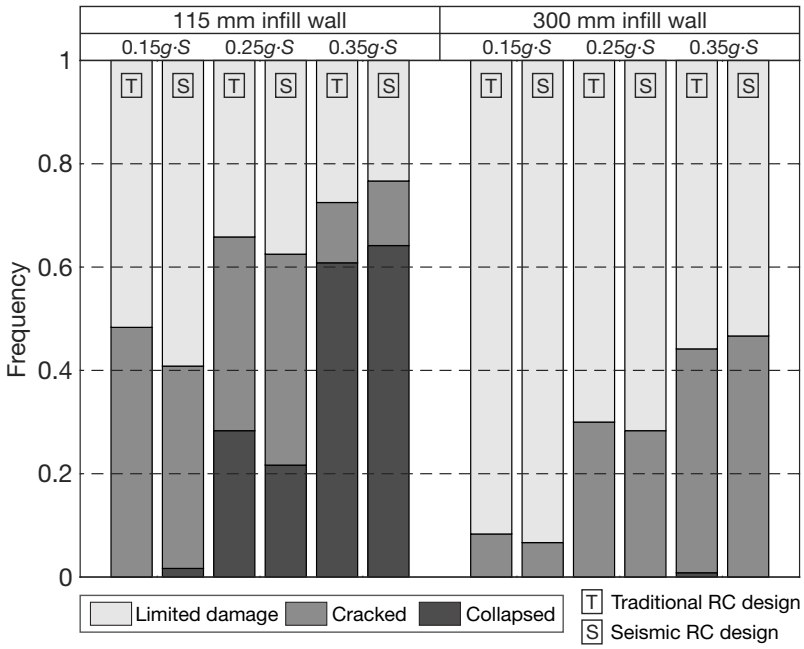

*Fig. 5.37Frequency of damage to the infill walls at the end of the analyses for **3×3** frame configurations. Aggregated data from EQ01-10 ground motions, considering both "**Or1**" **and** "**Rev**" orientations of the ground motion components.*

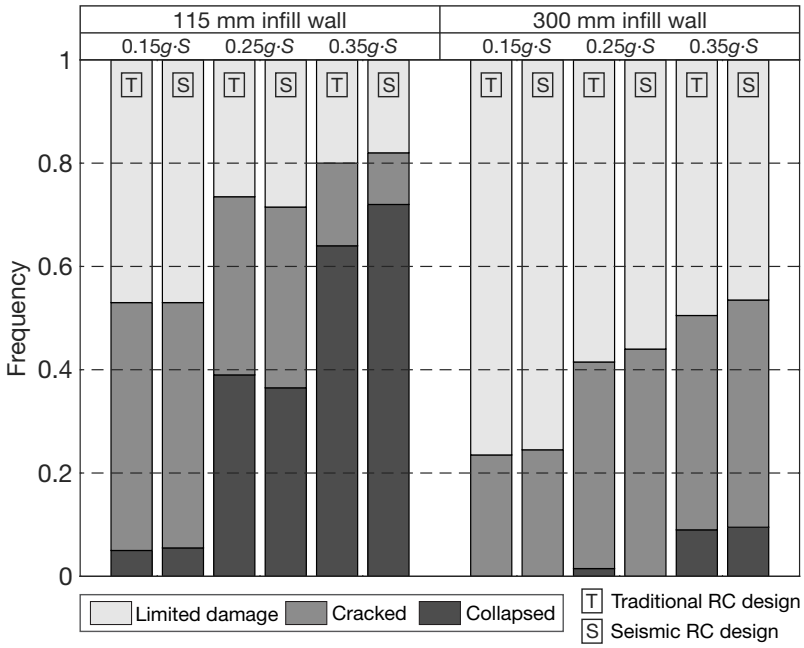

*Fig. 5.38Frequency of damage to the infill walls at the end of the analyses for **5×3** frame configurations. Aggregated data from EQ01-10 ground motions, considering both "**Or1**" **and** "**Rev**" orientations of the ground motion components.*

5.4.2 Discussion of the results

First, it is worth comparing the aggregated results of analyses EQ01-EQ10 to the results from EQ01(rev)-EQ10(rev), represented in Fig. 5.33-Fig. 5.34 for the 3×3 frames, and in Fig. 5.35-Fig. 5.36 for the 5×3 frames. It can be noted that, in spite of some variations, differences in the frequencies of collapsed and cracked walls are mostly restrained into a 10% range, and in any case do not show significant trends. Since the aggregated results obtained in the "Or1" and "Rev" sets are essentially equal, further discussion on the aggregated outputs can be limited to Fig. 5.37 and Fig. 5.38, in which the results of both the sets are combined.

The bar plots clearly show that the infill wall typology has the greatest influence on the overall damage to URM infill walls. Specifically, slender infill panels are considerably more prone to damage and failure, which is coherent with experimental results on OOP strength of URM infill walls (Anderson 1984; Dawe and Seah 1989; Abrams, Angel, and Uzarski 1996). The frequency of cracked walls is between 39% and 48% for both the 3×3 and 5×3 models at the 0.15$g{\cdot}S$ scale factor, which corresponds to a moderately low design spectrum in many Mediterranean countries. Comparatively, at the same scale factor, the 300 mm walls have rates of cracked walls around 24% and less than 10% for the 5×3 and 3×3 configurations, respectively. This result is consistent with the observations of disproportionate damage, and particularly early cracking, to URM infill walls even after relatively low seismic events (Decanini et al. 2004; Penna et al. 2013). Aside from the unacceptable economic impact, this is particularly concerning because, as shown in the IP/OOP interaction domains, once cracked the infill walls are far more susceptible to OOP failures. In turn, the infill panels response would be already compromised in case of slightly higher (but not uncommonly higher) seismic demands or potential aftershocks. Indeed, the bar plots show that at larger ground motion scale factors, the proportion of collapsed walls in the overall damaged panels (cracked and collapsed) increases significantly for both infill wall thicknesses.

The behaviour of the two panel typologies is even more distinct when considering the frequency of collapse. The 300 mm infilled structures reach a maximum rate of collapsed walls of about 10% for the five-storey frame configuration at the highest scale factor and the frequency is very low in the three-storey configuration. For the 115 mm panels, conversely, collapse frequency is already between 21% and 39% at the 0.25$g{\cdot}S$ scale factor, and in the 60%-70% range when scaled to 0.35$g{\cdot}S$. These frequencies could be interpreted approximately with wall collapses resulting in about 1 storey in 3×3 frames at the 0.25$g{\cdot}S$ scale factor and in 2 storeys at the 0.35$g{\cdot}S$ scale factor; in 5×3 frames, with wall collapses resulting in 2 and at lest 3 storeys for

the 0.25*g*·*S* and the 0.35*g*·*S* scale factor respectively. These figures are in line with the damage patterns of the infill walls observed in 5.3.
The small influence of the RC frame design was observed both in the infill wall history paths (5.2.2) and discussed with the damage grids on the frames (5.3.2). The bar plots, by aggregating the data from all the walls and the analyses, substantially confirm this numerical result, with no substantial difference or trend to be noted.

6 CONCLUSIONS

6.1 Summary

A numerical study on the seismic response of unreinforced masonry (URM) infill walls in reinforced concrete frames has been carried out considering the interaction of in-plane (IP) and out-of-plane (OOP) forces and displacements in the panels.
Firstly, the experimental and theoretical research works most relevant to the scope of this study were presented, focusing on the out-of-plane response URM infill walls, the combined IP/OOP behaviour of the panels and numerical macro-models that were proposed to consider interaction. Subsequently, a recently proposed macro-model for masonry infill walls that takes into account combined in-plane and out-of-plane actions on the panels was adopted and then calibrated with already available experimental data on two types of hollow clay masonry blocks, characterized by different thicknesses. The macro-element was then integrated in the computational model of planar frames. Eight planar frame models were generated, combining two frame configurations with different number of storeys, two significantly different infill walls thicknesses, and two types of designs for the RC frame members; these characteristics were chosen to be representative of the current building stock in Italy and other countries of the Mediterranean area. Next, a suite of ten natural bi-directional ground motions was assembled to be compatible with Eurocode 8 Type 1 elastic spectrum at three seismic intensities. Nonlinear dynamic time-history analyses were performed on the realistic planar frames with the scaled ground motions. Since the objective of the study is the seismic behaviour of URM infill walls, the results from the analyses were focused on the response of the panels. In particular, the key aspect of IP/OOP interactions taking place in URM infill walls during an earthquake was studied with force and displacement history paths enclosed in the strength a displacement domains of the panels. The damage to the URM panels subjected to the suite of ground motions was investigated by taking into account cracked and collapse patterns on the frames. The patterns were studied to evaluate the influence of the model characteristics, including wall thicknesses, number of storeys and RC

design, and of the input ground motion, the scale factor and variability of the bi-directional records. Based on the results A summary of the conclusions resulting from this study and suggestions for further research are presented in the following sections.

6.2 Conclusions

In recent years, data from experimental tests on URM infill walls that investigated the combined behaviour of in-plane and out-of-plane actions on the panels have gradually started to become more viable as the role of interaction was recognised by the engineering community. These experimental results are being used by researchers to propose new macro-models for infill walls that include IP/OOP interaction. However, the application and systematic evaluation and discussion of these models in extensive nonlinear dynamic analysis of realistic structures has not been studied yet. In this context, this research represents a step in this direction.
The inclusion of IP/OOP interaction on the response of infill walls during numerical analyses provided results that are neglected by state-of-the-art traditional macro-models that account only for IP behaviour of the panels. The following conclusions summarize the observations and findings discussed in this work. Many of the numerical results obtained from the analyses are consistent with observations of damage to URM infill walls in similar buildings in recent earthquakes.

- Both cracking and collapse of the walls tend to happen in the lower stories of the frames first, and then possibly extend to the upper stories.
- Until first cracking, the OOP response of the walls is quite limited, and cracking of the panels is usually dominated by the IP axial force due to frame lateral drift.
- After cracking, OOP displacements of the infill walls increase significantly.
- Collapses of URM infill walls are governed by a combination of IP/OOP displacements, usually with the OOP components playing the predominant role.
- Both cracking and failure occur mainly in the lower two storeys; with the exception of high intensity ground motions, upper storeys experience little or no damage.
- Collapse usually occurs a few seconds later than the cracking, and the wall hysteretic IP/OOP displacements, significantly higher than before cracking, were visible in the displacement path plots. This is consistent with widely

accepted notion that URM infill walls can provide a significant source of energy dissipation during ground motions.

- Even though damage is concentrated in the lower storeys, the most damaged walls are not necessarily at the lowest levels. In fact, frames with at least one collapsed wall, but none of them at the first storey are not uncommon.
- This result is strongly correlated with the interaction between simultaneous IP and OOP forces and displacements acting on URM infill walls during seismic excitation; this role of interaction, while supported by increasing experimental evidence, is currently neglected in most design practice.
- The cracking and failure of one infill wall at a given storey tend to propagate to the other wall(s) on the same storey.
- The collapse of infill walls on a given frame storey can trigger the formation of a soft storey; if the soft storey forms above the first level of the buildings, infill walls at lower floors are less likely to collapse during the remainder of the ground motion.
- For a given frame configuration and seismic excitation, thinner panels, widely used as enclosures especially in the past, are much more vulnerable to both cracking and collapse compared to the thicker panels that are more common now.
- Neglecting the effects, including potential failures, of the seismic action on the RC frame structure, RC frame design itself has little influence on the IP/OOP behaviour and damage of URM infill walls.

6.3 Suggestions for future work

One limitation of the study presented is related to the restricted set of models investigated. A more complete study is necessary to verify the testing technique in order to probe the generality of the conclusions herein proposed. In particular, future works should include more infill walls typologies, including brick and concrete block masonry panels, possibly calibrated from experimental results. Additionally, the infill wall model should be applied to a wider range of RC frame structures, including building configurations with a different number of bays and storeys and arrangement of infill walls.

The macro-model with IP/OOP interaction that was presented and applied in this research, and similar others that have been proposed very recently (Furtado et al. 2015), represent the state-of-the-art to represent combined actions on infill panels

during seismic excitation. The model proved to be adequate to represent the seismic response of URM infill walls, with results consistent with experimental evidences and field observations from past earthquakes. However, in order to evaluate the effect of seismic action on the global response of infilled RC frames, including damage and failures that occur in the RC members, a likewise state-of-the-art model should be used for representing the RC frame. Related to this aspect, more analyses are also required to validate the observation of the minor influence of the RC members design on the response of the panels. In particular, more varied detailing for traditional and seismic RC members need to be considered. Furthermore, a very interesting development would be the inclusion of local effects due to the interaction between the infill walls and the frame members.

The macro-element model needs also to be applied to three-dimensional models of the RC frames, in order to avoid potential influence of the elastic springs that were used to simulate the structure in the orthogonal direction.

This work confirmed the significant role of the interaction between IP and OOP actions on URM infill walls. It was noted that natural bi-directional ground motions, even when scaled at the same PGA, can result in significantly different response of the panels. More research is required to identify the influence ground motions characteristics on the damage to the infill walls. Emphasis should be given to different scaling methods for the records and on the orientation of the ground motion components.

REFERENCES

Abou-Zeid, B., W. El-Dakhakhni, A. Razaqpur, and S. Foo. 2011. 'Response of Arching Unreinforced Concrete Masonry Walls to Blast Loading'. *Journal of Structural Engineering* 137 (10): 1205–14. doi:10.1061/(ASCE)ST.1943-541X.0000344.

———. 2014. 'Time-Response Analysis of Arching Unreinforced Concrete Block Walls Subjected to Blast Loads'. *Journal of Structural Engineering* 140 (4): 04013099. doi:10.1061/(ASCE)ST.1943-541X.0000893.

Abrams, Daniel P., Richard Angel, and Joseph Uzarski. 1993. 'Transverse Strength of Damaged Urm Infills'. In *Proc of 6th North American Masonry Conference*, edited by A. A. Hamid and H. G. Harris, 1:347–58. Philadelphia: Masonry Society.

———. 1996. 'Out-of-Plane Strength of Unreinforced Masonry Infill Panels'. *Earthquake Spectra* 12 (4): 825–44. doi:10.1193/1.1585912.

Akhoundi, Farhad, Graça Vasconcelos, Paulo B. Lourenço, Carlos Palha, and Luis Silva. 2015. 'In-Plane and Out-of Plane Experimental Characterization of Rc Masonry Infilled Frames'. In *Proceedings of the 6th International Conference on Mechanics and Materials in Design*, 427–40. Ponta Delgada/Azores.

Anderson, C. 1984. 'Arching Action in Transverse Laterally Loaded Masonry Wall Panels'. *The Structural Engineer* 62 (13).

Angel, Richard, Daniel P. Abrams, D. Shapiro, J. Uzarski, and M. Webster. 1994. 'Behavior of Reinforced Concrete Frames with Masonry Infills'. Text SRS-589. Civil Engineering Studies. University of Illinois at Urbana-Champaign. https://www.ideals.illinois.edu/handle/2142/14210.

Asteris, P., S. Antoniou, D. Sophianopoulos, and C. Z. Chrysostomou. 2011. 'Mathematical Macromodeling of Infilled Frames: State of the Art'. *Journal of Structural Engineering* 137 (12): 1508–17. doi:10.1061/(ASCE)ST.1943-541X.0000384.

Asteris, P. G., D. M. Cotsovos, C. Z. Chrysostomou, A. Mohebkhah, and G. K. Al-Chaar. 2013. 'Mathematical Micromodeling of Infilled Frames: State of the Art'. *Engineering Structures* 56 (November): 1905–21. doi:10.1016/j.engstruct.2013.08.010.

Baker, Jack W., and C. Allin Cornell. 2006a. 'Which Spectral Acceleration Are You Using?' *Earthquake Spectra* 22 (2): 293–312. doi:10.1193/1.2191540.

———. 2006b. ‘Correlation of Response Spectral Values for Multicomponent Ground Motions’. *Bulletin of the Seismological Society of America* 96 (1): 215–27. doi:10.1785/0120050060.

Bennett, R. M., J Fowler J., and R. D. Flanagan. 1996. ‘Shake Table Testing of Structural Clay Tile Infilled Frames’. Y/EN--5491.

Beyer, Katrin, and Julian J. Bommer. 2006. ‘Relationships between Median Values and between Aleatory Variabilities for Different Definitions of the Horizontal Component of Motion’. *Bulletin of the Seismological Society of America* 96 (4A): 1512–22. doi:10.1785/0120050210.

———. 2007. ‘Selection and Scaling of Real Accelerograms for Bi-Directional Loading: A Review of Current Practice and Code Provisions’. *Journal of Earthquake Engineering* 11 (sup1): 13–45. doi:10.1080/13632460701280013.

Bommer, Julian J., and Ana Beatriz Acevedo. 2004. ‘The Use of Real Earthquake Accelerograms as Input to Dynamic Analysis’. *Journal of Earthquake Engineering* 08 (spec01): 43–91. doi:10.1142/S1363246904001596.

Braga, F., V. Manfredi, A. Masi, A. Salvatori, and M. Vona. 2010. ‘Performance of Non-Structural Elements in RC Buildings during the L’Aquila, 2009 Earthquake’. *Bulletin of Earthquake Engineering* 9 (1): 307–24. doi:10.1007/s10518-010-9205-7.

Bramerini, F., and G. Di Pasquale. 2008. ‘Aggiornamento delle mappe di rischio sismico in Italia’. *Ingegneria sismica* XXV (2): 5–23.

Bruneau, Michel. 1995. ‘Performance of Masonry Structures during the 1994 Northridge (Los Angeles) Earthquake’. *Canadian Journal of Civil Engineering* 22 (2): 378–402. doi:10.1139/l95-048.

Brzev, Svetlana. 2007. *Earthquake-Resistant Confined Masonry Construction*. Kanpur, India: NICEE.

Calvi, Gian Michele, and Davide Bolognini. 2001. ‘Seismic Response of Reinforced Concrete Frames Infilled with Weakly Reinforced Masonry Panels’. *Journal of Earthquake Engineering* 5 (2): 153–85. doi:10.1080/13632460109350390.

Calvi, G Michele, Davide Bolognini, and Andrea Penna. 2004. ‘Seismic Performance of Masonry-Infilled RC Frames: Benefits of Slight Reinforcements’. In , 253–76. Guimarães, Portugal.

Celarec, Daniel, Paolo Ricci, and Matjaž Dolšek. 2012. ‘The Sensitivity of Seismic Response Parameters to the Uncertain Modelling Variables of Masonry-Infilled Reinforced Concrete Frames’. *Engineering Structures* 35 (February): 165–77. doi:10.1016/j.engstruct.2011.11.007.

CEN. 2006. ‘Eurocode 6: Design of Masonry Structures - Part 1-1: General Rules for Reinforced and Unreinforced Masonry Structures’. EN 1996-1-1:2006. European Committee for Standardization.

———. 2013. ‘Eurocode 8: Design of Structures for Earthquake Resistance - Part 1: General Rules, Seismic Actions and Rules for Buildings’. EN 1998-1. European Committee for Standardization.

Chopra, Anil K. 2011. *Dynamics of Structures*. 4 edition. Upper Saddle River, N.J: Prentice Hall.

Crisafulli, Francisco J., Athol J. Carr, and Robert Park. 2000. 'Analytical Modelling of Infilled Frame Structures: A General Review'. *Bulletin of the New Zealand National Society for Earthquake Engineering* 33 (1): 30–47.

Crowley, Helen, and Rui Pinho. 2010. 'Revisiting Eurocode 8 Formulae for Periods of Vibration and Their Employment in Linear Seismic Analysis'. *Earthquake Engineering & Structural Dynamics* 39 (2): 223–35. doi:10.1002/eqe.949.

Dafnis, A., H. Kolsch, and H. Reimerdes. 2002. 'Arching in Masonry Walls Subjected to Earthquake Motions'. *Journal of Structural Engineering* 128 (2): 153–59. doi:10.1061/(ASCE)0733-9445(2002)128:2(153).

da Porto, Francesca, Giovanni Guidi, Massimo Dalla Benetta, and Nicolò Verlato. 2013. 'Combined In-Plane/Out-of-Plane Experimental Behaviour of Reinforced and Strengthened Infill Masonry Walls'. In *Proc. of 12th Canadian Masonry Symposium*, 10. Vancouver, Canada: The Masonry Society.

Dawe, J. L., and C. K. Seah. 1989. 'Out-of-Plane Resistance of Concrete Masonry Infilled Panels'. *Canadian Journal of Civil Engineering* 16 (6): 854–64. doi:10.1139/l89-128.

Decanini, Luis D., Adriano De Sortis, Agostino Goretti, Laura Liberatore, Fabrizio Mollaioli, and Paolo Bazzurro. 2004. 'Performance of Reinforced Concrete Buildings During the 2002 Molise, Italy, Earthquake'. *Earthquake Spectra* 20 (S1): S221–55. doi:10.1193/1.1765107.

Deierlein, Gregory G., Andrei M. Reinhorn, and Michael R. Willford. 2010. 'Nonlinear Structural Analysis for Seismic Design.' NIST GCR 10-917-. NEHRP Seismic Design Technical Brief No. 4. National Istitute of Standards and Technology.

De Sortis, Adriano, Paolo Bazzurro, Fabrizio Mollaioli, and Silvia Bruno. 2007. 'Influenza Delle Tamponature Sul Rischio Sismico Degli Edifici in Calcestruzzo Armato'. *Atti Del XII Convegno ANIDIS L'ingegneria Sismica in Italia, Pisa*, 10–14.

D.M. 14.01.2008 'Nuove Norme Tecniche per le costruzioni'. 2008.

Dolatshahi, Kiarash M., and Mohammad Yekrangnia. 2015. 'Out-of-Plane Strength Reduction of Unreinforced Masonry Walls because of in-Plane Damages'. *Earthquake Engineering & Structural Dynamics* 44 (13): 2157–76. doi:10.1002/eqe.2574.

Dolšek, Matjaž, and Peter Fajfar. 2001. 'Soft Storey Effects in Uniformly Infilled Reinforced Concrete Frames'. *Journal of Earthquake Engineering* 5 (1): 1–12. doi:10.1080/13632460109350383.

———. 2008. 'The Effect of Masonry Infills on the Seismic Response of a Four-Storey Reinforced Concrete Frame — a Deterministic Assessment'. *Engineering Structures* 30 (7): 1991–2001. doi:10.1016/j.engstruct.2008.01.001.

Drysdale, R., and A. Essawy. 1988. 'Out-of-Plane Bending of Concrete Block Walls'. *Journal of Structural Engineering* 114 (1): 121–33. doi:10.1061/(ASCE)0733-9445(1988)114:1(121).

EERI. 2009. ‘The Mw 6.3 Abruzzo, Italy, Earthquake of April 6, 2009’. EERI Special Earthquake Report. EERI. https://www.eeri.org/site/images/lfe/pdf/laquila-eq-report.pdf.

El-Dakhakhni, Wael Wagih, A. A. Hamid, Z. H. R. Hakam, and M. Elgaaly. 2006. ‘Hazard Mitigation and Strengthening of Unreinforced Masonry Walls Using Composites’. *Composite Structures* 73 (4): 458–77. doi:10.1016/j.compstruct.2005.02.017.

ESM working group. 2015. ‘European Strong-Motion Database, Version 0.1, Network Activity 3: Networking Acceleration Networks and SM Data Users. Project NERA (www.nera-Eu.org)’. http://esm.mi.ingv.it/.

Fardis, Michael N., and T. B. Panagiotakos. 1997. ‘Seismic Design and Response of Bare and Masonry-Infilled Reinforced Concrete Buildings. Part II: Infilled Structures’. *Journal of Earthquake Engineering* 1 (3): 475–503. doi:10.1080/13632469708962375.

FEMA. 1997. ‘NEHRP Guidelines for the Seismic Rehabilitation of Buildings’. FEMA-273. Washington, D.C.: Building Seismic Safety Council.

———. 2000. ‘Prestandard and Commentary for the Seismic Rehabilitation of Buildings. FEMA-356’. FEMA-356. Washington, D.C.: Federal Emergency Management Agency.

Flanagan, R., and R. Bennett. 1999a. ‘Arching of Masonry Infilled Frames: Comparison of Analytical Methods’. *Practice Periodical on Structural Design and Construction* 4 (3): 105–10. doi:10.1061/(ASCE)1084-0680(1999)4:3(105).

———. 1999b. ‘Bidirectional Behavior of Structural Clay Tile Infilled Frames’. *Journal of Structural Engineering* 125 (3): 236–44. doi:10.1061/(ASCE)0733-9445(1999)125:3(236).

Furtado, André, Hugo Rodrigues, António Arêde, and Humberto Varum. 2015. ‘Simplified Macro-Model for Infill Masonry Walls Considering the out-of-Plane Behaviour’. *Earthquake Engineering & Structural Dynamics*, n/a – n/a. doi:10.1002/eqe.2663.

Gabrielsen, B.L., and K. Kaplan. 1977. ‘Arching in Masonry Walls Subjected to Out-of-Plane Forces’. In *Proceedings of National Workshop on Earthquake Resistant Masonry Construction*. Vol. 106. NBS Science Series. Boulder, CO: National Bureau of Standards.

Grant, Damian. 2011. ‘Response Spectral Matching of Two Horizontal Ground-Motion Components’. *Journal of Structural Engineering* 137 (3): 289–97. doi:10.1061/(ASCE)ST.1943-541X.0000227.

Günay, Selim, and Khalid M. Mosalam. 2010a. ‘Infill Wall Model and Element Removal - OpenSeesWiki’. http://opensees.berkeley.edu/wiki/index.php/Infill_Wall_Model_and_Element_Removal.

———. 2010b. ‘Structural Engineering Reconnaissance of the April 6, 2009, Abruzzo, Italy, Earthquake, and Lessons Learned’. PEER 2010/105. PEER Research Reports. University of California, Berkeley: Pacific Earthquake Engineering Research Center.

http://peer.berkeley.edu/publications/peer_reports/reports_2010/web_PEER10_105_GUNAY&Mosalam_ITALY.pdf.

Hak, Sanja, Paolo Morandi, and Guido Megenes. 2013. *Damage Control of Masonry Infills in Seismic Design*. Research Report EUCENTRE, No. 01.2013. Pavia, Italy: IUSS Press.

Hak, Sanja, P. Morandi, G. Magenes, and T. J. Sullivan. 2012. 'Damage Control for Clay Masonry Infills in the Design of RC Frame Structures'. *Journal of Earthquake Engineering* 16 (sup1): 1–35. doi:10.1080/13632469.2012.670575.

Haldar, Putul, Yogendra Singh, and D. K. Paul. 2012. 'Effect of URM Infills on Seismic Vulnerability of Indian Code Designed RC Frame Buildings'. *Earthquake Engineering and Engineering Vibration* 11 (2): 233–41. doi:10.1007/s11803-012-0113-5.

Haseltine, B. A., H. W. H. West, and J. N. Tutt. 1977. 'The Resistance of Brickwork to Lateral Loading. Part 2 Design of Walls to Resist Lateral Loads'. *The Structural Engineer* 55 (10).

Hashemi, Alidad, and Khalid M. Mosalam. 2007. 'Seismic Evaluation of Reinforced Concrete Buildings Including Effects of Masonry Infill Walls'. Text PEER 2007/100. PEER Research Reports. University of California, Berkeley: Pacific Earthquake Engineering Research Center. http://peer.berkeley.edu/publications/peer_reports/reports_2007/webR_PEER7100_HASHEMI_mosalam.pdf.

Henderson, R. Craig, K. E. Fricke, W. Dale Jones, J. E. Beavers, and R. M. Bennett. 2003. 'Summary of a Large- and Small-Scale Unreinforced Masonry Infill Test Program'. *Journal of Structural Engineering* 129 (12): 1667–75. doi:10.1061/(ASCE)0733-9445(2003)129:12(1667).

Henderson, R. Craig, W. Dale Jones, E. G. Burdette, and Max L. Porter. 1993. 'The Effect of Prior Out-of-Plane Damage on the In-Plane Behavior of Unreinforced Masonry Infilled Frames'. In . Atlanta, GA. http://cedb.asce.org/cgi/WWWdisplay.cgi?9301064.

Henderson, R. Craig, Max L. Porter, W. Dale Jones, and E. G. Burdette. 2006. 'Influence of Prior Out-of-Plane Damage on the In-Plane Behavior of Masonry Infilled Frames'. *TMS Journal* 24 (No. 1).

Hendry, A. W. 1973. 'The Lateral Strength of Unreinforced Brickwork'. *The Structural Engineer* 51 (2).

Hill, James A. 1994. 'Out - of - Plane Response of Unreinforced Masonry Infill Frame Panels'. In *Technical Report*, NCEER 94-0004:33–38. Buffalo, NY: National Center for Earthquake Engineering Research.

Hong, H. P., and K. Goda. 2007. 'Orientation-Dependent Ground-Motion Measure for Seismic-Hazard Assessment'. *Bulletin of the Seismological Society of America* 97 (5): 1525–38. doi:10.1785/0120060194.

Humar, Jag Mohan, David Lau, and Jean-Robert Pierre. 2001. 'Performance of Buildings during the 2001 Bhuj Earthquake'. *Canadian Journal of Civil Engineering* 28 (6): 979–91. doi:10.1139/l01-070.

Iervolino, Iunio, Carmine Galasso, and Edoardo Cosenza. 2009. 'REXEL: Computer Aided Record Selection for Code-Based Seismic Structural Analysis'. *Bulletin of Earthquake Engineering* 8 (2): 339–62. doi:10.1007/s10518-009-9146-1.

Iervolino, Iunio, Carmine Galasso, Roberto Paolucci, and Francesca Pacor. 2011. 'Engineering Ground Motion Record Selection in the ITalian ACcelerometric Archive'. *Bulletin of Earthquake Engineering* 9 (6): 1761–78. doi:10.1007/s10518-011-9300-4.

Iervolino, Iunio, Giuseppe Maddaloni, and Edoardo Cosenza. 2008. 'Eurocode 8 Compliant Real Record Sets for Seismic Analysis of Structures'. *Journal of Earthquake Engineering* 12 (1): 54–90. doi:10.1080/13632460701457173.

ISTAT. 2011. 'Censimento delle Popolazione e delle Abitazioni, 2011'. http://dati-censimentopopolazione.istat.it/#.

Kadysiewski, Stephen, and Khalid M. Mosalam. 2009. 'Modeling of Unreinforced Masonry Infill Walls Considering In-Plane and Out-of-Plane Interaction'. Text PEER 2008/102. PEER Research Reports. University of California, Berkeley: Pacific Earthquake Engineering Research Center. http://peer.berkeley.edu/publications/peer_reports/reports_2008/web_PEER8102_Kadysiewski_Mosalam_R.pdf.

Karakostas, Christos, Vassilios Lekidis, Triantafyllos Makarios, Thomas Salonikios, Issam Sous, and Milton Demosthenous. 2005. 'Seismic Response of Structures and Infrastructure Facilities during the Lefkada, Greece Earthquake of 14/8/2003'. *Engineering Structures* 27 (2): 213–27. doi:10.1016/j.engstruct.2004.09.009.

Kaushik, Hemant B., Durgesh C. Rai, and Sudhir K. Jain. 2006. 'Code Approaches to Seismic Design of Masonry-Infilled Reinforced ConcreteFrames: A State-of-the-Art Review'. *Earthquake Spectra* 22 (4): 961–83. doi:10.1193/1.2360907.

Kent, Dudley Charles, and Robert Park. 1971. 'Flexural Members with Confined Concrete'. *Journal of the Structural Division* 97 (7): 1969–90.

Klingner, Richard E., Tarek R. Bashandy, Nestor R. Rubiano, and Steven C. Sweeney. 1996. 'Evaluation and Analytical Verification of Shaking Table Data from Infilled Frames Part II: Out-of-Plane Behavior'. In *Proceedings of Seventh North American Masonry Conference*, Volume 1:521–32. University of Notre Dame, South Bend, Indiana, USA.

Komaraneni, S., Durgesh C. Rai, and Vaibhav Singhal. 2011. 'Seismic Behavior of Framed Masonry Panels with Prior Damage When Subjected to Out-of-Plane Loading'. *Earthquake Spectra* 27 (4): 1077–1103. doi:10.1193/1.3651624.

Kong, Jing-Chang, Chang-Hai Zhai, and Chun-Hui Liu. 2015. 'Two-Way Seismic Behaviour of Concrete Frames with Infill Walls'. *Proceedings of the Institution of Civil Engineers - Structures and Buildings* 168 (9): 649–63. doi:10.1680/jstbu.14.00055.

Lam, N. T. K., M. Griffith, J. Wilson, and K. Doherty. 2003. 'Time–history Analysis of URM Walls in out-of-Plane Flexure'. *Engineering Structures* 25 (6): 743–54. doi:10.1016/S0141-0296(02)00218-3.

Liauw, T. C. 1979. 'Tests on Multistory Infilled Frames Subject to Dynamic Lateral Loading'. *Journal Proceedings* 76 (4): 551–64.

Liel, Abbie B., and Kathryn P. Lynch. 2009. 'Vulnerability of Reinforced Concrete Frame Buildings and Their Occupants in the 2009 L'Aquila, Italy Earthquake'. 213. Quik Response Report. Boulder, CO: Natural Hazard Center. http://www.colorado.edu/hazards/research/qr/qr213.pdf.

Lourenço, Paulo B. 1996. 'Computational Strategy for Masonry Structures'. Porto, Portugal: Faculdade de Engenharia da Universidade do Porto.

Luca, Flavia De, Gerardo M. Verderame, Fernando Gómez-Martínez, and Agustín Pérez-García. 2013. 'The Structural Role Played by Masonry Infills on RC Building Performances after the 2011 Lorca, Spain, Earthquake'. *Bulletin of Earthquake Engineering* 12 (5): 1999–2026. doi:10.1007/s10518-013-9500-1.

Maheri, Mahmoud R., and M. A. Najafgholipour. 2012. 'In-Plane Shear and Out-of-Plane Bending Capacity Interaction in Brick Masonry Walls'. In *Proc. of 15th World Conference on Earthquake Engineering*. Lisbon, Portugal.

Mander, J., M. Priestley, and R. Park. 1988. 'Theoretical Stress-Strain Model for Confined Concrete'. *Journal of Structural Engineering* 114 (8): 1804–26. doi:10.1061/(ASCE)0733-9445(1988)114:8(1804).

McDowell, E. L., K. E. McKee, and E. Sevin. 1956. 'Arching Action Theory of Masonry Walls'. *Journal of the Structural Division* 82 (ST2): 915–1 – 915–18.

McKenna, F., G. L. Fenves, and M. H. Scott. 2000. 'Open System for Earthquake Engineering Simulation (OpenSees). Pacific Earthquake Engineering Research Center'. *University of California, Berkeley, CA*. http://opensees.berkeley.edu/.

Menegotto, M., and P. E. Pinto. 1973. 'Method of Analysis for Cyclically Loaded Reinforced Concrete Plane Frames Including Changes in Geometry and Non-Elastic Behaviour of Elements under Combined Normal Force and Bending'. In *Proceedings of IABSE Symposium on Resistance and Ultimate Deformability of Structures Acted on by Well Defined Repeated Loads*, 15–22. Lisbon.

Miyamoto, H. Kit. 2013. 'L'Aquila Earthquake Journal Entry #1 | Kit Miyamoto Field Journals'. http://kitmiyamoto.com/earthquake-field-reports/laquila-earthquake-journal-entry-1/.

Moghaddam, Hassan, and Nabi Goudarzi. 2010. 'Transverse Resistance of Masonry Infills'. *ACI Structural Journal* 107 (4). doi:10.14359/51663819.

Mohyeddin, Alireza, Helen Goldsworthy, and Emad Gad. 2013a. 'Sensitivity Analysis of Nonlinear Behaviour of Infill-Frames Under In-Plane and Out-of-Plane Loading'. *Advances in Structural Engineering* 16 (10): 1729–48. doi:10.1260/1369-4332.16.10.1729.

Mohyeddin, Alireza, Helen M. Goldsworthy, and Emad F. Gad. 2013b. 'FE Modelling of RC Frames with Masonry Infill Panels under in-Plane and out-of-Plane Loading'. *Engineering Structures* 51: 73–87. doi:10.1016/j.engstruct.2013.01.012.

Mondal, Goutam, and Sudhir K. Jain. 2008. 'Lateral Stiffness of Masonry Infilled Reinforced Concrete (RC) Frames with Central Opening'. *Earthquake Spectra* 24 (3): 701–23. doi:10.1193/1.2942376.

Monk, Clarence B. 1958. 'Resistance of Structural Clay Masonry to Dynamic Forces; a Design Manual for Blast Resistance'. Text Research Report No. 7. Geneva, Illinois: Structural Clay Products Research Foundation.

Mosalam, Khalid M., and Selim Günay. 2014. 'Progressive Collapse Analysis of Reinforced Concrete Frames with Unreinforced Masonry Infill Walls Considering In-Plane/Out-of-Plane Interaction'. *Earthquake Spectra* 31 (2): 921–43. doi:10.1193/062113EQS165M.

Murty, C. V. R., Svetlana Brzev, Heidi Faison, Craig D. Comartin, and Ayhan Irfanoglu. 2006. 'AT RISK: The Seismic Performance of Reinforced Concrete Frame Buildings with Masonry Infill Walls'. WHE-2006-03. World Housing Encyclopedia. Oakland, CA: EERI.

Najafgholipour, M. A., Mahmoud R. Maheri, and P. B. Lourenço. 2013. 'Capacity Interaction in Brick Masonry under Simultaneous in-Plane and out-of-Plane Loads'. *Construction and Building Materials*, 25th Anniversary Session for ACI 228 – Building on the Past for the Future of NDT of Concrete, 38: 619–26. doi:10.1016/j.conbuildmat.2012.08.032.

———. 2014. 'Definition of Interaction Curves for the in-Plane and out-of-Plane Capacity in Brick Masonry Walls'. *Construction and Building Materials* 55 (March): 168–82. doi:10.1016/j.conbuildmat.2014.01.028.

Neuenhofer, A., and F. Filippou. 1998. 'Geometrically Nonlinear Flexibility-Based Frame Finite Element'. *Journal of Structural Engineering* 124 (6): 704–11. doi:10.1061/(ASCE)0733-9445(1998)124:6(704).

NOAA. 2007. 'NOAA/NESDIS/NGDC/MGG-Natural Hazards Images'. *Http://www.noaa.gov/*. February 21. http://www.ngdc.noaa.gov/hazardimages/.

OPCM 3274. 2003. *Opcm n. 3274 del 20 marzo 2003: primi elementi in materia di criteri generali per la classificazione sismica del territorio nazionale e di normative tecniche per le costruzioni in zona sismica*. *Gazz. Uff. 8 maggio 2003, n. 108*.

Ozkaynak, H., E. Yuksel, C. Yalcin, A. A. Dindar, and O. Buyukozturk. 2013. 'Masonry Infill Walls in Reinforced Concrete Frames as a Source of Structural Damping'. *Earthquake Engineering & Structural Dynamics* 43 (7): 949–68. doi:10.1002/eqe.2380.

Paolucci, R., F. Pacor, R. Puglia, G. Ameri, C. Cauzzi, and M. Massa. 2011. 'Record Processing in ITACA, the New Italian Strong-Motion Database'. In *Earthquake Data in Engineering Seismology*, edited by Sinan Akkar, Polat Gülkan, and Torild van Eck, 99–113. Geotechnical, Geological, and Earthquake Engineering 14. Springer Netherlands. http://link.springer.com/chapter/10.1007/978-94-007-0152-6_8.

Penna, Andrea, Paolo Morandi, Maria Rota, Carlo Filippo Manzini, Francesca da Porto, and Guido Magenes. 2013. 'Performance of Masonry Buildings during

the Emilia 2012 Earthquake'. *Bulletin of Earthquake Engineering* 12 (5): 2255–73. doi:10.1007/s10518-013-9496-6.

Pereira, Manuel Fernando Paulo, M. F. Neto Pereira, J. E. Dias Ferreira, and Paulo B. Lourenço. 2011. 'Behavior of Masonry Infill Panels in RC Frames Subjected to in Plane and out of Plane Loads'. In *7th Int. Conf. AMCM2011*. Kraków, Poland. http://repositorium.sdum.uminho.pt/handle/1822/14880.

Preti, M., N. Bettini, and G. Plizzari. 2012. 'Infill Walls with Sliding Joints to Limit Infill-Frame Seismic Interaction: Large-Scale Experimental Test'. *Journal of Earthquake Engineering* 16 (1): 125–41. doi:10.1080/13632469.2011.579815.

Pujol, S., Amadeo Benavent-Climent, Mario E Rodriguez, and J. Paul Smith-Pardo. 2008. 'Masonry Infill Walls: An Effective Alternative for Seismic Strengthening of Low-Rise Reinforced Concrete Building Structures'. In . Beijing, China.

Rodrigues, Hugo, Humberto Varum, and Aníbal Costa. 2010. 'Simplified Macro-Model for Infill Masonry Panels'. *Journal of Earthquake Engineering* 14 (3): 390–416. doi:10.1080/13632460903086044.

Scott, Andrew. 2009. 'L' Aquila, Italy Earthquake Reconnaissance'. *L' Aquila, Italy Earthquake Reconnaissance*. April 21. http://andrewnscott.blogspot.it/.

Sezen, Halil, Kenneth J. Elwood, Andrew S. Whittaker, Khalid M. Mosalam, John W. Wallace, and John F. Stanton. 2000. 'Structural Engineering Reconnaissance of the August 17, 1999, Kocaeli (Izmit), Turkey, Earthquake'. PEER 2000/09. PEER Research Reports. University of California, Berkeley: Pacific Earthquake Engineering Research Center. http://peer.berkeley.edu/publications/peer_reports/reports_2000/0009.pdfrts/reports_2007/webR_PEER7100_HASHEMI_mosalam.pdf.

Shahi, Shrey K., and Jack W. Baker. 2013. 'NGA-West2 Models for Ground Motion Directionality'. *Earthquake Spectra* 30 (3): 1285–1300. doi:10.1193/040913EQS097M.

Shapiro, D., J. Uzarski, M. Webster, R. Angel, and Daniel P. Abrams. 1994. 'Estimating Out-of-Plane Strength of Cracked Masonry Infills'. Text SRS-588. University of Illinois at Urbana-Champaign. https://www.ideals.illinois.edu/handle/2142/14209.

Smith, Brian Stafford. 1962. 'Lateral Stiffness of Infilled Frames' 88 (6): 183–99.

———. 1967. 'Methods for Predicting the Lateral Stiffness and Strength of Multi-Storey Infilled Frames'. *Building Science* 2 (3): 247–57.

Stavridis, A., and P. Shing. 2010. 'Finite-Element Modeling of Nonlinear Behavior of Masonry-Infilled RC Frames'. *Journal of Structural Engineering* 136 (3): 285–96. doi:10.1061/(ASCE)ST.1943-541X.116.

Stewart, Jonathan P., Norman Abrahamson, Gail M. Atkinson, Jack W. Baker, David M. Boore, Yousef Bozorgnia, Kenneth W. Campbell, et al. 2011. 'Representation of Bidirectional Ground Motions for Design Spectra in Building Codes'. *Earthquake Spectra* 27 (3): 927–37. doi:10.1193/1.3608001.

Tasligedik, A. S., S. Pampanin, and A. Palermo. 2011. 'Damage Mitigation Strategies of "Non-Structural" Infill Walls: Concept and Numerical-Experimental Validation Program'. In *Proceedings of the Ninth Pacific Conference on Earthquake Engineering*, paper n.120. Auckland, New Zealand. http://ir.canterbury.ac.nz:80/handle/10092/6135.

Thomas, F. G. 1953. 'The Strength of Brickwork'. *The Structural Engineer* 31 (2).

Timoshenko, S., and S. Woinowsky-Krieger. 1959. *Theory of Plates and Shells,*. 2 edition. Engineering Societies Monographs. Mcgraw-Hill College.

Tu, Yi-Hsuan, Tsung-Hua Chuang, Pai-Mei Liu, and Yuan-Sen Yang. 2010. 'Out-of-Plane Shaking Table Tests on Unreinforced Masonry Panels in RC Frames'. *Engineering Structures* 32 (12): 3925–35. doi:10.1016/j.engstruct.2010.08.030.

Vicente, R., H. Rodrigues, A. Costa, H. Varum, and J. A. R. Silva. 2010. 'Masonry Enclosure Walls: Lessons Learnt from the Recent Abruzzo Earthquake'. In *Proc. of 14th ECEE*. Ohrid, Macedonia. http://ria.ua.pt/handle/10773/6866.

Watson-Lamprey, Jennie, and Norman Abrahamson. 2006. 'Selection of Ground Motion Time Series and Limits on Scaling'. *Soil Dynamics and Earthquake Engineering* 26 (5): 477–82. doi:10.1016/j.soildyn.2005.07.001.

West, H. W. H. 1973. 'Lateral loading test on walls with different boundary conditions'. In *Proc. of Third International Brick Masonry Conference*. Essen, Germany.

Yuen, Y. P., and J. S. Kuang. 2012. 'Nonlinear Response and Failure Mechanism of Infilled RC Frame Structures under Biaxial Seismic Excitation'. In *Proc. of 15th World Conference on Earthquake Engineering*. Lisbon, Portugal.

———. 2013a. 'Masonry-Infilled Rc Frames Subjected to Combined in-Plane and out-of-Plane Loading'. *International Journal of Structural Stability and Dynamics* 14 (02): 1350066. doi:10.1142/S0219455413500661.

Yuen, Y P, and J S Kuang. 2013b. 'Simulations of Masonry-Infilled Reinforced Concrete Frame Failure'. *Proceedings of the ICE - Engineering and Computational Mechanics* 166 (4): 179–93. doi:10.1680/eacm.13.00002.

Žarnić, Roko, Samo Gostič, Adam J. Crewe, and Colin A. Taylor. 2001. 'Shaking Table Tests of 1:4 Reduced-Scale Models of Masonry Infilled Reinforced Concrete Frame Buildings'. *Earthquake Engineering & Structural Dynamics* 30 (6): 819–34. doi:10.1002/eqe.39.

APPENDIX A

In this Appendix, the full series of force and displacement history paths are reported for EQ10 analyses. The figures follow the same order of the history paths shown in section 5.2 for the EQ06 analyses, as summarized in Table A 1.
The EQ06-D1 and EQ06-D2 records are natural records taken in L'Aquila during the 2009 Abruzzo (Italy) earthquake. The EQ10-D1 and EQ10-D2 records are natural records from the 1999 Düzce (Turkey) earthquake.

	Analysis EQ06 scaled to a_g =			*Analysis EQ10 scaled to a_g =*		
Model	*0.15g*	*0.25g*	*0.35g*	*0.15g*	*0.25g*	*0.35g*
3×3_115T	Fig. 5.5	Fig. 5.9	Fig. 5.13	Fig. A 1	Fig. A 5	Fig. A 9
3×3_300T	Fig. 5.6	Fig. 5.10	Fig. 5.14	Fig. A 2	Fig. A 6	Fig. A 10
3×3_115S	Fig. 5.7	Fig. 5.11	Fig. 5.15	Fig. A 3	Fig. A 7	Fig. A 11
3×3_300S	Fig. 5.8	Fig. 5.12	Fig. 5.16	Fig. A 4	Fig. A 8	Fig. A 12
5×3_115T	Fig. 5.17	Fig. 5.21	Fig. 5.25	Fig. A 13	Fig. A 17	Fig. A 21
5×3_300T	Fig. 5.18	Fig. 5.22	Fig. 5.26	Fig. A 14	Fig. A 18	Fig. A 22
5×3_115S	Fig. 5.19	Fig. 5.23	Fig. 5.27	Fig. A 15	Fig. A 19	Fig. A 23
5×3_300S	Fig. 5.20	Fig. 5.24	Fig. 5.28	Fig. A 16	Fig. A 20	Fig. A 24

Table A 1 Summary and references of the force and displacements paths figures.

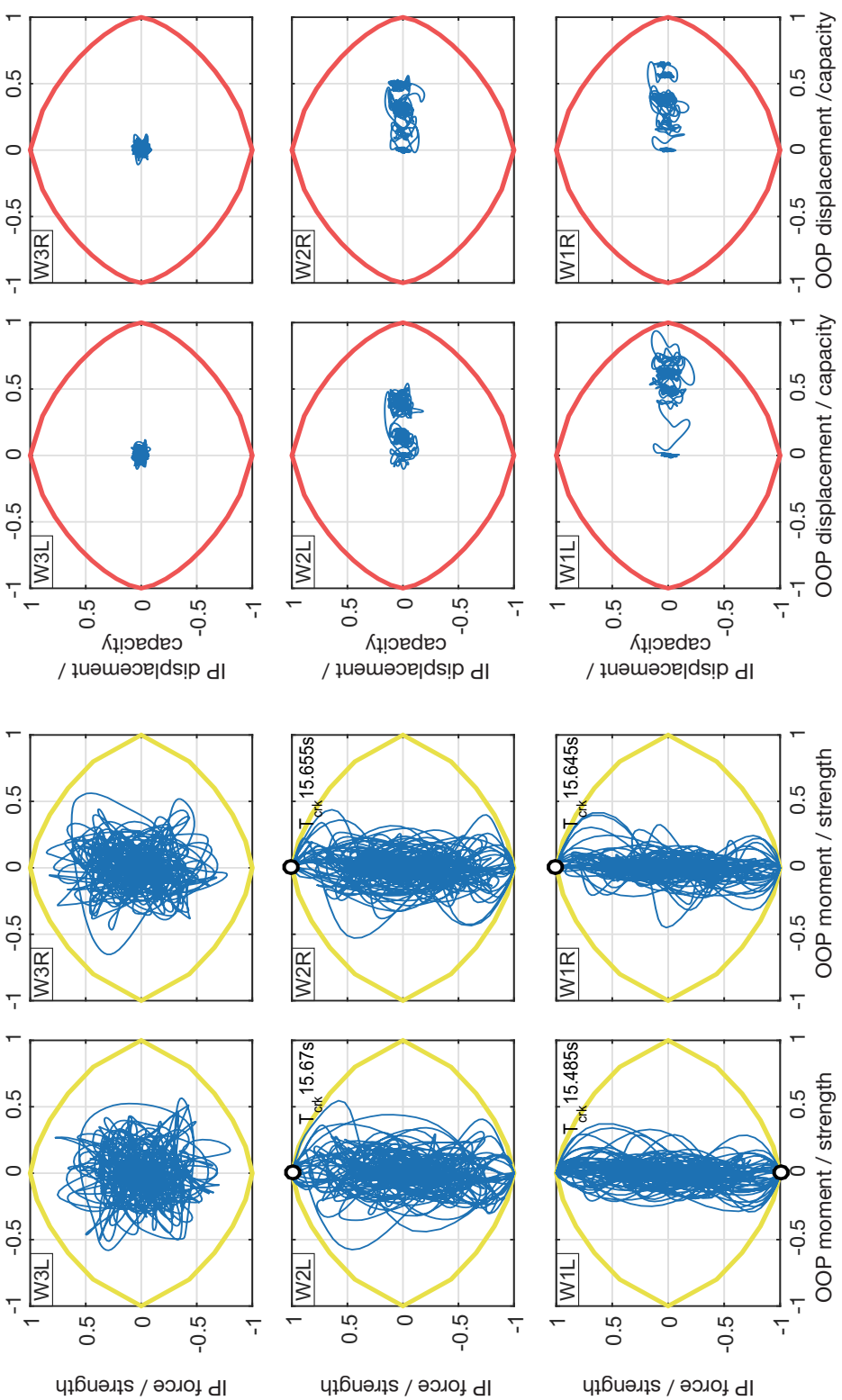

Fig. A 1 Force and displacement paths of infill walls in frame ***3×3_115T*** *for analysis* ***EQ10*** *scaled to* a_g **= *0.15g***

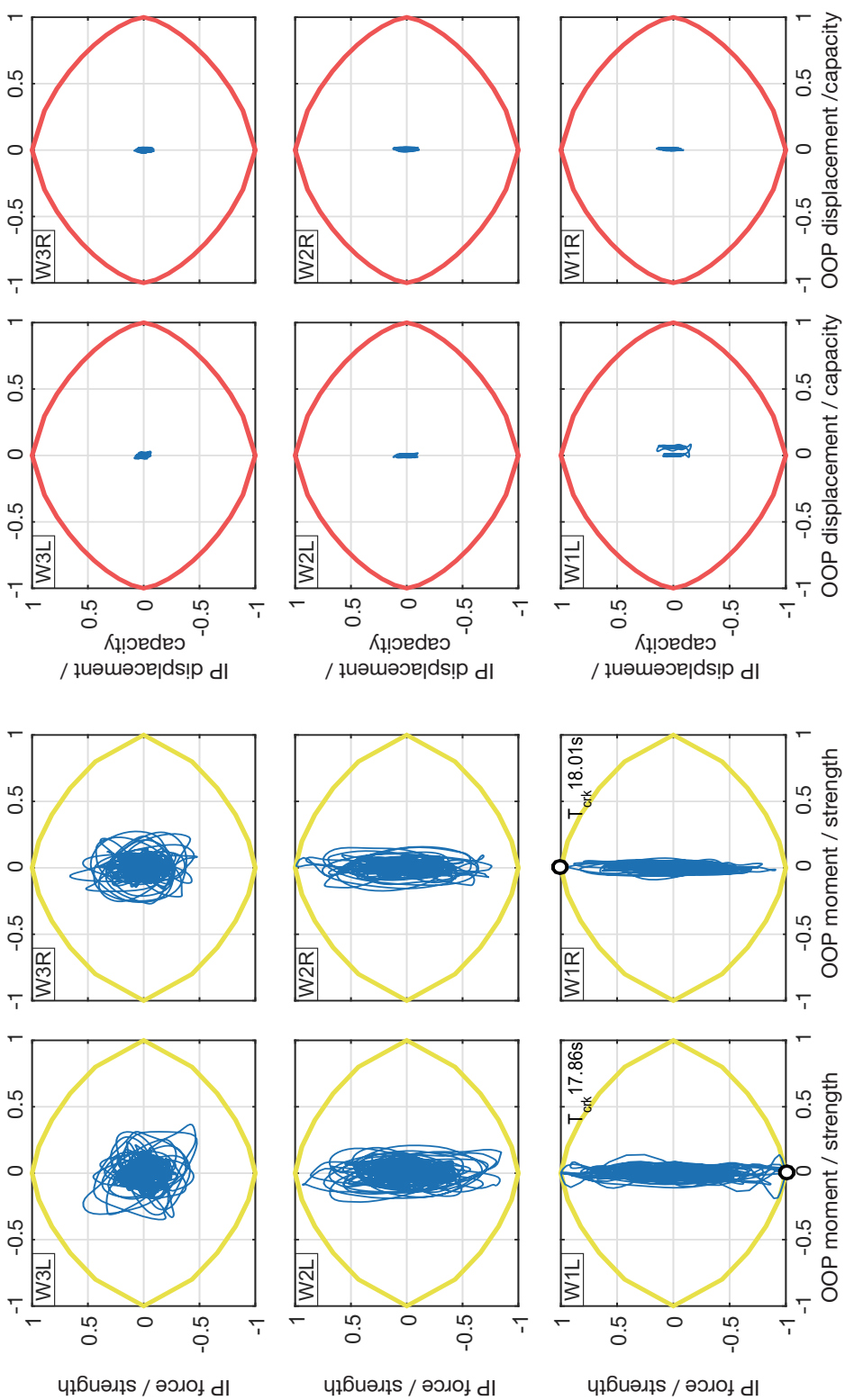

*Fig. A 2 Force and displacement paths of infill walls in frame **3×3_300T** for analysis **EQ10** scaled to a_g = **0.15g***

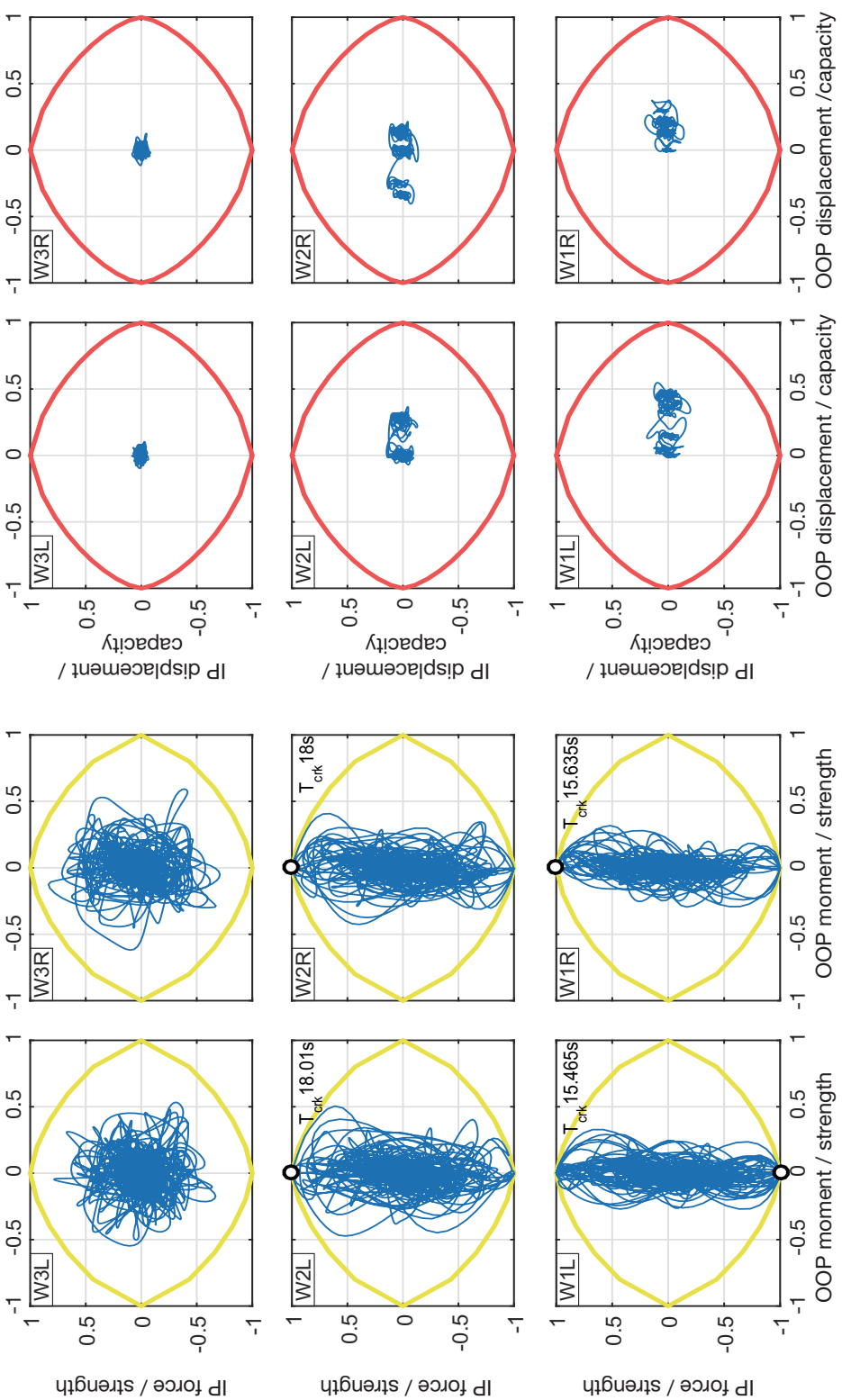

*Fig. A 3 Force and displacement paths of infill walls in frame **3×3_115S** for analysis **EQ10** scaled to a_g = **0.15g***

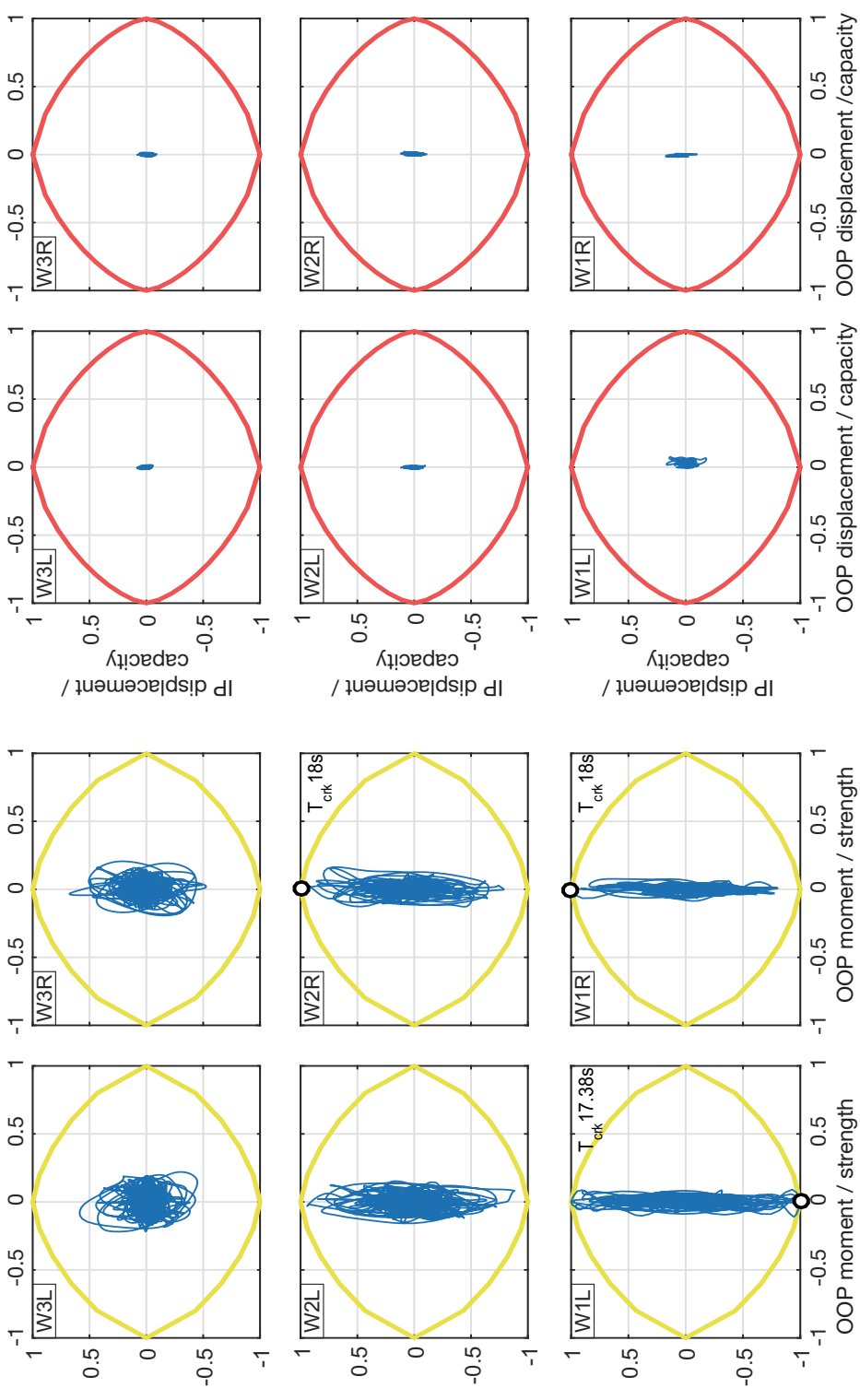

*Fig. A 4 Force and displacement paths of infill walls in frame **3×3_300S** for analysis **EQ10** scaled to a_g = **0.15g***

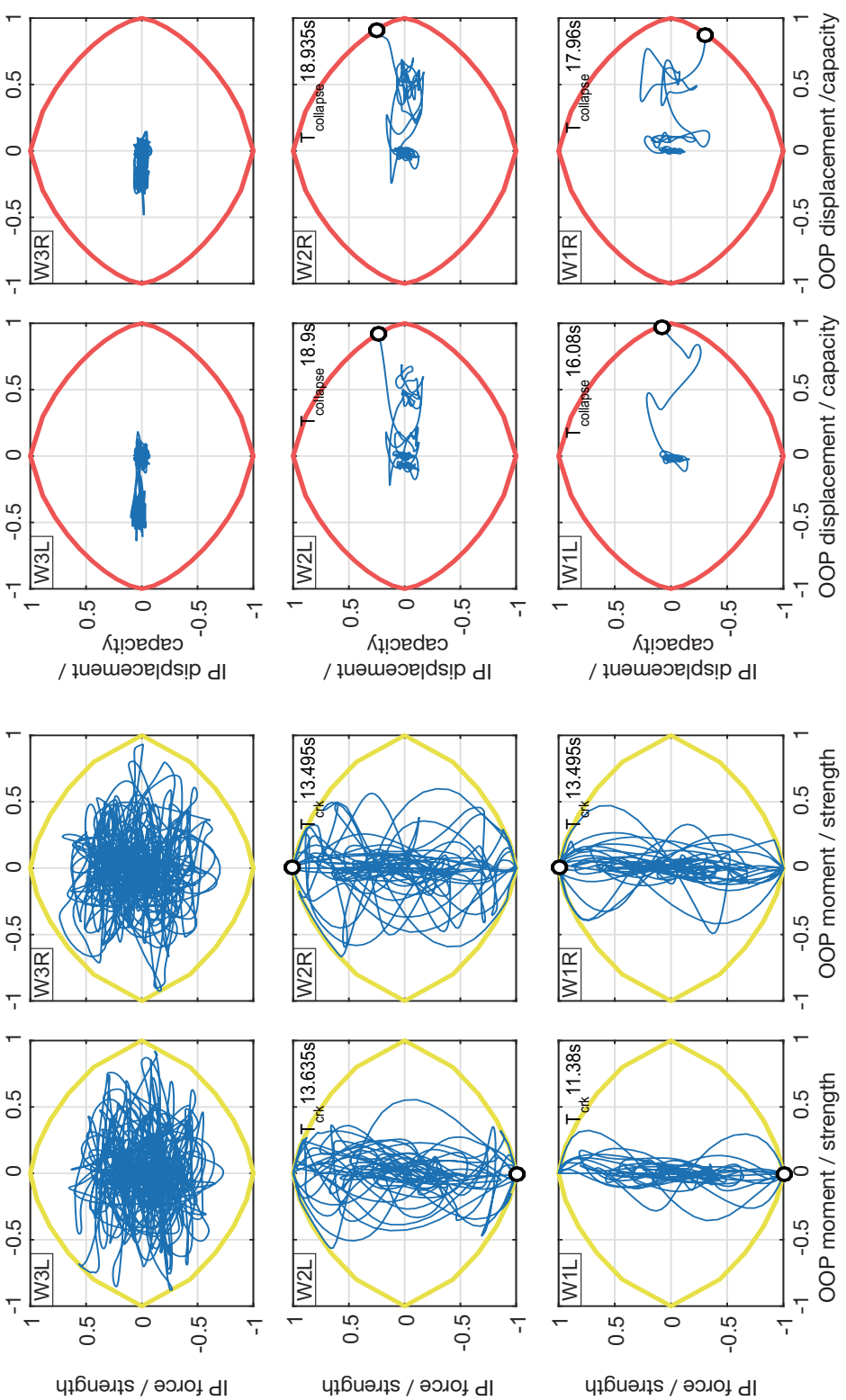

Fig. A 5 Force and displacement paths of infill walls in frame ***3×3_115T*** *for analysis* ***EQ10*** *scaled to* $\mathbf{a_g = 0.25g}$

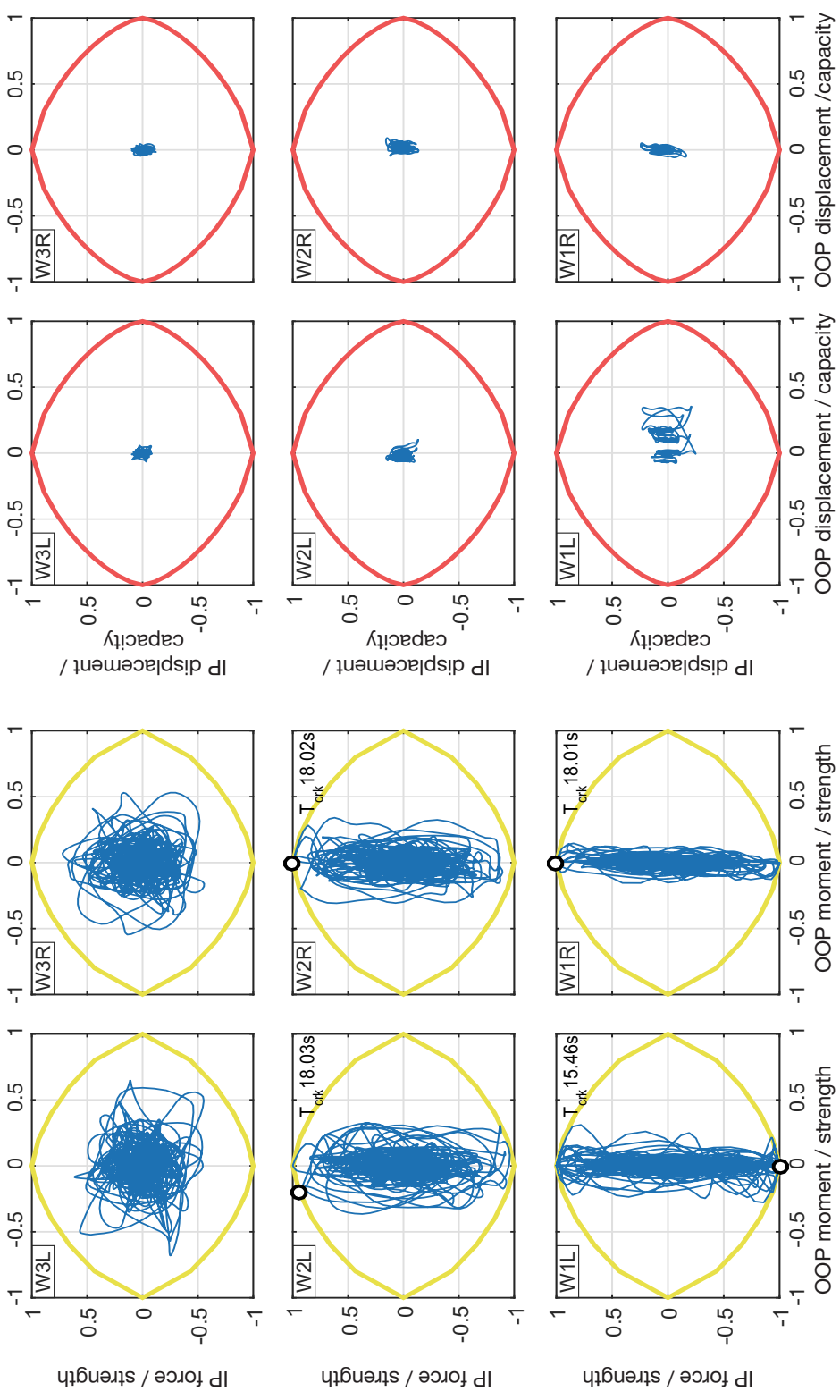

*Fig. A 6 Force and displacement paths of infill walls in frame **3×3_300T** for analysis **EQ10** scaled to a_g = **0.25g***

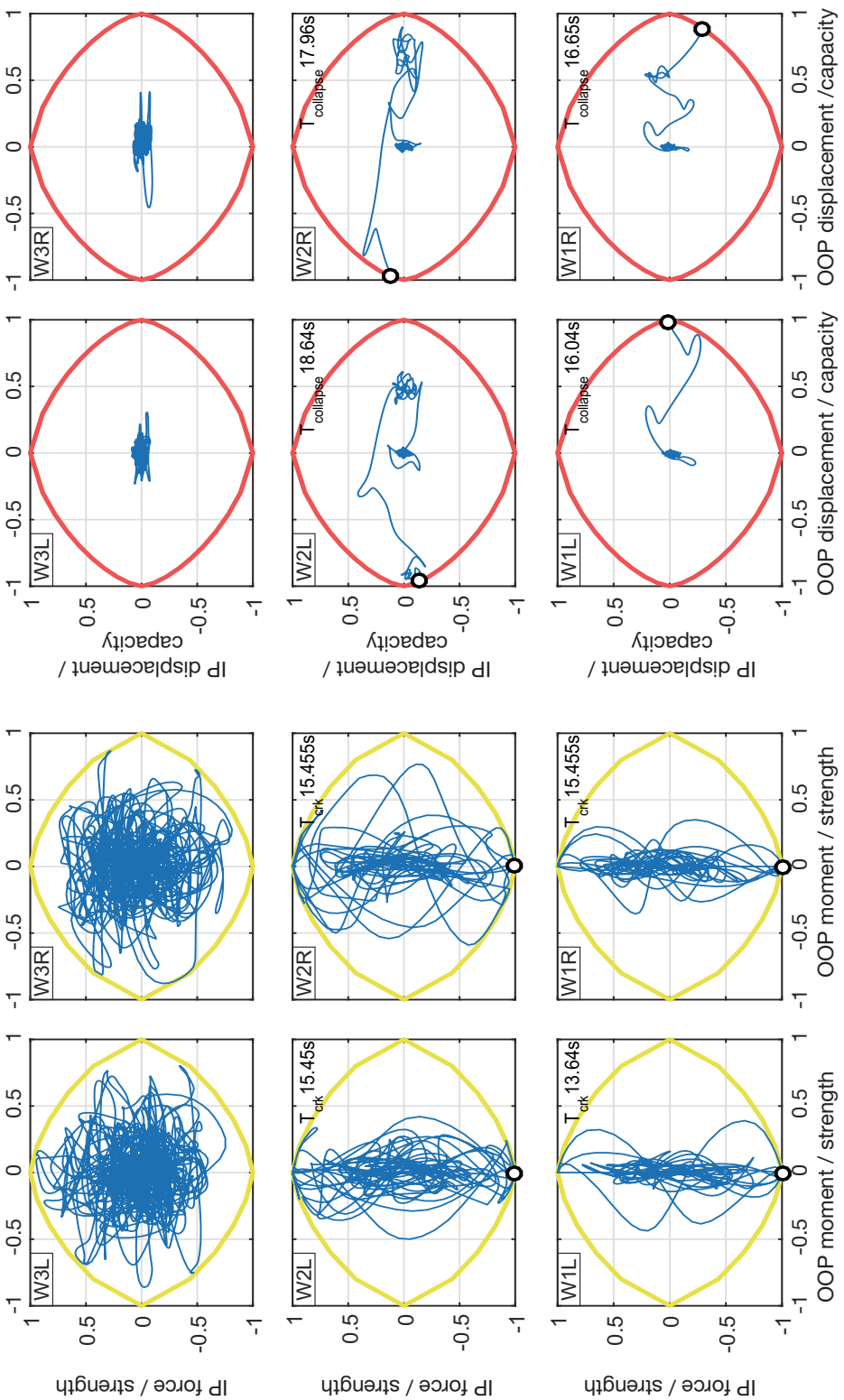

Fig. A 7 Force and displacement paths of infill walls in frame ***3×3_115S*** *for analysis* ***EQ10*** *scaled to* a_g **= 0.25*g***

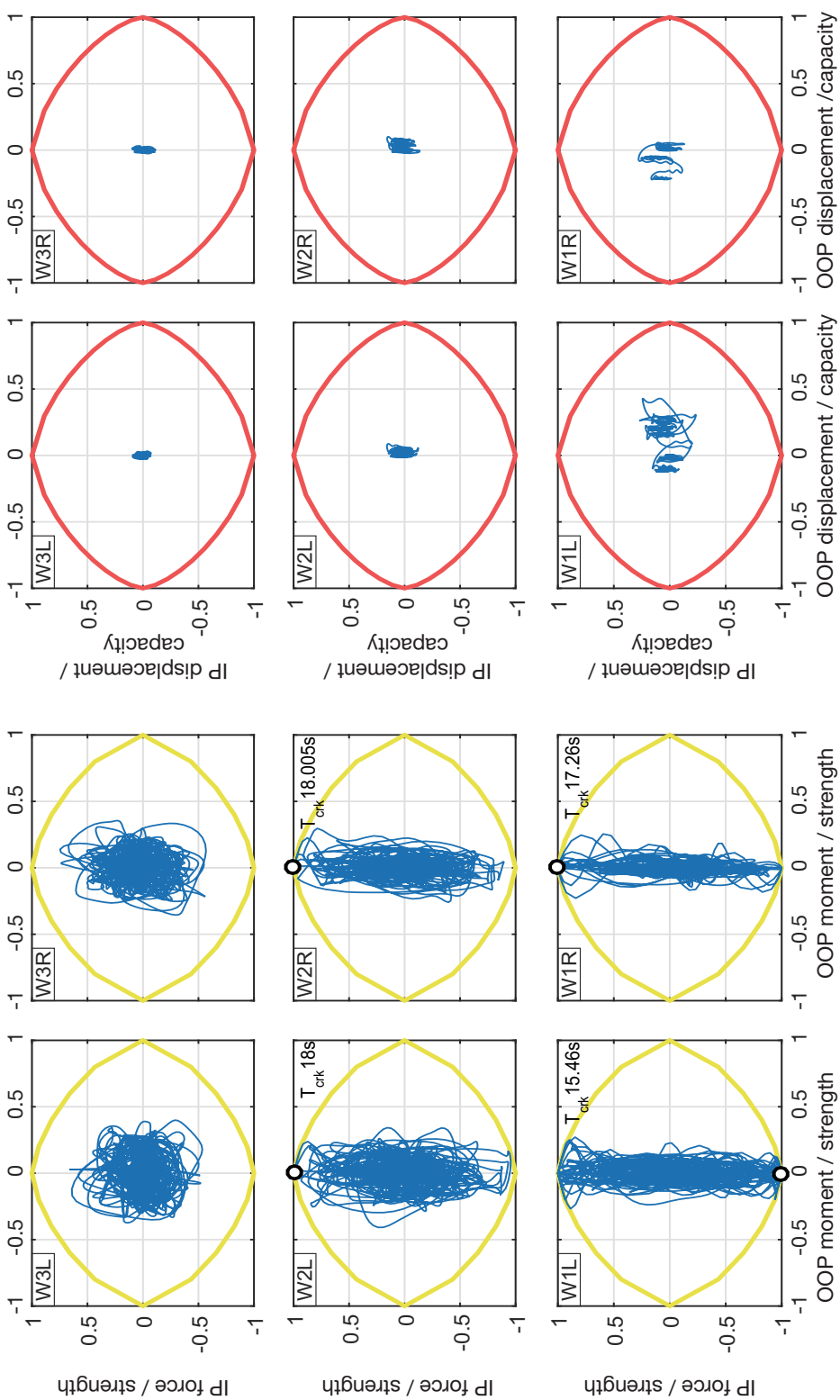

*Fig. A 8 Force and displacement paths of infill walls in frame **3×3_300S** for analysis **EQ10** scaled to a_g = **0.25g***

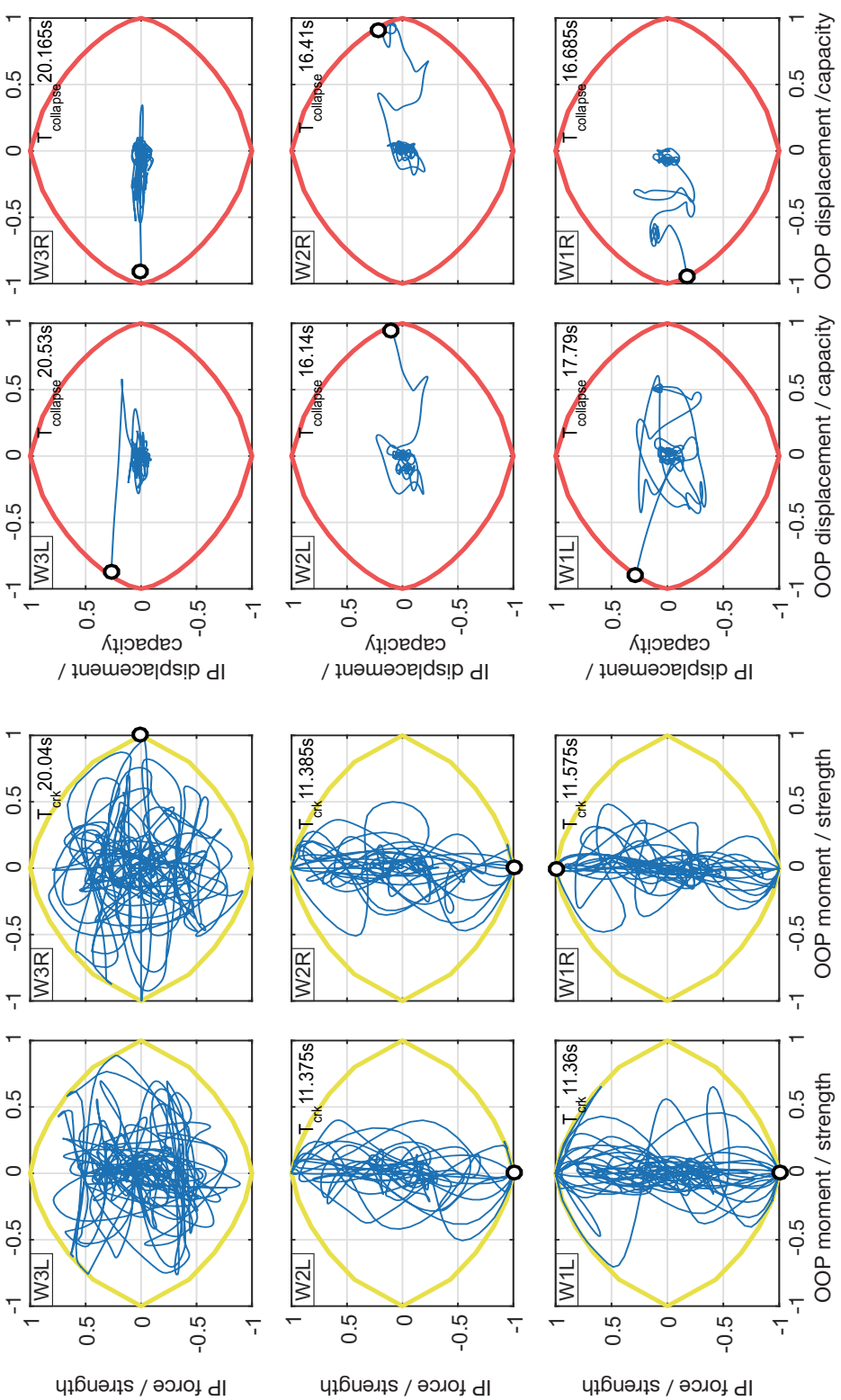

Fig. A 9 Force and displacement paths of infill walls in frame ***3×3_115T*** *for analysis* ***EQ10*** *scaled to* a_g **= 0.35g**

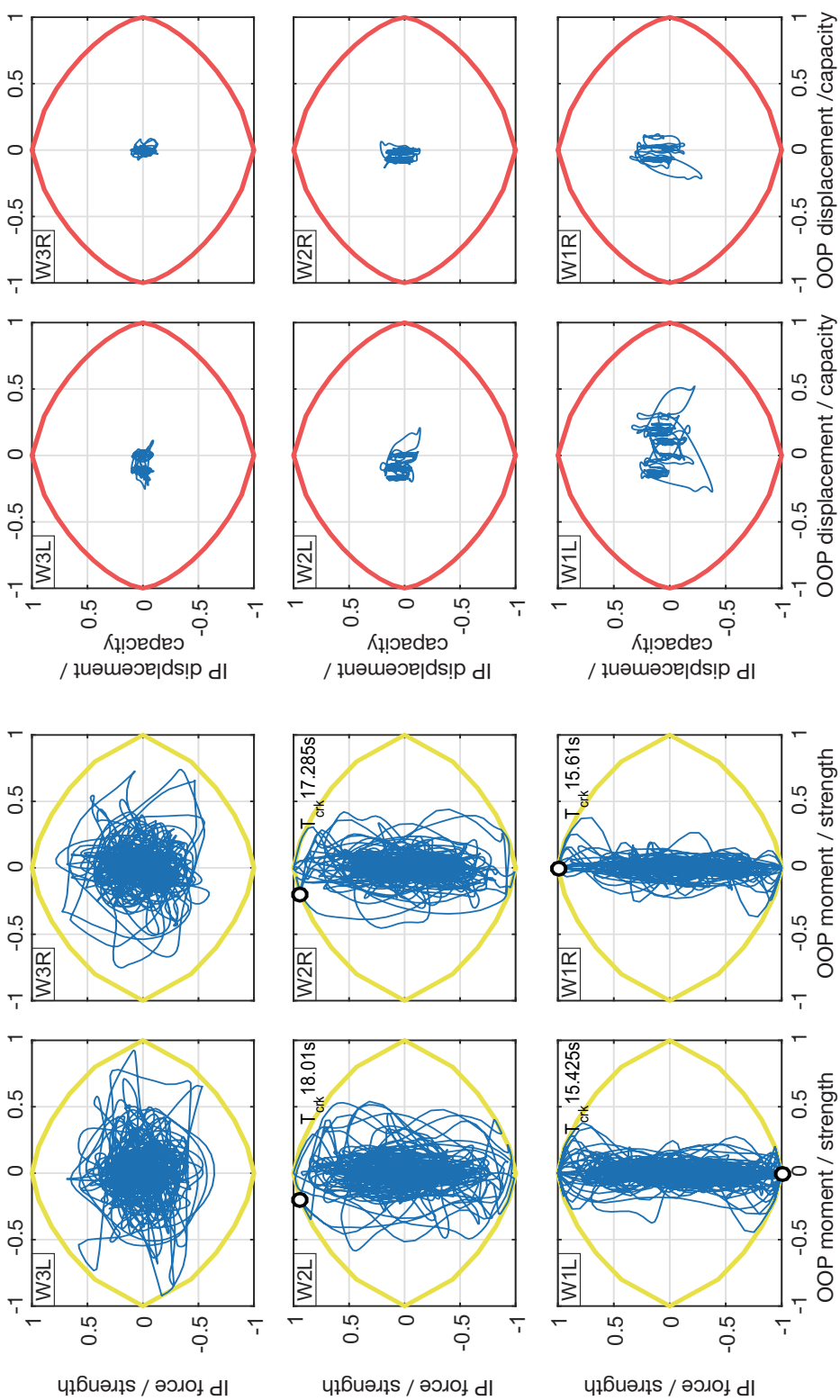

*Fig. A 10 Force and displacement paths of infill walls in frame **3×3_300T** for analysis **EQ10** scaled to a_g = **0.35g***

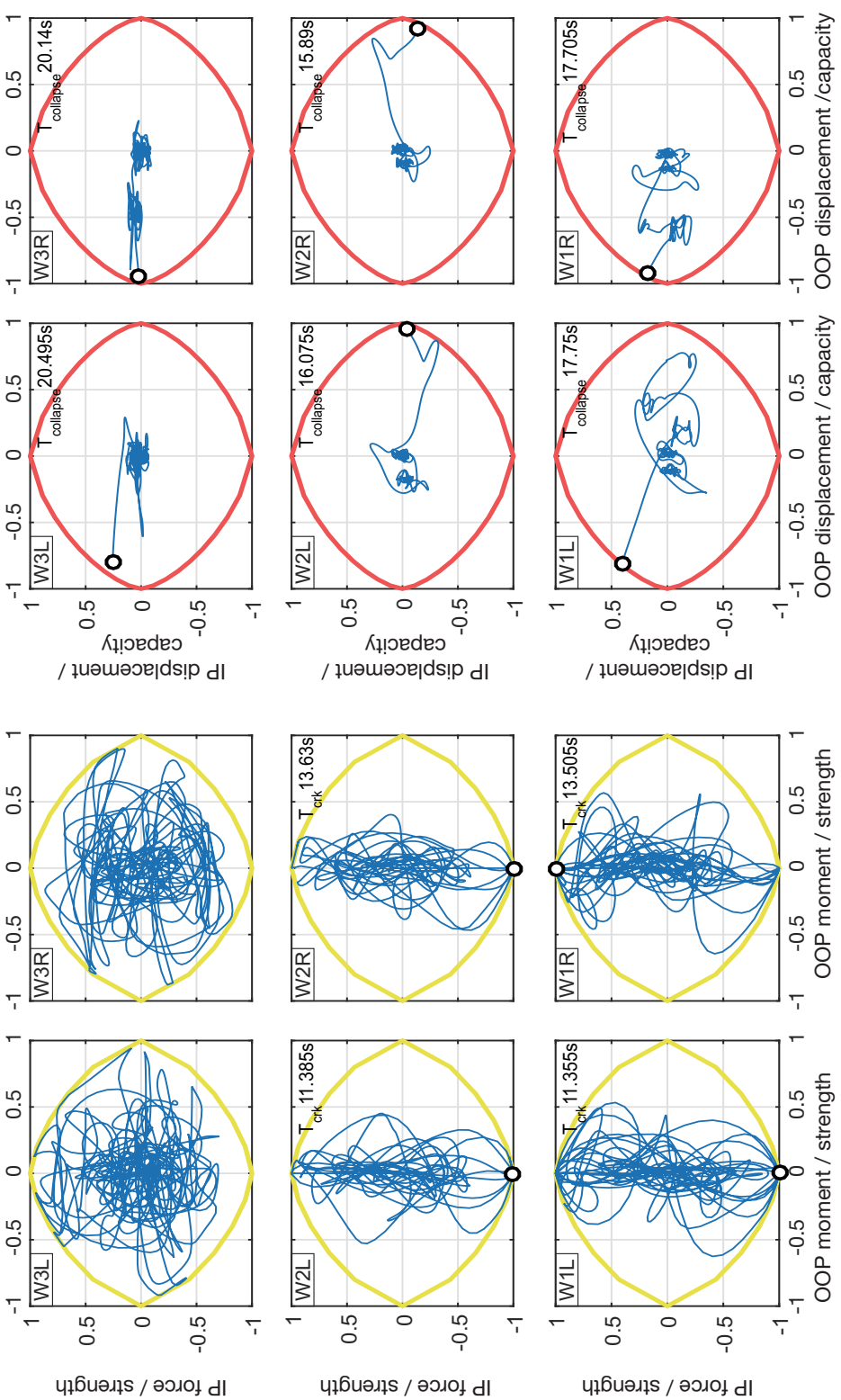

*Fig. A 11 Force and displacement paths of infill walls in frame **3×3_115S** for analysis **EQ10** scaled to a_g = **0.35g***

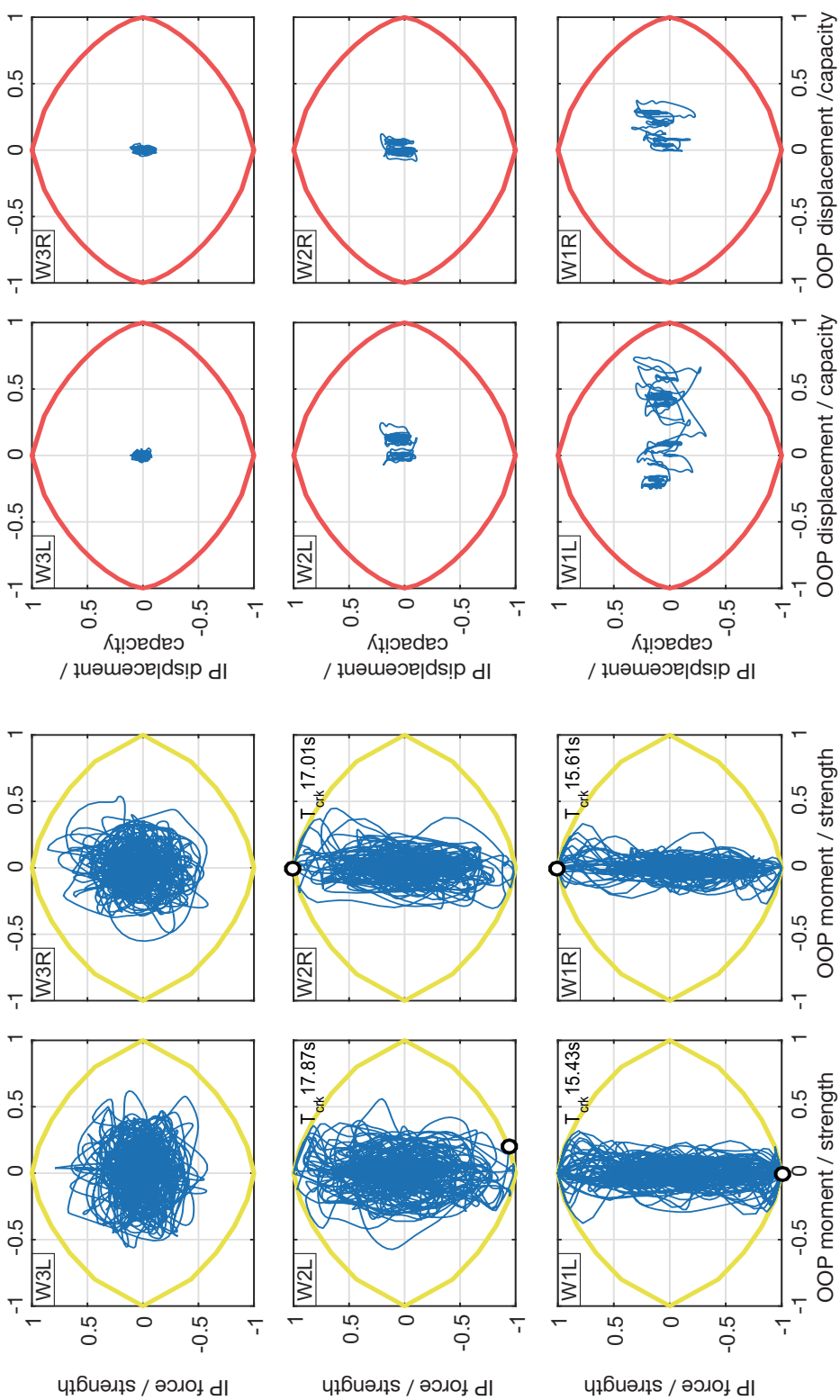

*Fig. A 12 Force and displacement paths of infill walls in frame **3×3_300S** for analysis **EQ10** scaled to a_g = **0.35g***

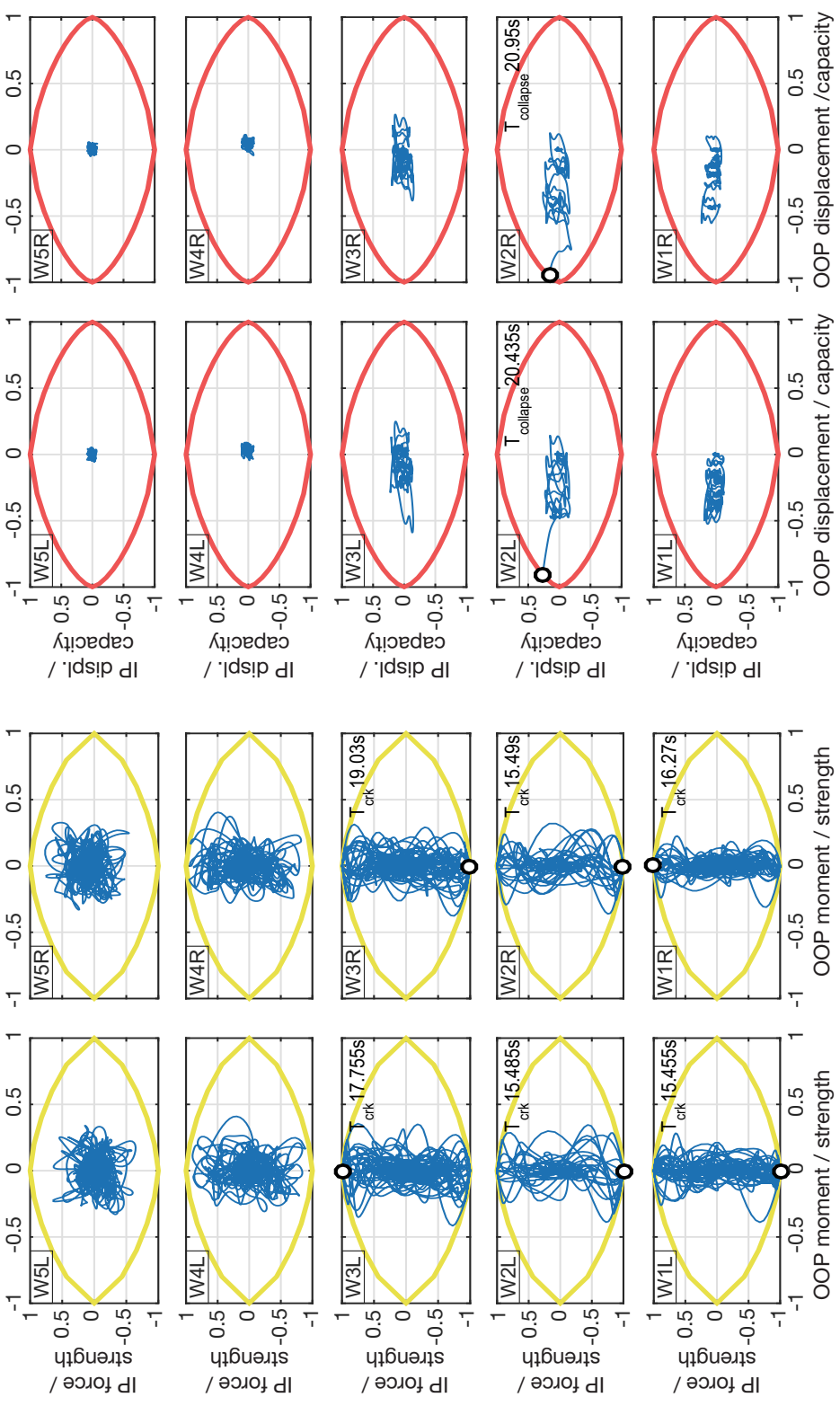

Fig. A 13 Force and displacement paths of infill walls in frame ***5×3_115T*** *for analysis* ***EQ10*** *scaled to* a_g **= 0.15g**

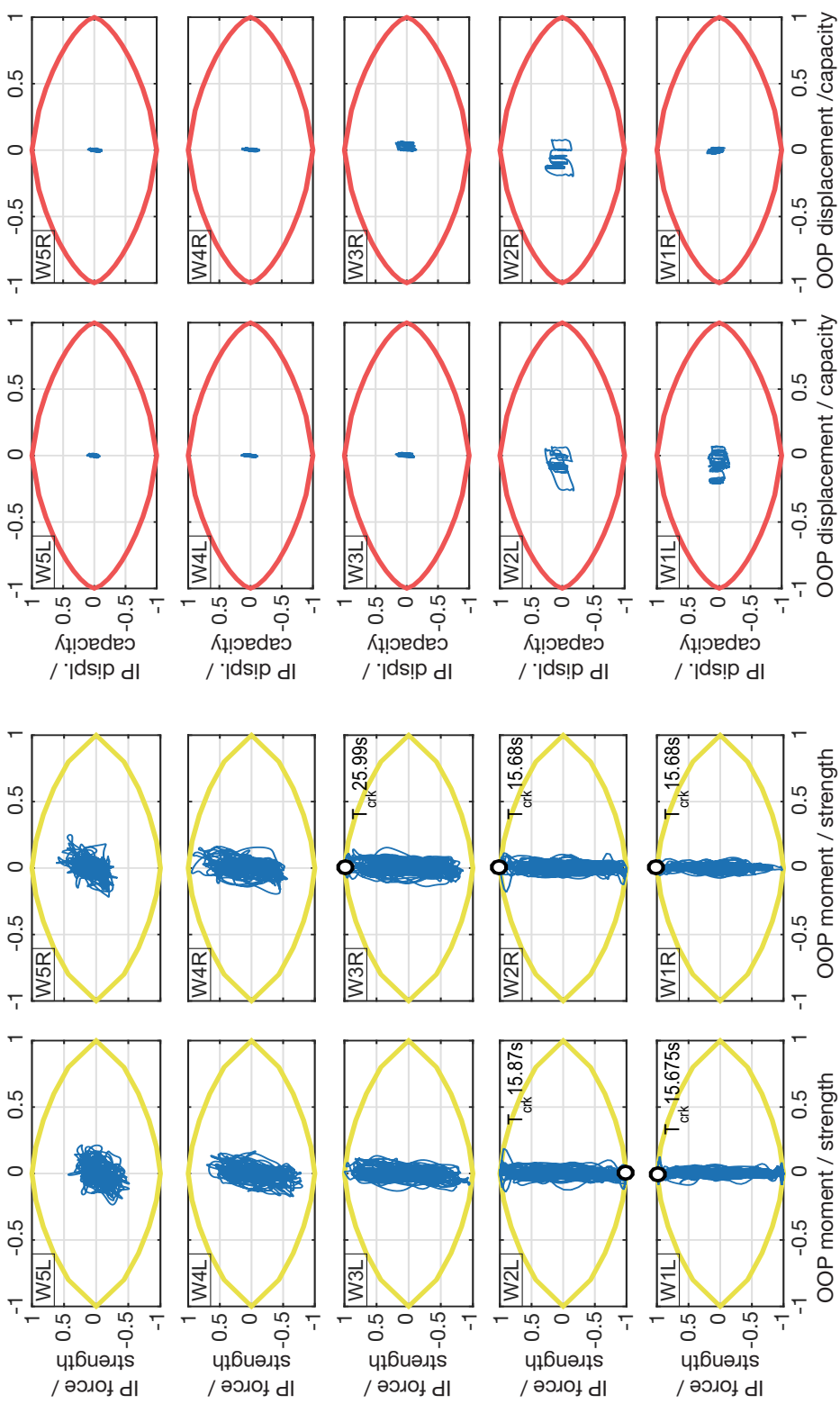

*Fig. A 14 Force and displacement paths of infill walls in frame **5×3_300T** for analysis **EQ10** scaled to a_g = **0.15g***

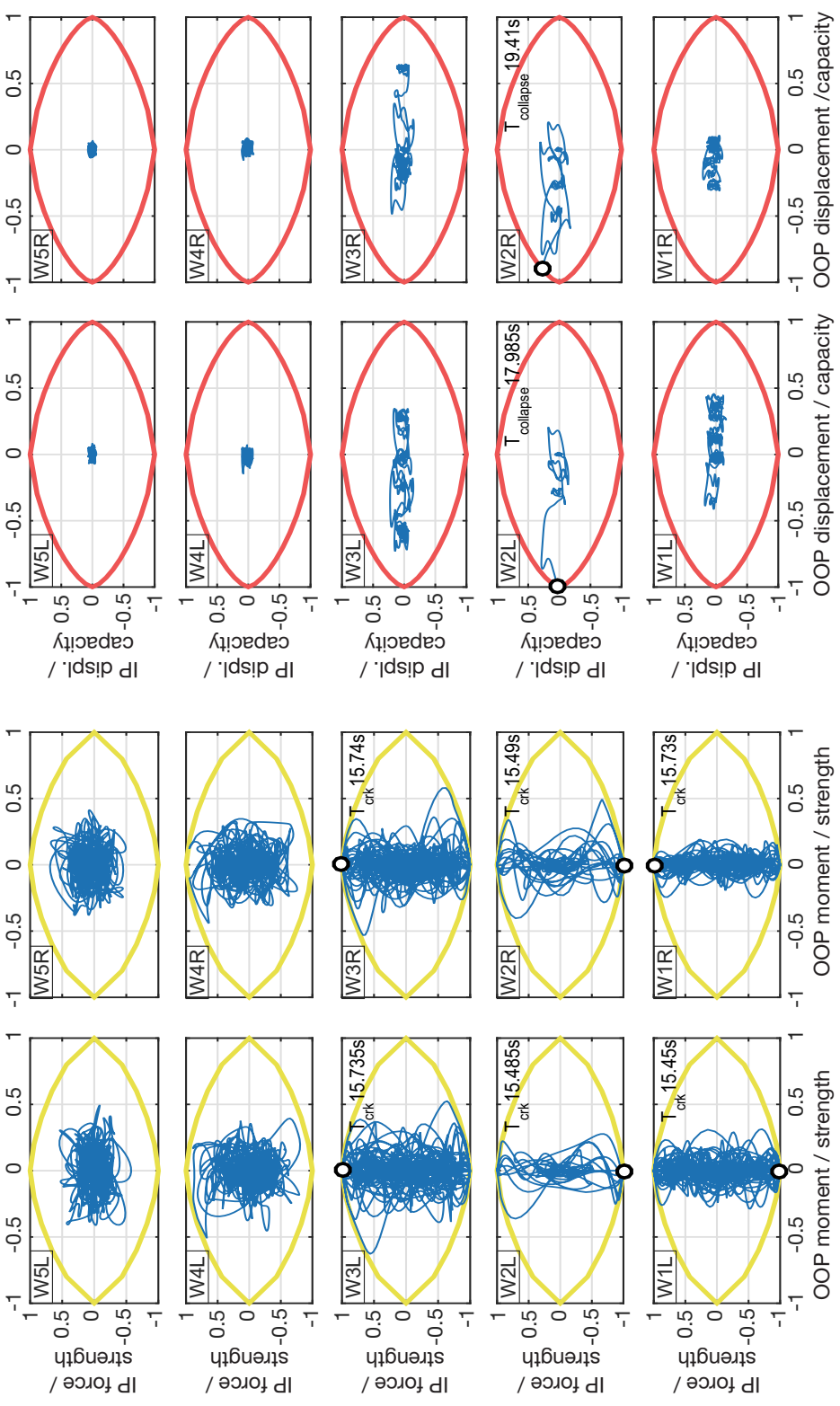

Fig. A 15 Force and displacement paths of infill walls in frame ***5×3_115S*** *for analysis* ***EQ10*** *scaled to* a_g **= 0.15g**

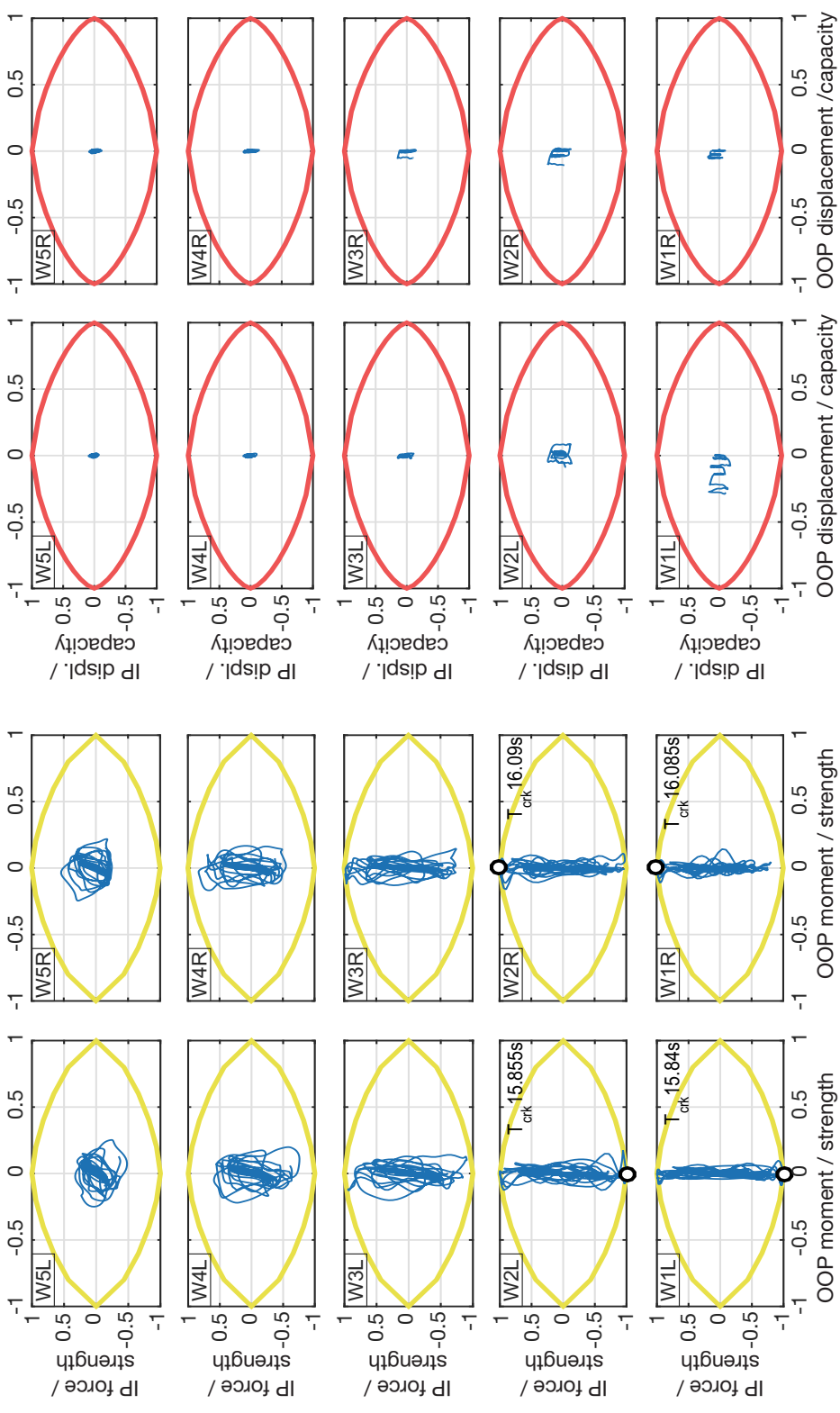

*Fig. A 16 Force and displacement paths of infill walls in frame **5×3_300S** for analysis **EQ10** scaled to a_g = **0.15g***

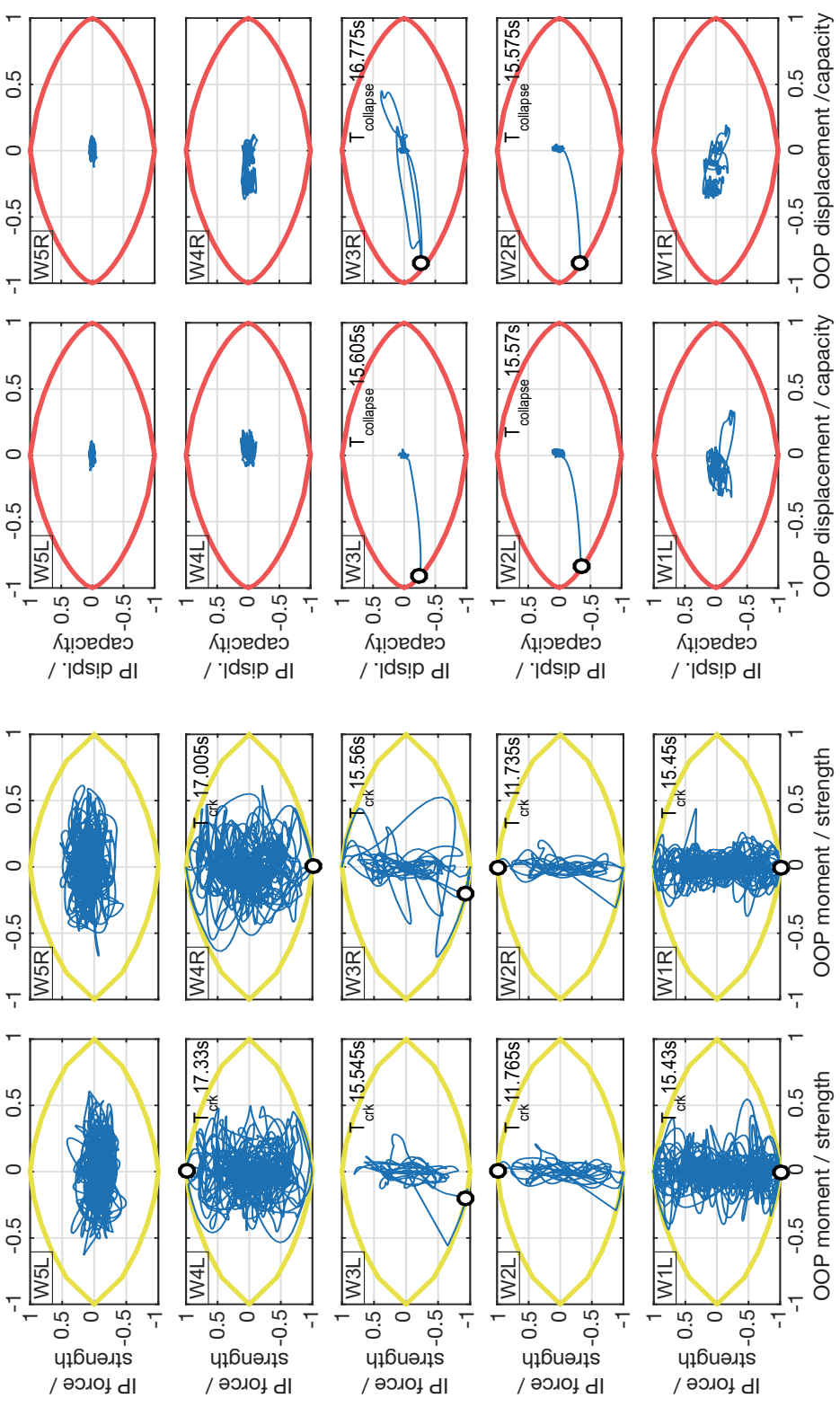

Fig. A 17 Force and displacement paths of infill walls in frame ***5×3_115T*** *for analysis* ***EQ10*** *scaled to* a_g **= 0.25*g***

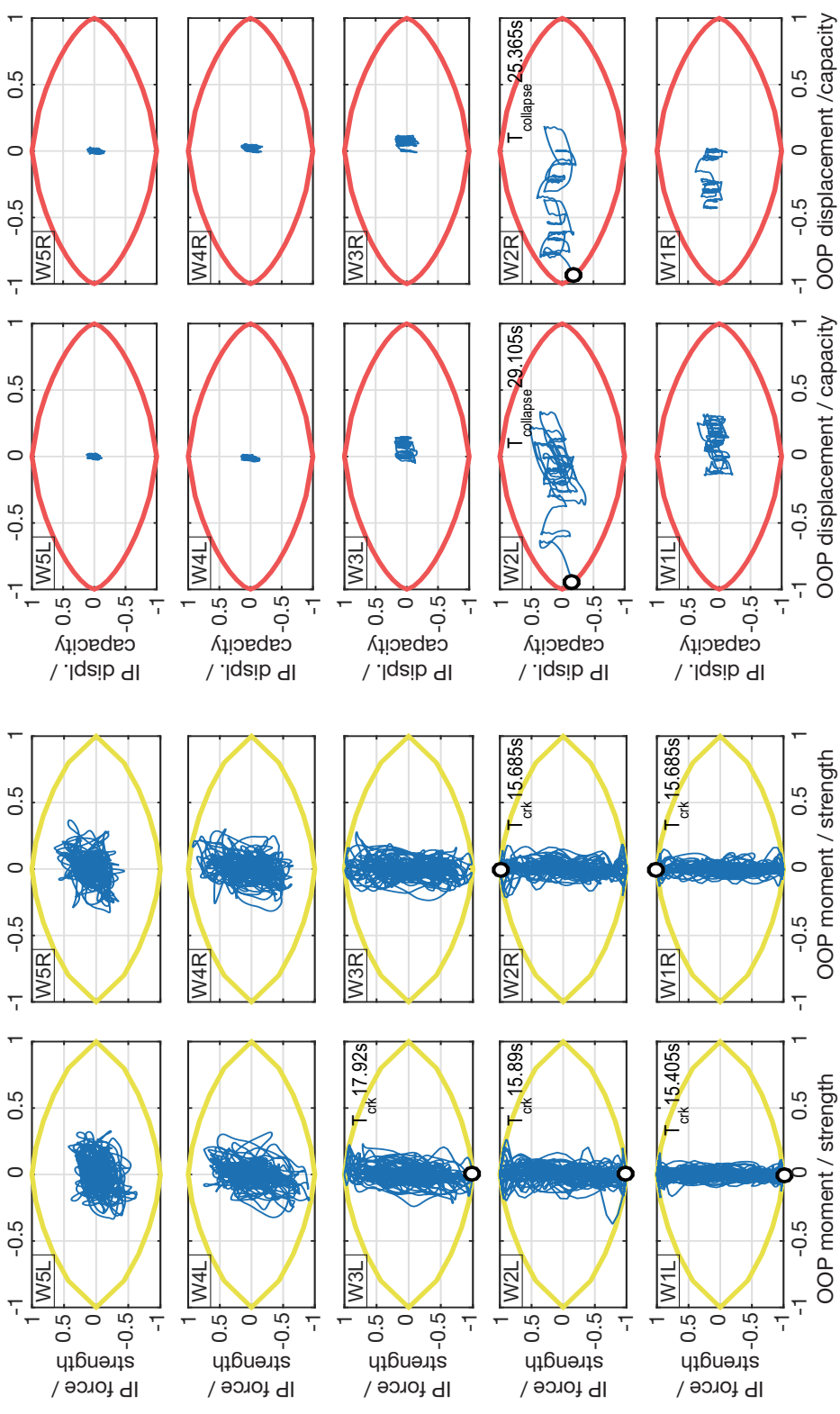

*Fig. A 18 Force and displacement paths of infill walls in frame **5×3_300T** for analysis **EQ10** scaled to a_g = **0.25g***

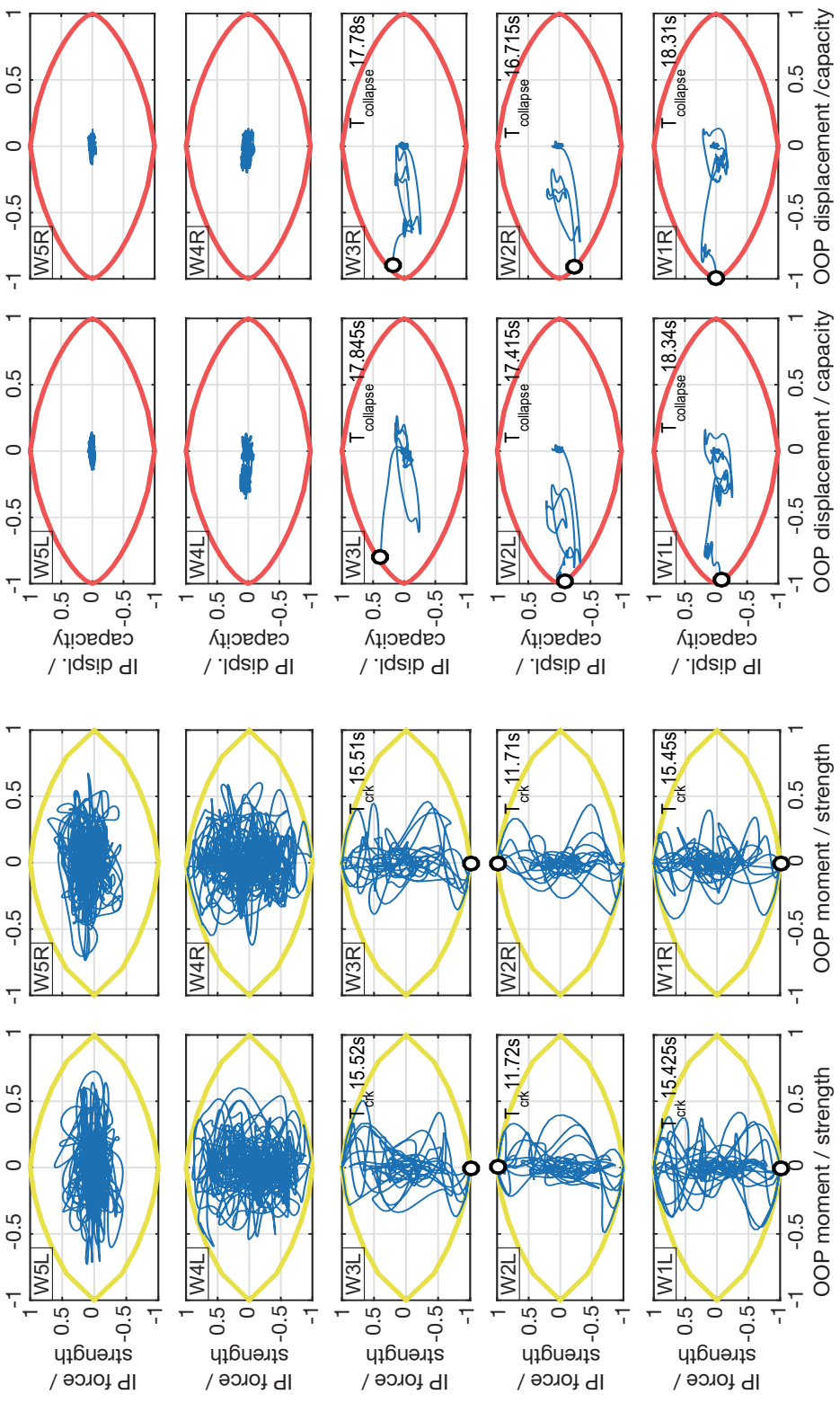

Fig. A 19 Force and displacement paths of infill walls in frame ***5×3_115S*** *for analysis* ***EQ10*** *scaled to* a_g **= 0.25g**

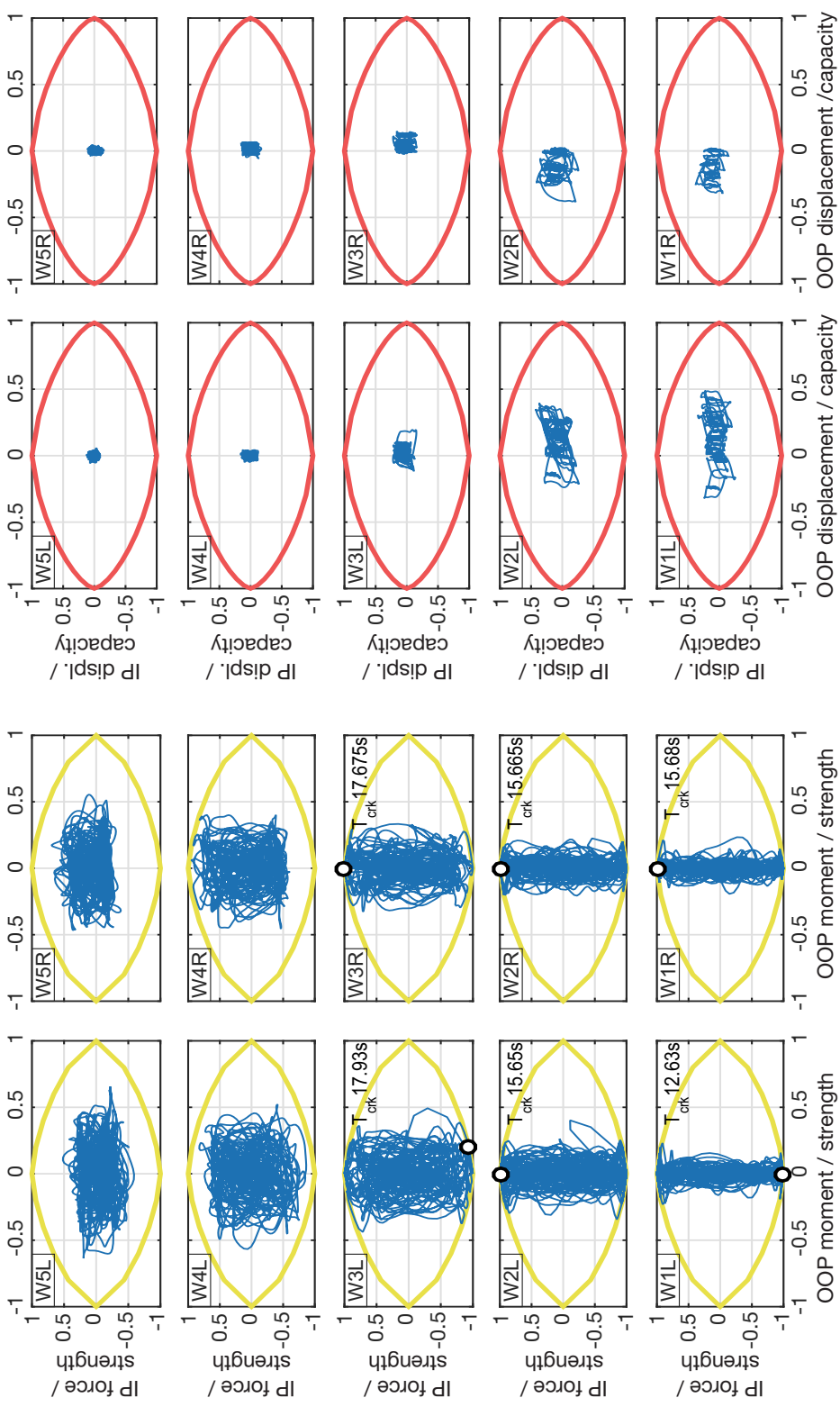

Fig. A 20 Force and displacement paths of infill walls in frame ***5×3_300S*** *for analysis* ***EQ10*** *scaled to* a_g **= 0.25g**

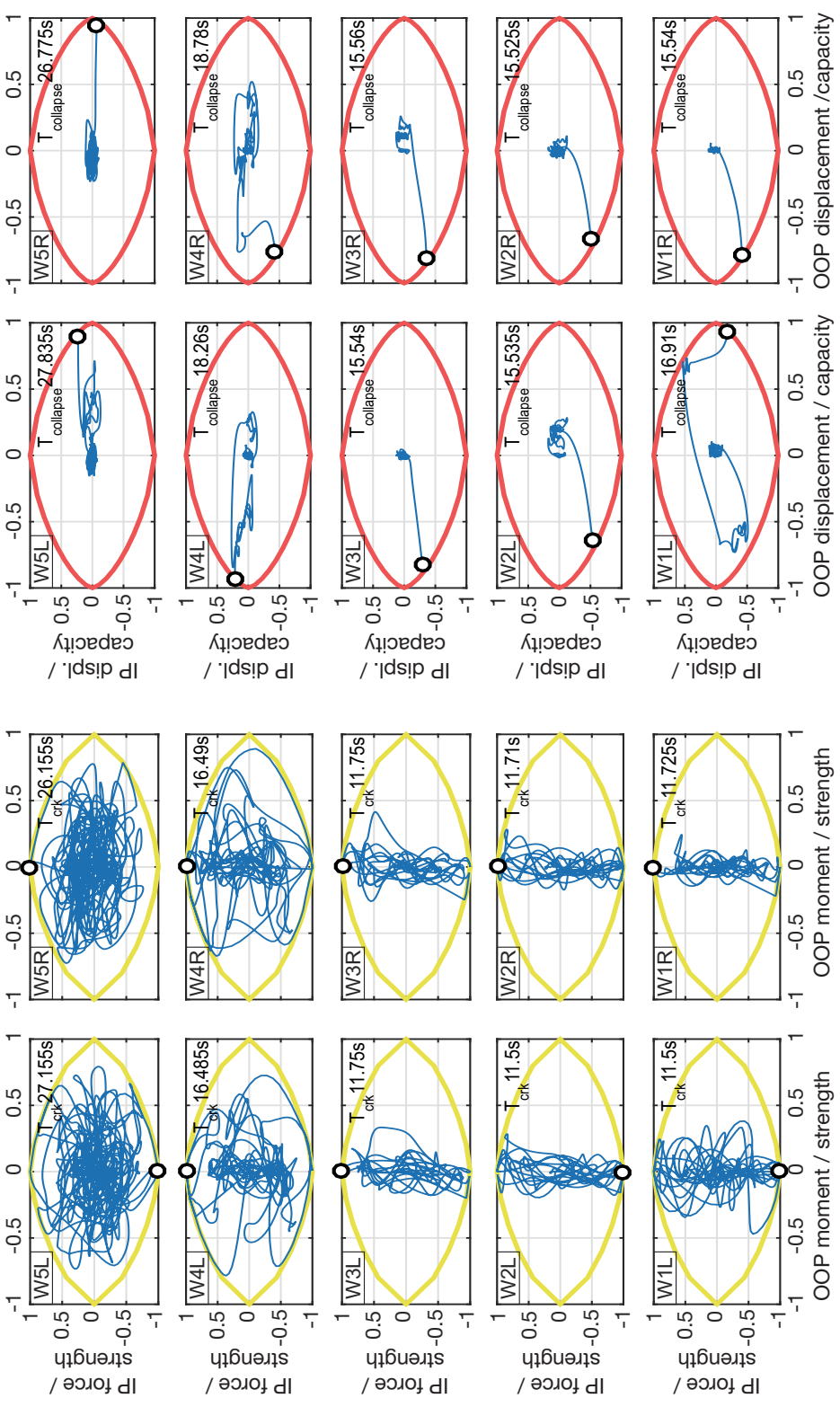

Fig. A 21 Force and displacement paths of infill walls in frame ***5×3_115T*** *for analysis* ***EQ10*** *scaled to* a_g **= 0.35*g***

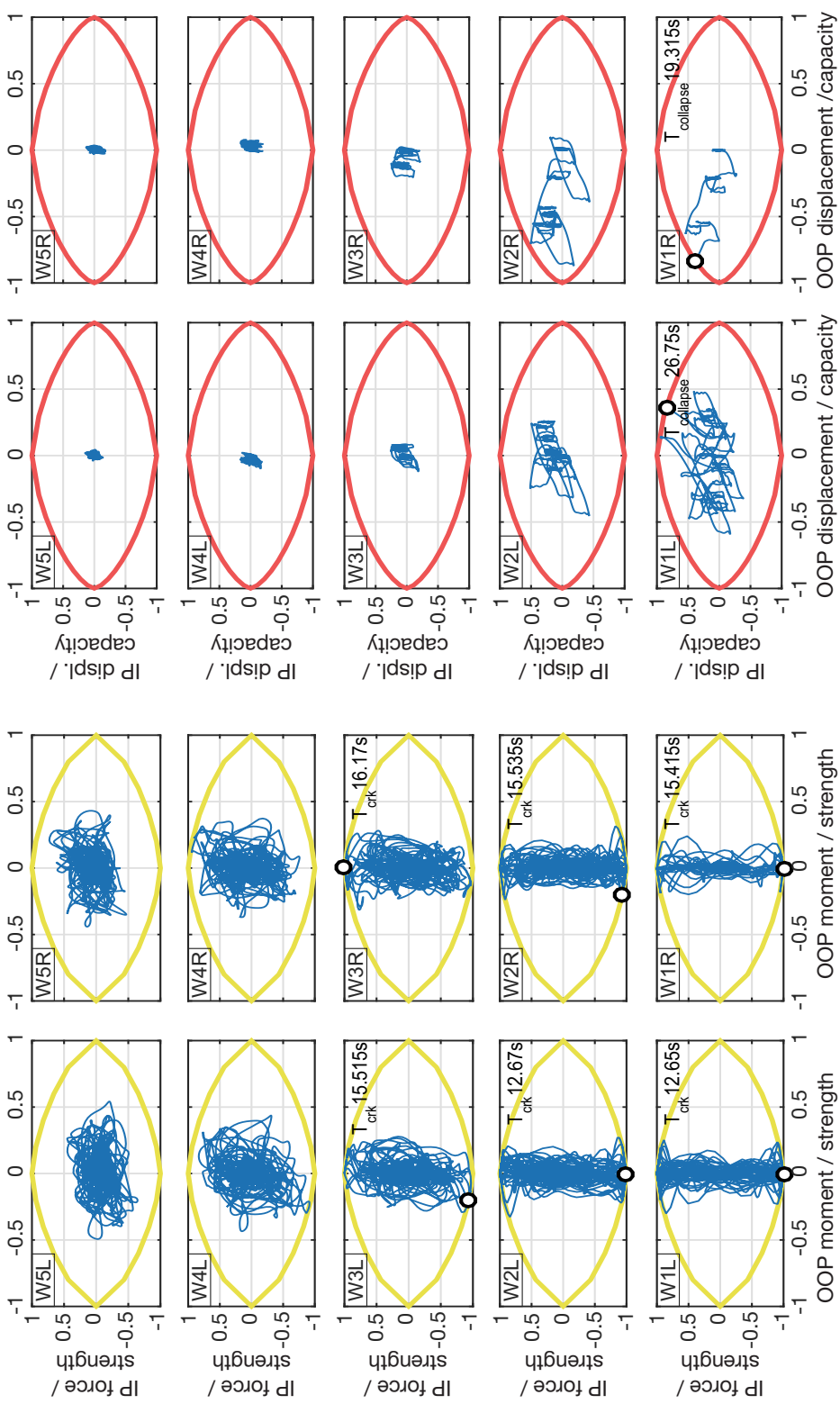

*Fig. A 22 Force and displacement paths of infill walls in frame **5×3_300T** for analysis **EQ10** scaled to a_g = **0.35g***

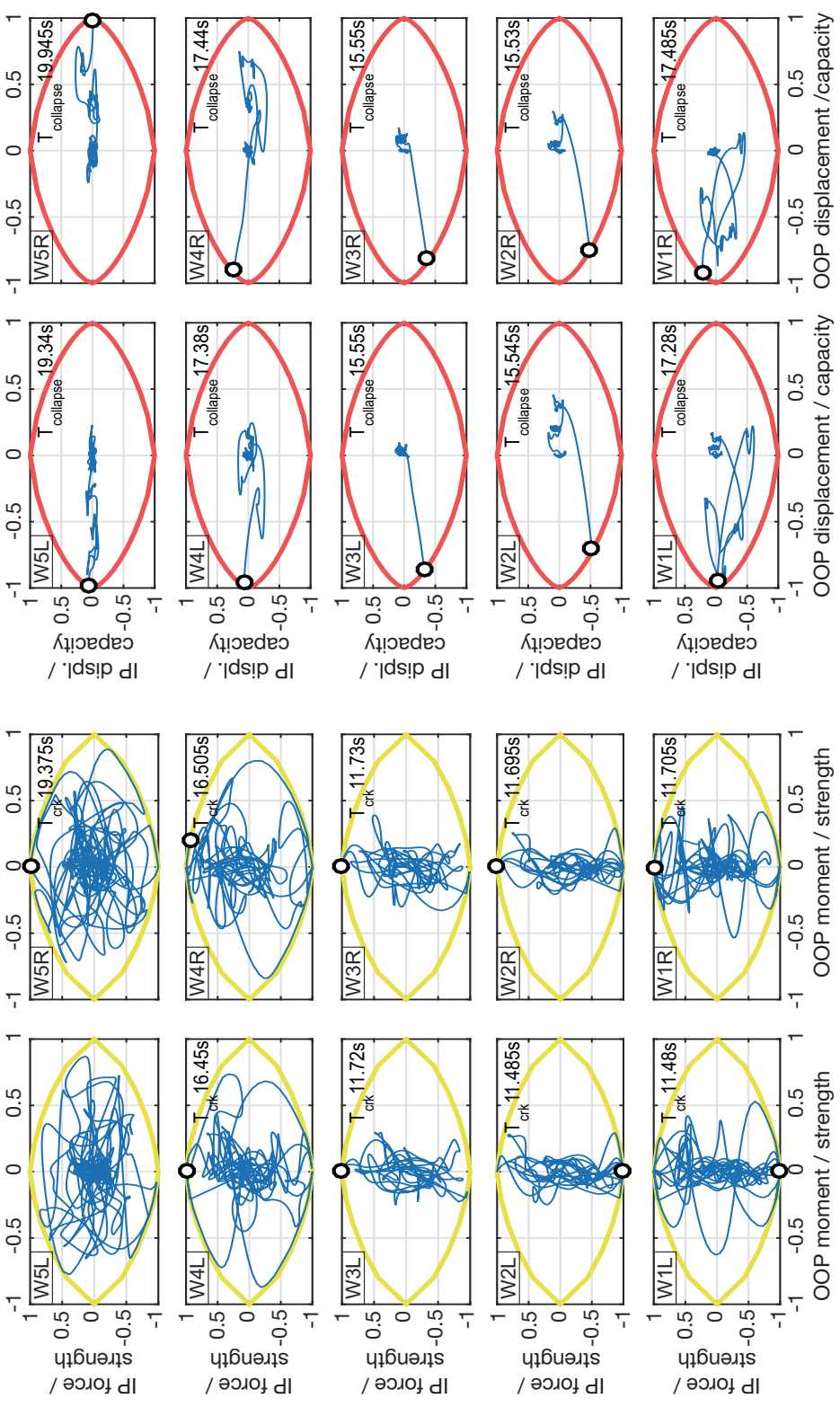

Fig. A 23 Force and displacement paths of infill walls in frame ***5×3_115S*** *for analysis* ***EQ10*** *scaled to* a_g **= 0.35g**

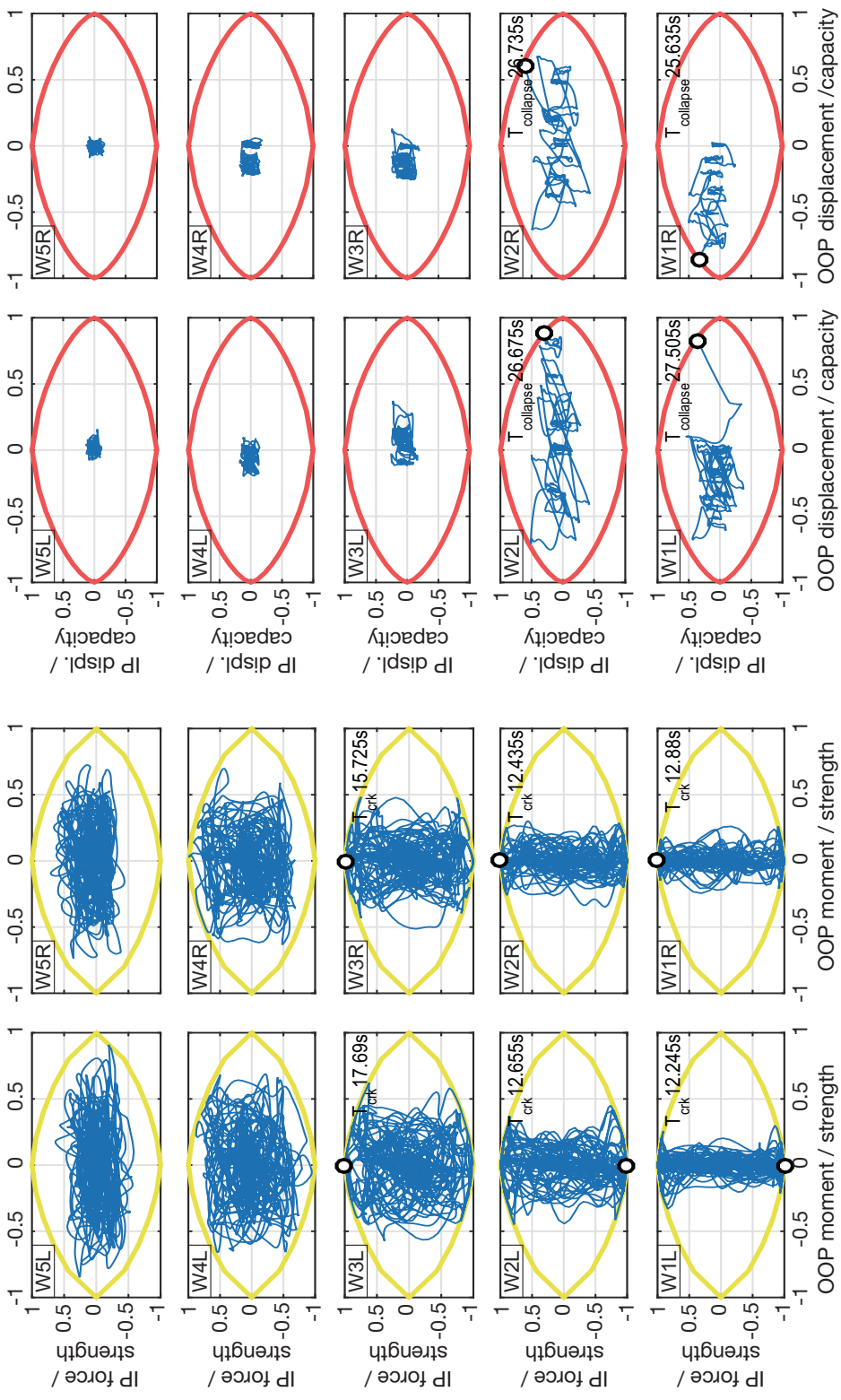

*Fig. A 24 Force and displacement paths of infill walls in frame **5×3_300S** for analysis **EQ10** scaled to a_g = **0.35g***